universität wien

MASTERARBEIT | MASTER'S THESIS

Titel | Title

Accessing Flexibly Modified Prion Protein Variants by Combining Genetic Code Expansion and Protein Semi-Synthesis

verfasst von | submitted by

Jacqueline Bittner Bc. BSc

angestrebter akademischer Grad | in partial fulfilment of the requirements for the degree of

Master of Science (MSc)

Wien | Vienna, 2026

Studienkennzahl lt. Studienblatt | Degree programme code as it appears on the student record sheet:	UA 066 863
Studienrichtung lt. Studienblatt | Degree programme as it appears on the student record sheet:	Masterstudium Biologische Chemie
Betreut von | Supervisor:	Univ.-Prof. Dr. Christian Friedrich Wilhelm Becker

Acknowledgements

Firstly, I want to thank Christian F. W. Becker for accepting me into his group and for introducing me to the interesting world of prions, proteins and semi-synthesis. Your patience and guidance during both the experimental parts but also the writing process of this thesis were fundamental and did mean a lot to me, especially in the final stretches.

I also want to thank Gerhard Niederacher for introducing me to a lot of new laboratory techniques, to which I was not accustomed to before, and for sharing his laboratory space with me. Whenever I needed help with troubleshooting, regardless of whether in the lab or outside, you had an open ear and good advice.

Special thanks go to Anna Mägde, who joined me in this prion adventure and helped me immensely with syntheses and experimental questions. I hope you find the answers for some of my findings during your PhD.

Lastly, I want to thank Herwig Weißinger for his organic inputs and help with NMR elucidation and wish him the very best for his remaining PhD journey.

Most importantly, I want to thank my family who always promoted and supported my scientific interests and education, regardless of age or location, and continue to do so with unchanged enthusiasm.

Abstract

The focus of this thesis lies on the combination of genetic code expansion (GCE), expressed protein selenoester ligation (EPSL) as well as copper catalyzed azide alkyne cycloaddition (CuAAC) techniques to obtain flexibly modified full-length variants of the bank vole prion protein (bvPrP). Further development of these techniques will enable the generation of mg-amounts of homogenous bvPrP variants with glycan mimics as well as a C-terminal glycosylphosphatidylinositol (GPI) mimic to study their impact on PrP folding, aggregation and pathogenic events in cells.

In this work, the two native N-glycosylation sites at positions 181 and 197 in the bvPrP amino acid sequence were individually substituted with an amber stop codon, allowing the site-specific introduction of non-canonical amino acids (ncAAs) such as N-*ε*-((2-azidoethoxy)carbonyl)-L-lysine (AzK) and N-*ε*-(prop-2-ynyloxycarbonyl)-L-lysine (YnK). YnK was used from commercial sources as well as self-synthesized due to economic reasons. Both batches were successfully applied. Over the course of this work, four distinct bvPrP intein fusion protein variants, namely bvPrP-WT, bvPrP-N181X-AzK, bvPrP-N197X-AzK and bvPrP-N181X-YnK, were produced through recombinant protein expression. Following purification, the protein hydrazides used for CuAAC or selenoester conversion were generated through hydrazinolysis of the intein fusion construct. However, it was discovered that the azide moiety within bvPrP-N181X-AzK was reduced to an amine by DTT in the process. Thus, the focus shifted to YnK and the bvPrP-N181X mutant, as this variant exhibits increased expression efficiency. Moreover, YnK incorporation and CuAAC reaction capability was demonstrated through conjugation to Fluor 488 azide. However, during subsequent CuAAC reactions conducted to conjugate the bvPrP-N181X-YnK hydrazide to an azidomannose glycan mimic, monitoring and precipitation issues were encountered. Therefore, product formation could not be confirmed. Furthermore, previously made bvPrP-WT hydrazide was converted to a selenoester and ligated to an GPI-anchor mimic, affording the bvPrP-GPI product.

Zusammenfassung

Der Fokus dieser Arbeit liegt auf der Kombination der Techniken der Expansion des Genetischen Codes (GCE), der Exprimiertes Protein Selenoester Ligation (EPSL) als auch der Kupfer katalysierten Azid Alkin Cycloaddition (CuAAC) um flexibel modifizierte Volllängenvarianten des Rötelmaus Prion Proteins (bvPrP) zu erhalten. Die Weiterentwicklung dieser Techniken wird die Herstellung von mg-Mengen homogener bvPrP Varianten mit Glykanmimetika sowie einem C-terminalem Glycosylphosphatidylinositol (GPI) Mimetikum erlauben, um deren Effekt auf PrP Faltung, Aggregation und pathologischen Ereignissen in Zellen zu erforschen.

In dieser Arbeit wurden die zwei nativen N-Glykosilierungsstellen an den Positionen 181 und 197 in der bvPrP Aminosäuresequenz individuell mit einem Amber-Stopcodon substituiert, was die positionsspezifische Einführung von nicht-kanonischen Aminosäuren (ncAAs) wie N-*ε*-((2-azidoethoxy)carbonyl)-L-Lysin (AzK) und N-*ε*-(prop-2-inyloxycarbonyl)-L-Lysin (YnK) ermöglicht. YnK von kommerziellen Quellen wurde verwendet, sowie aufgrund von ökonomischen Gründen selbst synthetisiert. Beide Chargen wurden erfolgreich angewandt. Während dem Verlauf dieser Arbeit wurden vier unterschiedliche bvPrP Inteinfusionsproteinvarianten, nämlich bvPrP-WT, bvPrP-N181X-AzK, bvPrP-N197X-AzK und bvPrP-N181X-YnK durch rekombinante Proteinexpression produziert. Nach der Aufreinigung wurden die für CuAAC oder Selenoesterkonversion verwendeten Proteinhydrazide durch Hydrazinolyse des Inteinfusionskonstrukts generiert. Jedoch wurde entdeckt, dass der Azid-Rest innerhalb von bvPrP-N181X-AzK während des Vorgangs von DTT zu einem Amin reduziert wurde. Folglich ist der Fokus auf YnK und die bvPrP-N181X Mutante übergegangen, da diese Variante eine erhöhte Expressionseffizienz aufweist. Überdies wurde der YnK Einbau und die CuAAC Reaktionsfähigkeit durch eine Konjugation zum Fluor 488 Azid demonstriert. Allerdings sind während der anschließend durchgeführten CuAAC Reaktionen, um das bvPrP-N181X-YnK Hydrazid an ein Azidomannoseglykanmimetikum zu konjugieren, Monitoring- und Niederschlagsprobleme aufgetreten. Daher konnte die Produktformation nicht bestätigt werden. Darüber hinaus wurde ein zuvor hergestelltes bvPrP-WT Hydrazid in einen Selenoester konvertiert und an ein GPI-Ankermimetikum ligiert um das bvPrP-GPI Produkt zu erhalten.

Table of Contents

Abbreviations

aaRS	Aminoacyl-tRNA synthetase
ACN	Acetonitrile
APS	Ammonium persulfate
Azidomannose	2,3,4,6-tetra-O-acetyl-*α*-D-mannopyranosyl azide
AzK	N-*ε*-((2-azidoethoxy)carbonyl)-L-lysine
Boc-L-Lys-OH	N-*α*-(tert-Butoxycarbonyl)-L-lysine
BSE	Bovine spongiform encephalopathy
bvPrP	Bank vole prion protein
$CaCl_2$	Calcium chloride
CBD	Chitin-binding domain
CJD	Creutzfeldt-Jakob disease
$CoCl_2 \cdot 6\ H_2O$	Cobalt(II) chloride hexahydrate
CuAAC	Copper catalyzed azide alkyne cycloaddition
$CuSO_4$	Copper(II) sulfate
$CuSO_4 \cdot 5\ H_2O$	Copper(II) sulfate pentahydrate
dH_2O	Deionized water
DI-MS	Direct injection-mass spectrometry
DMF	Dimethylformamide
DMSO-d6	Deuterated dimethyl sulfoxide
DNA	Desoxyribonucleic acid
DPDS	Diphenyldiselenide
DSL	Diselenide-selenoester ligation
DTT	Dithiothreitol
E. coli	*Escherichia coli*

EDTA	Ethylenediaminetetraacetic acid
equiv.	Equivalents
EPL	Expressed protein ligation
EPSL	Expressed protein selenoester ligation
ESI	Electrospray ionization
EtOAc	Ethyl acetate
$FeCl_2 \cdot 4\ H_2O$	Iron(II) chloride tetrahydrate
GCE	Genetic code expansion
GdnHCl	Guanidine hydrochloride
GPI	Glycosylphosphatidylinositol
H_3BO_3	Boric acid
HCl	Hydrochloric acid
HEPES	2-(4-(2-hydroxyethyl)-1-piperazinyl)-ethanesulfonic acid
HPLC	High performance liquid chromatography
HRMS	High resolution mass spectrometry
IPTG	Isopropyl *β*-d-1-thiogalactopyranoside
KH_2PO_4	Potassium dihydrogen phosphate
LC-MS	Liquid chromatography-mass spectrometry
MESNa	Sodium 2-mercaptoethanesulfonate
$MgSO_4$	Magnesium sulfate
$MnCl_2 \cdot 4\ H_2O$	Mangansese(II) chloride tetrahydrate
mRNA	Messenger ribonucleic acid
MS	Mass spectrometry
Na_2HPO_4	Disodium hydrogen phosphate
NaCl	Sodium chloride

NaOH	Sodium hydroxide
NaPi	Sodium phosphate
NCL	Native chemical ligation
ncAA	non-canonical amino acid
NH_4Cl	Ammonium chloride
Ni-NTA	Nickel-nitrilotriacetic acid
$NiSO_4$	Nickel(II) sulfate
NMR	Nuclear magnetic resonance
OD_{600}	Optical density at a wavelength of 600 nm
PES	Polyethersulfone
pI	Isoelectric point
POI	Protein of interest
PrP	Prion protein
PrP^{C}	Cellular prion protein
PrP^{Sc}	Scrapie prion protein
RF1	Release factor 1
RF2	Release factor 2
RP-HPLC	Reversed phase high performance liquid chromatography
rpm	Rounds per minute
RT	Room temperature
SDS	Sodium dodecyl sulfate
SDS-PAGE	Sodium dodecyl sulfate-polyacrylamide gel electrophoresis
SPPS	Solid phase peptide synthesis
TBS	Tris(hydroxymethyl)aminomethane buffered saline
TBTA	Tris((1-benzyl-4-triazolyl)methyl)amine

TCEP	Tris(2-carboxyethyl)phosphine
TEMED	Tetramethylethylenediamine
TFA	Trifluoroacetic acid
THF	Tetrahydrofuran
THPTA	Tris(3-hydroxypropyltriazolylmethyl)amine
Tris	Tris(hydroxymethyl)aminomethane
TrisHCl	Tris(hydroxymethyl)aminomethane hydrochloride
tRNA	Transfer ribonucleic acid
TSE	Transmissible spongiform encephalopathy
WT	Wild-type
xg	Times gravitational force
YnK	N-*ε*-(prop-2-ynyloxycarbonyl)-L-lysine
$ZnCl_2$	Zinc chloride

1. Introduction

1.1 The prion protein PrP

1.1.1 Prion diseases – History, transmission and pathology

The prion protein (PrP) is the main causative agent of a set of fatal neurodegenerative diseases termed transmissible spongiform encephalopathies (TSE), which are observed in mammals as well as humans. Historically, prion diseases in animals endemically occurred in sheep and goats in the form of scrapie, as well as in cervids, such as elk, deer or moose, as chronic wasting disease. However, several new forms of zoonotic TSEs arose during the 20th century, with the infections ascribed to the application of contaminated ovine bonemeal in cattle feed. The novel bovine spongiform encephalopathy (BSE) led to further spread of pathological prions through the consumption of infected meat, causing small outbreaks of TSEs in humans and primates, among others.[1,2]

In addition to the zoonotic infection pathway, humans can also develop a prion disease through cannibalistic consumption of infected tissue, due to genetic predisposition, after accidental prion exposure during medical procedures, or sporadically. Human TSEs include Creutzfeldt-Jakob disease (CJD), Kuru, Gerstmann-Sträussler-Scheinker disease, fatal familial insomnia and variable protease-sensitive prionopathy. While CJD can arise *via* all four pathways, Kuru is a result of ritualistic cannibalism of the dead practiced by the Foré people in Papua New Guinea during mourning.[1,3] After major outbreaks in the 1940ies and 1950ies, naturally occurring Kuru practically disappeared after the Foré abandoned their endocannibalistic traditions and thereby stopped further prion transmission within their communities.[3] Gerstmann-Sträussler-Scheinker disease, fatal familial insomnia and variable protease-sensitive prionopathy are classified as genetic prion diseases. The underlying mutations are solely acquired through autosomal dominant inheritance.[1,3] Genetic prion diseases typically first emerge after 50 to 60 years of life.[1] Similar to CJD, fatal familial insomnia may also occur sporadically, thus called sporadic familial insomnia.[3] It is hypothesized that sporadic prion diseases originate from non-inherited, somatic mutations or sudden protein instability, resulting in the novel generation of pathogenic PrP aggregates.[1] Sporadic TSEs constitute up to 90 % of all known cases, while between 5 and 10 % are attributed to inherited prion diseases.[1,4] TSEs which have been acquired due to exposure to dietary or iatrogenic PrP are connected to less than 1 out of 100 patients.[4]

While diverse in their symptomatic manifestations, all human TSE pathologies encompass the loss of brain matter due to neuronal death caused by PrP aggregation, ultimately leading to a spongiform cerebral physiology. These structural changes are typically accompanied by mental changes, like atypical behavior or cognitive deterioration, and motoric dysfunctions like ataxia, which ultimately depend on the TSE type and allow their clinical differentiation. Although incubation times vary depending on the source of infection, most patients die within the first year after showing symptoms as no functional treatments exist and the diseases normally progress rapidly.[1–3] Experimental exposure to human pathological PrP from CJD and Kuru patients led to the development of TSE symptoms in primates, monkeys, cats, mice, hamsters and bank vole.[2]

Interestingly, high susceptibility to TSE development after exposure to pathological PrP is not universal in mammals. Indeed, horses, dogs and pigs with known exposure to human, ovine or bovine pathological PrP did not evolve TSEs, even after direct cerebral injections.[2] Moreover, rabbits, which are classically considered as TSE resistant animals, only developed TSE related symptoms after extensive treatment employing the protein misfolding cyclic amplification technique.[2,5,6] However, the infection rate using non-rabbit derived pathological PrP was extremely low. Nevertheless, inoculating other rabbits with brain homogenate from a symptomatic animal from the first passage led to a 100 % infection rate, indicating the possibility of a rabbit TSE formation.[2,6] In contrast, the bank vole, whose genetic PrP variant is used during the experimental work of this thesis, is considered as an exceptional model organism to study prion diseases. Wild-type bank voles exhibit an almost universal susceptibility to a wide range of both human and other mammalian pathological PrP, thereby overcoming the species barrier. Additionally, TSE development rates of 100 % are recorded regularly for bank voles subjected to infectious material. Equally high infection rates are also reported when using transgenic mice expressing the bank vole PrP homolog instead of their native PrP variant. Furthermore, bank vole PrP also typically maintains the structural properties of the original infective protein variant and can be applied to study genetic and sporadic forms of prion disease.[4]

Overall, resistance and susceptibility to a TSE in different species are attributed to polymorphisms of the PrP encoding gene *PRNP*, the accompanying changes in amino acid composition and protein structure as well as alterations of its post-translational modifications.[1,2,4]

1.1.2 Function and structure of human PrP^C

The human non-pathogenic, or cellular PrP variant PrP^C, encoded by the evolutionarily conserved gene *PRNP* located on chromosome 20, has a mature length of 208 amino acids and is expressed universally within the body.[1,7,8] However, the majority of PrP^C is produced by neurons, where its ultimate destination is the exterior of the cell membrane.[7] Here, it is associated with a wide array of functions, ranging from mitochondrial, myelin and ion homeostatic activities to neuroprotection and development, involvement in the circadian rhythm, cell adhesion as well as cell-to-cell signaling. Still, its exact role is yet to be determined.[1,7]

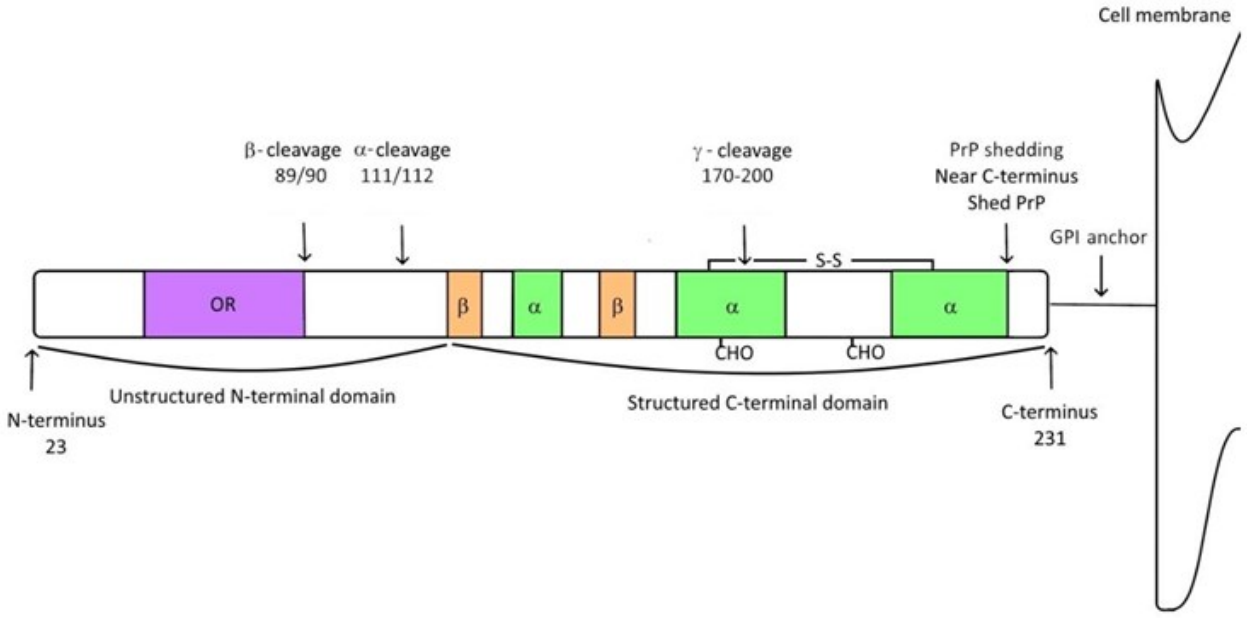

Figure 1: Structural peculiarities of PrP^C. The purple box denotes the octapeptide repeat within the unstructured, N-terminal domain. The green and orange rectangles represent the *α*-helices and *β*-sheets respectively. The *α*-, *β*-, *γ*- and shed PrP cleavage sites are each marked by an arrow. At the C-terminus, the glycosylphosphatidylinositol (GPI) anchor attaching the protein to the cell membrane is indicated. CHO denotes the N-glycosylation sites at asparagine residues 181 and 197. Adapted from Kovač & Šerbec.[7]

Structurally, PrP^C is a monomer and consists of an unorganized N-terminal domain, accommodating distinct octapeptide repeats, and a globular, highly organized C-terminal segment which is comprised of three *α*-helices and two *β*-pleated sheets (**Figure 1**).[7,8] Additionally, four distinct protease cleavage sites can be found along the protein. The *α*-cleavage site is situated in the N-terminal region between amino acids 111 and 112, within a region primarily composed of hydrophobic residues. Next, the *β*-cleavage site is located at the end of the octapeptide repeat containing domain, amid residues 89 and 90, while the *γ*-cleavage site is located within the second *α*-helical domain of the C-terminal region, with its exact position being unknown. However, experimental data suggests a location somewhere between amino acids 170 and 200. Lastly, a protein shedding site is located

proximally to the C-terminal end. While *α*-cleavages, *γ*-cleavages and PrP shedding are solely catalyzed proteolytically, *β*-cleavages primarily occur in the presence of reactive oxygen species.[7] In its native, tertiary protein structure a disulfide bond between the cysteine residues at positions 179 and 214 introduces additional conformational stability.[7,8] As a known glycoprotein, PrP^{C} is also found in varying proteoforms with N-glycans in positions 181 and 197.[7–10] However, PrP^{C} variants completely lacking or with only one glycosylation also exist.[9,10] A glycosylphosphatidylinositol (GPI) anchor, which attaches PrP^{C} to the exterior of the cell membrane, is added to serine residue 231 during post-translational modifications.[7–10] Similarly to the changing N-glycosylation pattern, PrP^{C} lacking the GPI anchor also occurs naturally.[10] Owing to a high diversity in glycan composition, the number of documented PrP^{C} variants exceeds 400 glycoforms. Moreover, each glycan is capable of carrying up to five terminal sialic acids, impacting the respective protein pI or overall net charge of each glycoform at native conditions.[9] These variations in post-translational modifications both positively and negatively impact PrP^{C} protein stability and impede or facilitate the transformation into the misfolded, pathological prion protein form named PrP scrapie (PrP^{Sc}).[8–10]

Similarly to the heterogeneity of PrP^{C} post-translational modifications, the sequence of the PrP^{C} encoding gene *PRNP* also impacts the likelihood of developing a TSE.[10] Mutations connected to hereditary prion diseases are mainly situated within the globular C-terminus and primarily affect the two terminal *α*-helical domains.[11] Insertions modifying the octapeptide repeat region of the unstructured N-terminus with further octapeptide copies are associated with hereditary CJD.[11,12] Moreover, selected sequence variations of *PRNP* found in the general population may promote the generation of sporadic or acquired forms of CJD, with the most prominent being a valine-methionine polymorphism at position 129. Here, general homozygosity is more likely to support TSE development.[11,13,14] In contrast, a glutamic acid-lysine polymorphism at position 219 native to Japan is suggested to exhibit protective characteristics against sporadic CJD in heterozygous individuals.[11,15] A similar heterozygous resistance polymorphism, in this instance involving glycine and valine at position 127, is reported for several individuals from areas previously afflicted with Kuru. Here, experiments in mice already showed that, in addition to Kuru, this polymorphism also prevents infection by CJD prion variants.[11,16]

1.1.3 The PrP^C to PrP^{Sc} conversion

Up to now, the exact conversion mechanism from PrP^C into the disease-causing PrP^{Sc} variant has not been completely elucidated. Nevertheless, it is indicated that the transformation occurs in a template-directed fashion (**Figure 2**).[1,10,17]

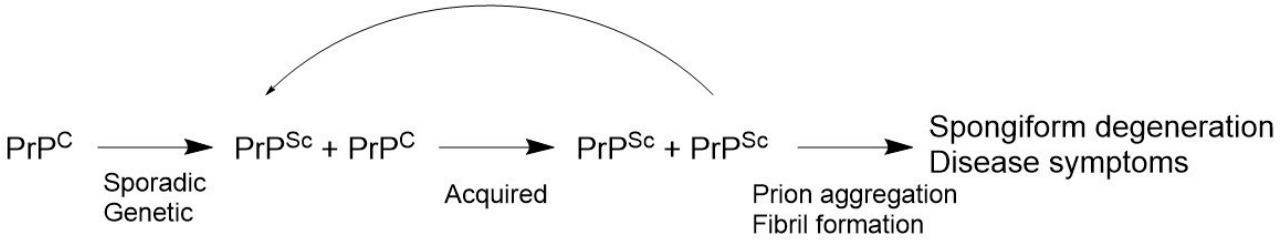

Figure 2: The TSE conversion mechanism: After acquiring PrP^{Sc} through sporadic or genetic misfolding or due to environmental exposure, it promotes subsequent misfolding of PrP^C to PrP^{Sc} with itself serving as a template in the process. After sufficient conversion cycles, PrP^{Sc} aggregates and forms fibrils, ultimately leading to spongiform cerebral degeneration and TSE symptoms.

Only differing in their three-dimensional structure, PrP^{Sc} presumably promotes the sequential unfolding of PrP^C into a denatured, primary state, followed by a subsequent refolding into the PrP^{Sc} tertiary structure, with the sporadically formed, genetically predisposed or externally acquired PrP^{Sc} serving as a blueprint in the process.[18] During remodeling, PrP^C loses its main *α*-helical structures, which are instead transformed into *β*-pleated sheets, ultimately leading to a *β*-solenoid protein conformation.[8,18] Thus, each refolded PrP^{Sc} monomer is structurally composed of four distinct rings arranged vertically, with a distance of 4.8 Å in between each level, giving the *β*-solenoid a total height of 19.2 Å. It is hypothesized that the *β*-strands at the top and bottom of each solenoid ultimately act as templates for the PrP^C to PrP^{Sc} conversion mechanism when encountering PrP^C in its primary state. After templating the formation of the first ringed *β*-solenoid level, the newly reconstructed *β*-strands then promote the sequential refolding of the remaining parts of the protein, finally generating a novel PrP^{Sc} molecule. The main intermolecular interactions involved are hydrogen bonds, electrostatic forces and π-π stacking, with steric effects also impacting the process.[18] Following their reconstruction, the newly converted PrP^{Sc} *β*-solenoids then tend to aggregate into quaternary structures called amyloids or fibrils.[10,11,18] Their spontaneous fragmentation accelerates further infection as each fragment serves as a potential nucleus for the PrP^C to PrP^{Sc} conversion. Finally, a TSE breaks out due to the damages caused by PrP^{Sc} amyloid fibril accumulation in neuronal tissue, resulting in cell death and spongiform degeneration.[1,10,11]

PrP keeps all post-translationally acquired glycan modifications during the whole structural reformation process.[9,17] Their individual charges as well as steric hindrances hence lead to

different prion strains, which have an impact on the types of fibrils formed due to their varying interstrain compatibility.[9,17,18] It is suggested that the aggregate amyloid structure is the main differentiator of which type of TSE evolves.[9,17] Additionally, a higher amount of PrP^{C} is correlated with a faster conversion into and accumulation of PrP^{Sc} and, thus, a more rapid advance of disease. Correspondingly, a mutation in the *PRNP* gene or the lack of endogenous PrP^{C} significantly decelerate or completely prevent the outbreak of disease respectively.[10] Interestingly, unlike PrP^{C}, PrP^{Sc} is largely resistant against proteases and insoluble, indicating increased stability and reinforcing the impact of protein folding on its biochemical properties.[10,19] However, these properties are primarily associated with PrP^{Sc} in its aggregated state.[19]

To be able to investigate the influence of individual glycan modifications on the conversion into and subsequent aggregation of PrP^{Sc} the homogenous generation of the respective PrP glycoform must be ensured. In the following chapters two distinct but compatible approaches, namely genetic code expansion and protein semi-synthesis, are explored.

1.2 Genetic code expansion

1.2.1 Natural background

The genetic code is the basis for the translation of the information encoded by the genome. Following transcription, which produces the required mRNA template, a ribosome generates the corresponding polypeptide chain according to the codon sequence of the mRNA. Thereby each codon, consisting of a set of three nucleotides, is recognized by a particular tRNA carrying a defined amino acid. Of the 64 possible codon triplet combinations, 61 code for one of the 20 canonical amino acids. The remaining three, namely TAG, TAA and TGA, also commonly known as amber, ochre and opal respectively, do not correspond to any amino acid. Instead, they solely act as termination signals and allow the binding of proteins called release factors that lead to the release of the polypeptide chain from the ribosome, thus concluding biosynthetic protein production.[20,21] However, the biochemical needs of various organisms across the domains of life exceed the number of functionalities provided by the canonical set of amino acids. Therefore, many organisms enzymatically adapt proteins post-translationally to acquire the necessary modifications.[22] In addition, various species evolutionarily adapted their genetic code to incorporate a non-canonical amino acid (ncAA) during translation when encountering a stop codon to achieve additional functional diversification through so called stop codon suppression, also known as genetic code expansion (GCE). Prominent examples of ncAAs naturally incorporated this way are

selenocysteine and pyrrolysine.[20–22] Stop codon suppression requires an additional tRNA identifying and binding to the reassigned triplet. Additionally, as is the case for most tRNAs, a matching aminoacyl-tRNA synthetase (aaRS) is also needed, which enzymatically binds an amino acid to its cognate tRNA through aminoacylation.[20,21] However, a notable exception to this rule is selenocysteine, whose biosynthesis occurs while already bound to its tRNA. Thereby the tRNA is first aminoacylated with serine which is subsequently converted enzymatically into selenocysteine prior to use in translation.[23]

1.2.2 Biotechnological application

To biotechnologically exploit the naturally occurring process of GCE, an orthogonal aaRS and tRNA pair that does not cross-react with the endogenous translational machinery is required. Thereby exclusively the ncAA, which is not naturally utilized by the species used for expression, is incorporated site-specifically into a growing polypeptide chain instead of a stop codon, which is reassigned in the process (**Figure 3**).[20,21]

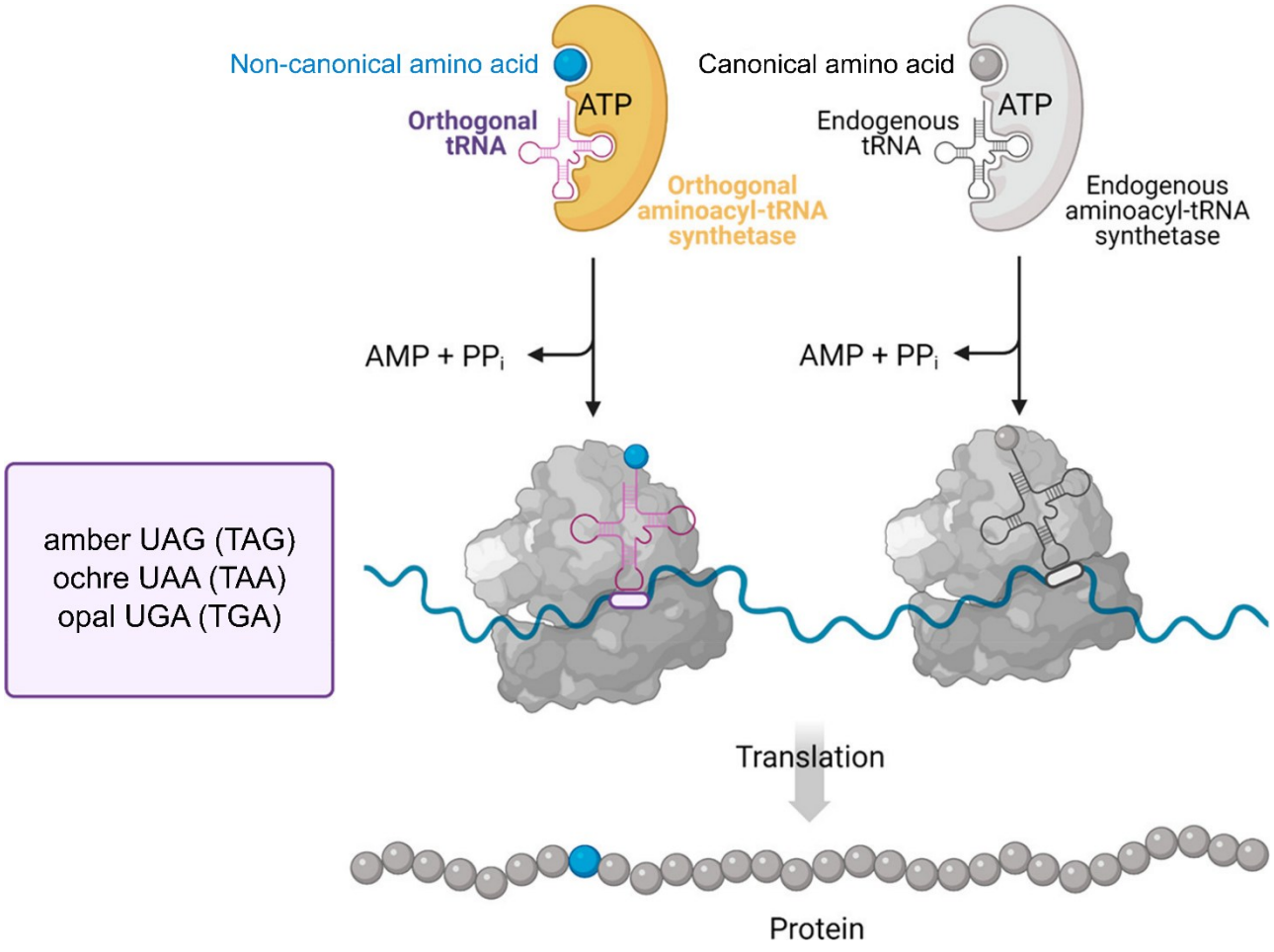

Figure 3: Translational process using a ncAA and canonical amino acid respectively. The pink rectangle denotes the stop codons available for GCE with their respective mRNA and DNA triplet code (in brackets). Adapted from Shandell *et al.*[24]

In most cases, a pair from an evolutionary distant species is introduced into the organism of interest as phylogenetic distance ensures that the interferences of the host with the newly added orthogonal pair are minimized.[20,25] The most heavily used stop codon suppression systems are derived from archaea such as *Methanococcus jannaschii* and *Methanosarcina mazei*. They provide a tRNA and aaRS combination that naturally supports incorporation of tyrosine or pyrrolysine instead of an amber stop codon.[20–22] Their amber codon suppression pairs have been successfully introduced into several organisms that allow efficient recombinant protein expression.[20,21] Nevertheless, *Escherichia coli* is the predominant species used for GCE and the accompanying protein production. *E. coli* is a naturally advantageous species for GCE as its genome is easily manipulated and only contains 314 genes ending with an amber codon, equating to a genome wide termination frequency of approximately 7 %.[21,26,27] Thus *E. coli* is highly suitable for amber codon suppression. Moreover, in selected strains as few as 7 of these genes are essential for the organism, and all of them encode an additional ochre or opal stop codon later in the sequence allowing to perform amber codon suppression without significant repercussions for the cell.[21] In addition to simply transferring an evolutionary distant aaRS and tRNA combination into *E. coli* or any other expression system, the pair used also may undergo further artificial evolutionary optimization to deter possible translational interferences within the host.[21,25] Moreover, the specific recognition of the aaRS with the ncAA of choice and its loading onto the cognate tRNA must be acquired through either rational changes or directed evolution approaches to change the aaRS binding pocket. Directed evolution generates orthogonality and ncAA specificity through repeated rounds of mutant selection, both positive and negative, and must be conducted in concert for both the aaRS and its cognate tRNA to maintain mutual interaction and ensure consistent orthogonality to the host.[20,21,25]

On a side note, it is also possible to incorporate ncAAs using an endogenous aaRS and tRNA if the structure of the ncAA of choice is similar to a canonical amino acid.[22,25] However, in such cases the expression organism must be auxotrophic for the native amino acid and the expression media must be depleted of this amino acid to prevent a mixed incorporation.[22] Moreover, as the native amino acid is replaced throughout the proteome, negative effect on structure and function of endogenous proteins, have to be evaluated.[25]

1.2.3 Sample applications and technical limitations

Site-selective insertion of new chemical functionalities into a protein of interest (POI) *via* GCE enables a large variety of new applications. NcAAs bearing fluorescent dyes are used to monitor protein synthesis, localization, trafficking, function, intermolecular interactions,

structure formation and disassembly, as well as responses to environmental conditions. Fluorophores can also be attached using biorthogonal conjugation chemistries, allowing the application of a larger variety of fluorescent molecules when compared to direct incorporation of fluorescent ncAAs. Furthermore, incorporation of ncAAs with reactive handles enables the post-translational attachment of affinity tags or protein-protein interaction studies by generating cross-links between the partaking entities.[28] Another application is caging of specific residues, which allows to control protein activity in space and time. Here, protected sidechain groups included in ncAAs at key sites disable their natural function and are released either chemically or *via* irradiation.[28–30] GCE also enables the generation of post-translationally modified proteins and thus allows to investigate the impact of these modifications on protein function. To obtain post-translationally modified proteins, both already modified ncAAs as well as ncAAs with conjugation handles are applied. Similarly, the active sites of enzymes can also be site-specifically altered to study but also to expand or optimize their functionalities and mechanisms. For various types of spectroscopies, isotope or probe-containing ncAAs facilitate studying structure and dynamics of POIs.[28]

The biotechnological applicability and overall efficiency of GCE depends on several factors: Firstly, the prokaryotic release factors RF1 and RF2, recruited by the amber and ochre as well as opal and ochre stop codons respectively, are always in competition with the orthogonal tRNA during translational termination. Thus, the POI containing the ncAA is generated with varying efficiency, due to early termination and the generation of a truncated form. For amber codon suppression this problem can be addressed by disabling the gene encoding RF1. However, depending on the *E. coli* strain used, this may lead to cytotoxic effects by direct effects of the missing RF1 and its connection to the vital genes mentioned above.[20,21,25] Therefore, additional measures like co-transformation of these genes in concert with the orthogonal tRNA are required.[21] Alternatively, whole genome replacements of TAG with ochre stop codons or selectively mutating the ribosome to prevent interaction also introduce RF1 redundancy and can be performed in parallel to a RF1 genomic knock-out.[20,21,25]

Another limitation is that the boundaries of the classical genetic code confine the number of simultaneously applicable ncAAs. For example, when performing amber codon suppression only one kind of ncAA can be incorporated.[20–22] Consequently, each additional ncAA used necessitates another reassigned codon with its unique aaRS and tRNA combination that must not interfere with the endogenous system and other orthogonal pairs, which is again

limited by the number of codons that can be suppressed.[20,22,25] Here, several solutions have been explored. For instance, whole genome mutational exchange of a sense codon with an analogue coding for the same amino acid and subsequent removal of the tRNA of the original codon enables the orthogonal reassignment of the selected codon.[20,25] Nonetheless, as each sense codon variant carries intrinsic properties beyond coding for an amino acid, only a few codons are considered viable for replacement.[20] Similarly, artificial codons consisting of four or five nucleotides can be assigned freely to an orthogonal set of aaRS and tRNA. However, the faithful implementation of this approach is mostly based on the generation of a mutated ribosome as the natural variant may exhibit difficulties in interacting with tRNAs accommodating elongated anticodons. Additionally, the forced translation of a quadruplet based genetic code by a native ribosome may lead to unwanted frameshifts and this leads to nonsense polypeptides, which can be associated with toxic effects. Lastly, not all ncAAs are applicable in the context of the native ribosomal environment. Apart from natural and structurally similar, non-canonical *α*-L amino acids, which are readily incorporated by endogenous ribosomes during bond formation, only a selected few amino acids of other types, such as *α*-D and *β*-amino acids, have been integrated this way. Consequently, their efficient incorporation requires mutations in the ribosome to facilitate interactions. These modifications lead to structural changes of the ribosomal subunits and introduce orthogonality against natural and affinity for orthogonal mRNAs containing the ncAA of interest. Cross-reaction between the orthogonal and native entities ought to be avoided due to their incompatibility that can impact translation and subsequently leads to toxic effects.[20,25]

Another approach to site-specifically incorporate ncAAs into a POI is protein semi-synthesis, which is covered in the next chapter.

1.3 Protein semi-synthesis

The generation of flexibly modified protein analogues is of vital importance for functional investigation, deciphering interaction networks and developing novel therapeutics. However, solely relying on chemical or biological synthesis severely limits the range of accessible protein variants.[31–33] Chemical means offer precise polypeptide synthesis through techniques such as solid phase peptide synthesis (SPPS), which enables the inclusion of post-translational modifications or other alterations to sidechains as well as to the protein backbone during synthesis itself.[32–34] However, chemical synthesis by SPPS is limited by incomplete coupling reactions, accumulation of closely related byproducts and losses during purification.[34] Due to this, an average peptide length of approximately 50 residues can be achieved in routine syntheses.[32–34] In contrast, recombinant production generates proteins

without size constraints but is instead restricted by the genetic code if any non-encoded chemical functionalities within the product are desired.[32,33,35] Thus, combining both protein synthesis methods allows to semi-synthetically produce POIs without functional or structural limitations through the ligation of separately manufactured fragments.[32,33,36]

1.3.1 Native chemical ligation

To overcome the size limit of SPPS condensation of protected peptide segments was applied for decades with limited success. Only with the introduction of a robust chemoselective ligation approach for unprotected peptides polypeptides with more than 100 amino acids became routinely accessible. This development was mainly driven by native chemical ligation (NCL). This reaction was introduced by the Kent lab in 1994 and has become the most successful ligation reaction for accessing synthetic protein synthesis.[33–35] The method requires at least two peptides assembled *via* SPPS, one carrying an *α*-thioester at its C-terminus and the other one bearing a cysteine at its N-terminus.[32–35] Nevertheless, each additional ligation step decreases the final yield and products exceeding a length of 200 residues are considered laborious and difficult to produce.[32,35,36]

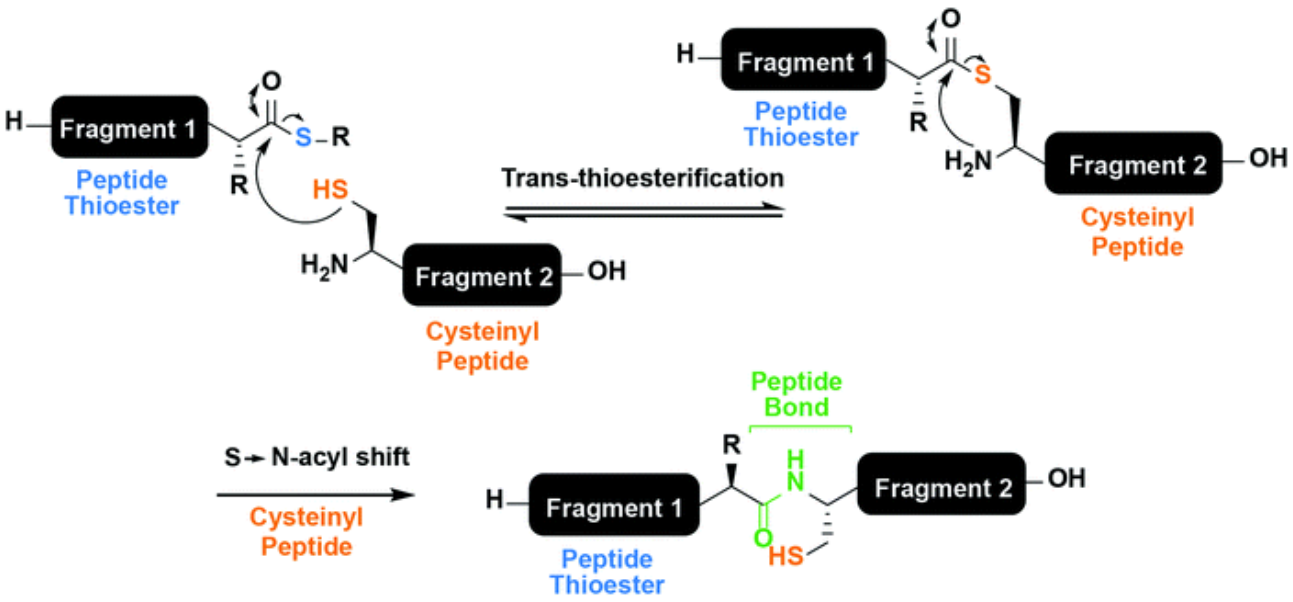

Figure 4: Schematic depiction of the NCL reaction mechanism.[35]

Mechanistically (**Figure 4**), NCL first encompasses a trans-thioesterification initiated by a nucleophilic attack of the C-terminal thioester carbonyl by the cysteine thiol group. Followed by rapid S → N intramolecular rearrangement of the intermediate between the cysteinyl *α*-amine and the carbonyl of the newly formed trans-thioester, a natural peptide bond conjugating the initial fragments is established.[33–35] The reaction kinetics are highly reliant on the nucleophilicity of the partaking cysteine as well as the immediate chemical

environment of the *α*-thioester, with the trans-thioesterification ultimately determining the reaction rate.[33] However, the rare natural abundance of cysteines in polypeptides restricts the functional applicability of this method. Thus, the development of desulfurization chemistries to convert cysteine residues into alanine, which is approximately five times more abundant in proteins, post ligation drastically increased its applicability.[34,35,37] This approach has been expanded to 14 additional site-specifically thiolated canonical residues, greatly facilitating the generation of suitable ligation sites.[35,37,38] However, one has to take into account that desulfurization usually not only affects the thiols required for NCL, but also any other cysteine residue present in the protein sequences if left unprotected.[33,37]

Another noteworthy expansion of the NCL methodology relies on the application of selenium instead of sulfur-based chemistry. Here, the exchange of the native cysteine with its selenium containing cognate, selenocysteine, enhances the nucleophilic property of the N-terminally functionalized peptide during NCL. Furthermore, it addresses the previously mentioned kinetic limitations posed by sterically challenged or electron rich C-terminal *α*-thioesters, which may drastically impact the overall reaction progression, *via* the use of acyl selenoesters.[33,35,37,39] Their increased reactivity has been attributed to the improved capability of selenolate as a leaving group compared to the classical thiolate during trans-selenoesterification.[33,37,39] The available selenium-based ligation techniques were further evolved by the use of selenocystine. During diselenide-selenoester ligation (DSL) selenocystine, which is a quite stable diselenide, is used instead of its reduced counterpart in concert with a C-terminal selenoester. Thereby even kinetically disfavored ligation reactions reach completion at room temperature without any additives within minutes compared to thiol-based NCL reactions.[35,37] Additionally, DSL is applicable within a pH range of three to seven.[37] If a non-selenium containing product is desired, a final deselenization step, which can be performed without affecting any unmasked cysteines within the product, is conducted after the ligation.[33,35,37,39] Thus, the final protein contains an alanine at the ligation site. Moreover, the alternative application of an oxidative deselenization protocol allows the generation of a serine residue if desired.[35,37,39] Any dimerized entities formed during the reaction are also removed during these processes.[37] Similarly to NCL, DSL also permits the use of non-canonical residues functionalized with a suitably placed selenol moiety.[35,37]

Two notable alternatives to NCL are ketoacid-hydroxylamine ligation and serine/threonine ligation. Both methods also generate a native amide bond at the ligation junction *via* a traceless, chemoselective reaction. However, unlike NCL, they do not require a cysteine

residue within the sequence. Instead, homoserine or serine/threonine are generated at the ligation junction respectively.[31,39]

1.3.2 Expressed protein ligation

Despite the functional advances provided by NCL and its technical extensions, its range is still constrained in routine applications by its practical size limitation to approximately 200 residues.[32,35,36] To address this issue, expressed protein ligation (EPL) was established in 1998 by Muir and collaborators. Classical EPL combines the advantages of the NCL technique with the recombinant production of the *α*-thioester protein segment, thus enabling the semi-synthetic assembly of functionalized proteins without comprises regarding their final length.[32,33,35,36,40] Similar to NCL, EPL is generally conducted in aqueous, neutral conditions at room temperature, with the reaction durations ranging from one to three days.[35,36] The generation of the thioester segment relies on a natural protein processing step termed protein splicing. Ubiquitous among the domains of life and also observed in various viruses, protein splicing encompasses the autocatalytic excision of a peptide segment from a biosynthetic polypeptide, the so-called intein. Ligation of the flanking polypeptides domains, named exteins, then affords the protein splicing product.[32,33,35,36] Two of the most prominent examples of inteins used in protein semi-synthesis are *Sce* VMA and *Mxe* GyrA. *Sce* VMA originates from the species *Saccharomyces cerevisiae*, more specifically its vacuolar ATPase, and was used in a mutated version which cannot undergo autosplicing during the foundational EPL experiments.[33,36] *Mxe* GyrA instead stems from the species *Mycobacterium xenopi* and was derived from its DNA gyrase A. Also applied in an altered state, *Mxe* GyrA has emerged as the intein of choice for most *α*-thioester fragment productions due to its early discovery and biotechnological availability, as well as comparatively short length and its ability to undergo splicing in a fairly chaotropic environment of up to 4 M of urea.[33,35,36] Furthermore, following unfolding it also tends to refold correctly on its own, facilitating the recombinant generation of protein fragments that tend aggregate and fall out of solution.[33,36]

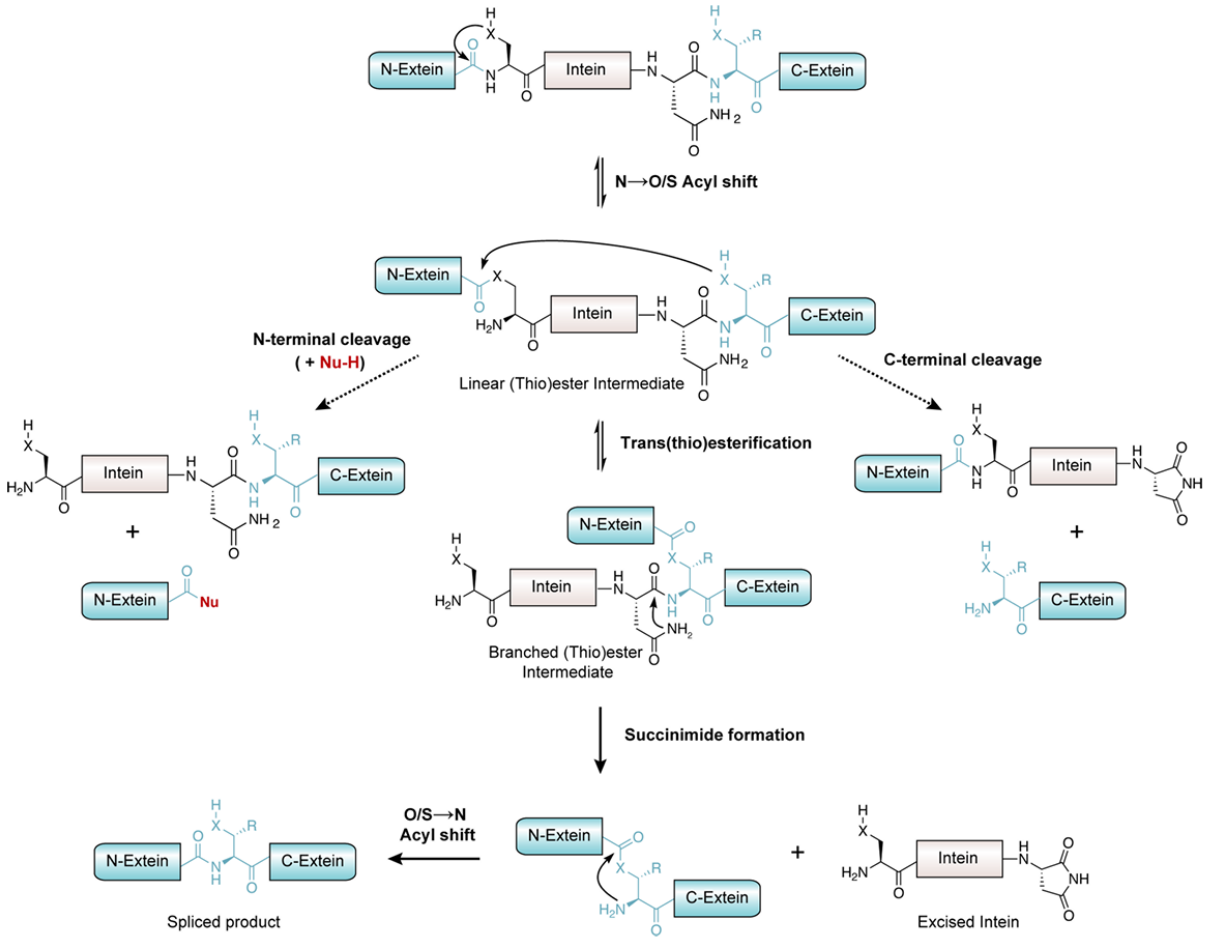

Figure 5: Schematic depiction of the protein splicing mechanism including N- and C-terminal cleavage sideproducts. The X either represents an oxygen or sulfur atom from a corresponding serine, threonine or cysteine residue.[33]

From a mechanistic point of view (**Figure 5**), the N-terminal cysteine or serine functionality of the intein first attacks the neighboring carbonyl following previous catalytic activation, leading to a temporary oxoester/thioester formation. Subsequently, a novel branched intermediate is generated *via* a reversible acyl transfer, connecting the ends of the N- and C- terminal extein fragments through another oxoester/thioester bond. Hereby only cysteine, serine or threonine amino acids are possible target residues. Next, intramolecular rearrangement results in the extrusion of the intein *via* cyclization, thereby creating a succinimide moiety from a conserved asparagine residue at its C-terminus. Lastly, the remaining extein intermediate undergoes an O/S → N acyl shift, producing the native extein-extein splice product.[32,33] Inteins with mutated, non-nucleophilic amino acids at their N-terminus may bypass the initial, linear intermediate formation and generate the second, branched variant instead. Nevertheless, normally this change causes premature asparagine cyclization within the intein, inducing the proteolytic removal of the C-terminal extein fragment.[33] In contrast, the replacement of the asparagine disables succinimide formation and induces N-terminal extein hydrolysis from the activated intermediate, thereby releasing

the N-extein as an acid. Through the supplementation of high amounts of thiols during this process the extein is instead released as an *α*-thioester and repurposed for EPL after purification.[31–33] The thiol-induced cleavage of the intein does not dramatically depend on sequence or structure of either extein, extending the biotechnological applicability. MESNa is usually the thiol reactant of choice for this process due to superior product stability compared to cleavage reactions performed with either *β*-mercaptoethanol or DTT.[31,33] Moreover, hydrazine induced cleavages have also been reported, exhibiting kinetic advantages and even higher chemical stability in the peptide hydrazide formed, which are already applied extensively during NCL. Nonetheless, regardless of their origin, peptide hydrazides need to be transformed chemically into the required thioester prior to ligation.[33,35] On a related note, the traceless cleavage from the intein, and any C-terminal extension, is further harnessed biotechnologically through the appendage of affinity tags, simplifying purification after recombinant production.[31,33,35] Prominent examples are chitin-binding domains (CBD), purified using chitin beads, and histidine-tags (His-tag), exhibiting affinity for metal cations.[31,35,41]

While diverting from the original protein splicing approach to create thioesters, EPL is also performed using recombinantly generated N-terminal cysteinyl peptides, if modifications within the thioester terminating entity are required. Here, protease cleavage sites are introduced within the sequence, enabling site-directed proteolysis and the production of desired protein fragment.[35,36]

The semi-synthetic method applied during this thesis, expressed protein selenoester ligation, emerged out of the influential native chemical ligation and expressed protein ligation techniques.[40]

1.3.3 Expressed protein selenoester ligation

In 2022 Becker, Payne and coworkers extended DSL towards recombinantly produced protein segments and termed this approach expressed protein selenoester ligation (EPSL). It was developed to overcome shortcomings of EPL, such as the need for high reactant concentrations and slow reactions.[40] EPSL therefore combines the functional virtues of DSL with the size augmentation provided by EPL through the use of selenoesters originating from recombinant production and synthetically generated N-terminal selenopeptides. However, unlike EPL based thiolysis methods, phenylselenol induced selenolysis does not generate aryl selenoesters due to solubility and decomposition issues of the selenol reactant under neutral, aqueous conditions.[40]

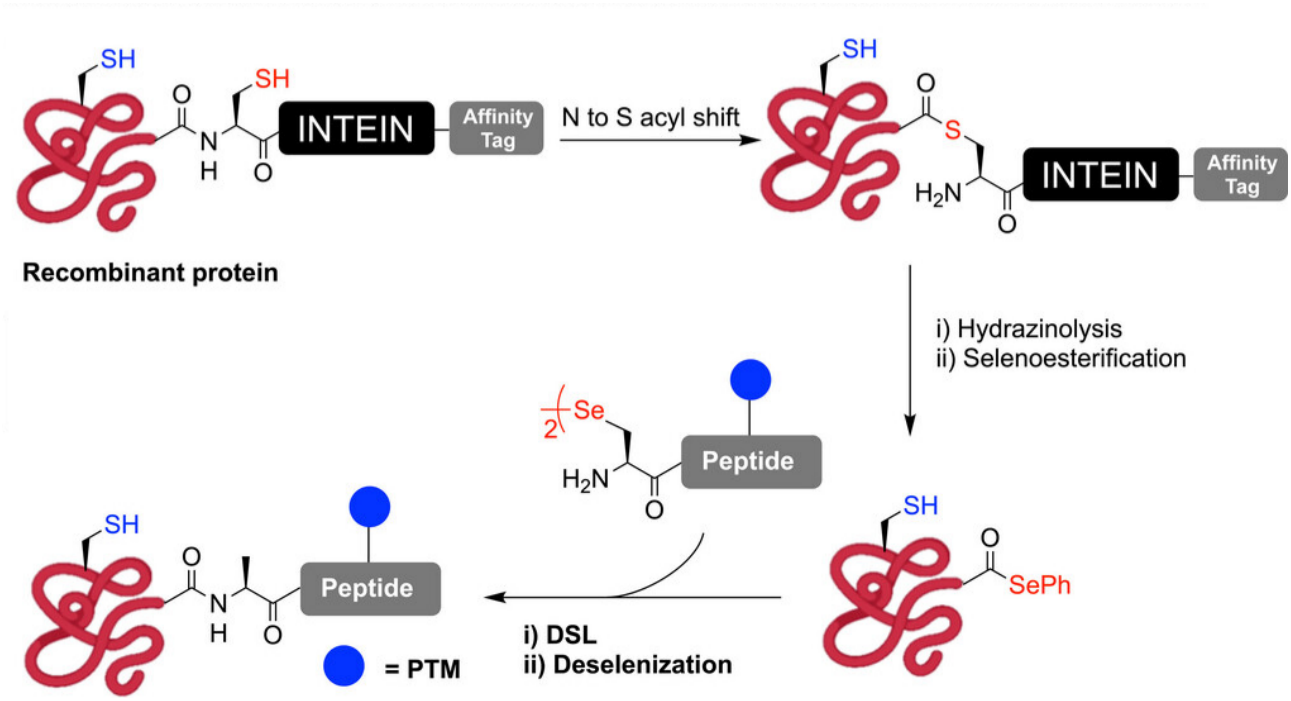

Figure 6: Schematic depiction of the EPSL methodology. Adapted from Becker and Payne *et al*.[40]

Therefore, aryl selenoesters are produced *via* a hydrazide intermediate (**Figure 6**). Following initial hydrazinolysis, the recombinant fragment is thus subjected to selenoesterification using diphenyldiselenide (DPDS) and acetylacetone, achieving selenoester creation through the formation of a Knorr pyrazole intermediate. The final product is then received after performing DSL with the appropriate selenopeptide previously assembled by SPPS. Analogous to DSL, EPSL products can then be subjected to chemoselective deselenization if desired.[40]

2. Aim

The aim of this work is the semi-synthetic generation of two glycan modified variants of the bank vole prion protein bvPrP C-terminally attached to a synthetic GPI mimic. Therefore, the mutants bvPrP-N181X and bvPrP-N197X are first produced as PrP-intein fusion proteins through recombinant expression in *E. coli* using amber codon suppression, introducing the ncAA N-*ε*-((2-azidoethoxy)carbonyl)-L-lysine (AzK) at positions 181 and 197 respectively. Alternatively, N-*ε*-(prop-2-ynyloxycarbonyl)-L-lysine (YnK) is introduced at position 181. Following Ni-NTA purification and hydrazinolysis of the attached intein, the C-terminal protein hydrazides are selenoesterified and ligated to a synthetic GPI-anchor mimic using the EPSL technique. After deselenization and HPLC purification of the semi-synthetic product, glycan mimics are conjugated to the incorporated ncAA within the protein *via* CuAAC reaction to generate the final products.

Further experiments with these ligation products may then be used to study the impact of glycan modifications on bvPrP structure and aggregation tendencies. Moreover, the combination of GCE, EPSL and CuAAC techniques employed during this thesis may provide an alternative access to semi-synthetically modified proteins.

3. Material and Methods

3.1 Reagents

All reagents were acquired commercially unless stated otherwise. In the case of protein expression both commercial and self-made YnK was applied. For the preparation of all aqueous solutions and buffers deionized water (dH_2O) generated by a Milli-Q purification system was used.

3.2 Production of C-terminal PrP hydrazides

3.2.1 Protein expression and harvest

For recombinant expression the *E. coli* strain BL21(DE3) Gold previously transformed with a T7x33 plasmid containing wild-type (WT) and two modified bank vole PrP variants, namely bvPrP-N181X and bvPrP-197X, was used. All three constructs consist of a full length bvPrP segment encompassing amino acids 23-231 followed by a *Mxe* GyrA intein segment with an appended 7x His-tag and a CBD, as shown in **Figure 7**, together with the structures of the AzK and YnK ncAAs.

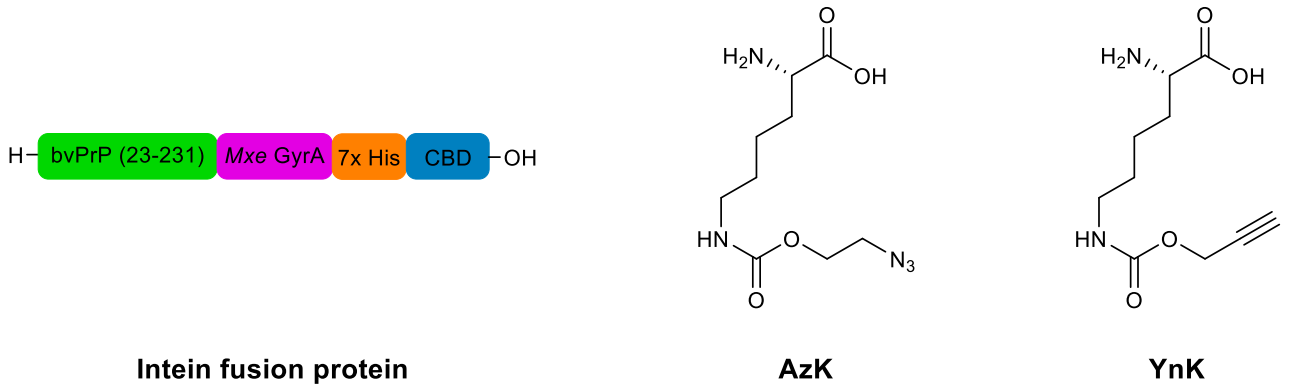

Figure 7: Scheme of the bvPrP fusion protein and the structures of the ncAAs AzK and YnK. The green segment represents the full length bvPrP segment, the pink segment denotes the Mxe GyrA intein, the orange segment the 7x His-tag and the blue segment the CBD.

The T7x33 plasmids originated from the Wiltschi lab and further contain a T7 expression system, which accommodates *Methanosarcina mazei* pyrrolysine specific aaRS and tRNA genes required for amber codon suppression as well as the respective bvPrP fusion constructs, enabling their IPTG inducible gene expression.[42,43]. Additionally, T7x33 also codes for a kanamycin resistance gene.[42] Recombinantly produced PrP tends to deposit in inclusion bodies, allowing purification from the insoluble fraction after cell lysis and purification.[44,45]

Protein expression was initiated by inoculating fresh M9 minimal medium prepared from sterile stock solutions with the relevant *E. coli* strain and incubating the starter culture overnight at 37 °C and 170 rpm. After dilution to an OD_{600} of 0.2 using fresh or recycled medium, the cell culture was reincubated and grown to an OD_{600} value between 0.6 and 0.8. Subsequently, target protein expression was induced *via* the addition of 1 mM of IPTG. At this step the relevant ncAA (AzK or YnK) was also added at a concentration of 5 mM if the protein variants produced through amber codon suppression were generated and fresh medium was used. The cells were left to grow for 4 h (WT) or overnight (AzK,YnK) at 37 °C and 170 rpm, with normalized samples taken for an analytical SDS-PAGE after 0 h, 2 h, 4 h (WT) or 0 h, 2 h as well as the next day (AzK, YnK) following IPTG induction. After centrifugation at 10,000 xg and 10 °C for 30 minutes, the supernatant was decanted and the cells homogenated in approximately 150 mL of TBS buffer using an Ultra Turrax disperser (IKA). The cell suspension was then put on ice and lysed by sonication for 45 minutes using the Ultrasonic Homogenizer 505 (Fisherbrand). Next, the PrP containing inclusion bodies were isolated through centrifugation at 30,000 xg at 10 °C for 30 minutes. Subsequently, the supernatant was discarded and the pellet dissolved through stirring overnight in approximately 30 mL of 6 M GdnHCl (pH=8) at RT. Following centrifugation at 30,000 xg and 10 °C for 30 minutes the supernatant containing recombinant bvPrP was collected, evaluated using LC-MS and stored at 4 °C until further use.

Table 1: Composition of M9 minimal medium (1 L)

Stock solution	Components	Stock concentration	Amount
M9 salts	KH_2PO_4	0.11 M	200 mL
	Na_2HPO_4	0.24 M	
	NaCl	0.04 M	
	NH_4Cl	0.09 M	
$CaCl_2$	$CaCl_2$	0.1 M	1 mL
$MgSO_4$	$MgSO_4$	1 M	1 mL
Trace elements	$FeCl_2 \cdot 4\ H_2O$	8.7 mM	1 mL
	$MnCl_2 \cdot 4\ H_2O$	3.5 mM	
	$CoCl_2 \cdot 6\ H_2O$	1.8 mM	
	$ZnCl_2$	0.4 mM	
	$CuSO_4 \cdot 5\ H_2O$	0.4 mM	
	H_3BO_3	0.5 mM	
Glucose	Glucose	1.1 M	20 mL

Yeast extract	Yeast extract	3 g/L	777 mL
Kanamycin	Kanamycin	30 mg/mL	1 mL

Table 2: TBS buffer (pH=8) components and their concentration

Component	Concentration
Tris	50 mM
NaCl	150 mM

3.2.2 Ni-NTA affinity purification

Nickel-nitrilotriacetic acid (Ni-NTA) affinity purification methodology exploits the tendency of proteins with domains consisting of multiple uninterrupted histidine residues, so called His-tags, to bind to metal cations. For this method nickel cations are bound to a matrix *via* a nitrilotriacetic acid ligand. Their immobilization allows the directed isolation of a recombinantly produced POI with an appended His-tag from the cell lysate.[41]

Ni-NTA purification was conducted using 15 mL plastic syringes with an internal plastic filter and a vertical rotator for their placement during extended incubation periods. First, fresh Ni-NTA beads were transferred to a new 15 mL syringe and washed twice with dH_2O, followed by their equilibration in a 6 M GdnHCl (pH=8) solution for approximately 1 hour. Then the beads were incubated with the 6 M GdnHCl bvPrP solution for 15 to 60 minutes followed by flow-through removal. This step was conducted repeatedly if more than 15 mL of solution was purified at a time. After washing the beads with fresh 6 M GdnHCl for 15 minutes the POI was then eluted using a 6 M GdnHCl solution supplemented with 500 mM of imidazole (pH=8) after an incubation period of 15 to 60 minutes. Twice a second washing step using 6 M GdnHCl containing either 20 mM or 40 mM of imidazole (pH=8) was also conducted prior to elution to remove impurities. The beads were then washed with dH2O for 15 minutes and stored in 20 % ethanol at 4 °C. The beads were regenerated before the next use by dH_2O washing and incubation in a stripping buffer for 5 minutes. Following a 5-minute dH_2O wash the beads were incubated in 0.1 M of NaOH for 5 minutes. After another 5-minute dH_2O wash the beads were submerged in a 0.1 M $NiSO_4$ solution for 5 minutes. Next, a 5-minute dH_2O was conducted and the beads equilibrated in 6 M GdnHCl (pH=8) for 5 minutes prior to the addition of the 6 M GdnHCl protein solution and the conductance of the subsequent steps mentioned above.

Samples were taken from each flow-through, wash, imidazole wash and eluate solution for analytical SDS-PAGE evaluation.

Table 3: Stripping buffer (pH=7.4) components and their concentration

Component	Concentration
NaPi	20 mM
NaCl	0.5 M
EDTA	50 mM

3.2.3 Intein hydrazinolysis

To generate the bvPrP hydrazide fragment from the intein fusion protein a cleavage reaction was conducted. First, the purified 6 M GdnHCl protein solution was concentrated to a multiple of 2.5 mL (approximately from 30 mL to 10 mL) *via* centrifugation at 3,000 xg and RT using 30 kDa Amicon centrifugal filters (Merck Millipore) previously washed with dH_2O. Then a buffer exchange to 8 M urea was performed with a PD10 desalting column (Cytiva). Here, the PD10 column was extended with a plastic funnel and washed with dH2O. Following subsequent equilibration with a neutralized 8 M urea solution, 2.5 mL of concentrated bvPrP solution were transferred to the column. After its complete diffusion 3.5 mL of neutralized 8 M urea were added to the column and the resulting flow-through was collected. If more than 2.5 mL of sample solution underwent buffer exchange, the two previous steps were repeated after performing an 8 M urea wash step. Subsequently, the generated 8 M urea protein solution was combined 1:1 with the cleavage solution, which was added dropwise, and stirred overnight at RT. Following cleavage, the product was isolated *via* RP-HPLC and dried through lyophilization. The used PD10 column was washed with dH2O, supplemented with 20 % ethanol and stored at RT until reuse.

During this process samples were taken for an analytical SDS-PAGE before and after the addition of the cleavage solution. Additionally, an LC-MS analysis of the product following hydrazinolysis as well as lyophilization was also conducted. The lyophilized product was evaluated by MS and additional HRMS analysis for non-WT samples. When performing a test cleavage SDS-PAGE and LC-MS samples were taken after 0 h, 3 h and the next day after the addition of the cleavage solution.

Table 4: Protein samples and the respective cleavage solutions with compositions, concentrations and pH prior to 1:1 dilution

Fusion protein	Component	Concentration	pH
bvPrP-WT	DTT	100 mM in TBS	Not adjusted
	Hydrazine	4 % in TBS	
	DTT	200 mM in TBS	neutralized
	Hydrazine	4 % in TBS	
bvPrP-N197X-AzK	DTT	200 mM in TBS	neutralized
	Hydrazine	4 % in TBS	
bvPrP-N181X-AzK	DTT	100 mM / 200 mM in TBS	neutralized
	Hydrazine	4 % in TBS	
bvPrP-N181X-YnK	DTT	100 mM in TBS	neutralized
	Hydrazine	4 % in TBS	

3.3 Expressed protein selenoester ligation of bvPrP-WT

All EPSL reactions were conducted according to an adapted internal protocol and utilized provided reactants previously produced and synthesized in our laboratory.

To C-terminally ligate the GPI-anchor to the bvPrP-WT hydrazide, 3.4 mg (0.148 µmol, 1 mM) of bvPrP-WT hydrazide were transferred to a 1.5 mL Eppendorf tube and dissolved in 150 µL of sonicated and degassed conversion buffer. Afterwards the solution was brought to a pH between 1.5 and 2, 20 equiv. of acetylacetone were added and the mixture incubated at RT for approximately 1 h. Subsequently, 2 equiv. (1.9 mg, 0.296 µmol) of GPI-diselenide were dissolved in 300 µL sonicated and degassed DSL buffer and introduced to the reaction solution. Following pH adjustment to 3-4, the solution was incubated at RT for 1-2 h. The reaction mixture was then repeatedly extracted with 450 µL hexane to remove excess DPDS by inverting the Eppendorf tube after hexane addition and subsequent centrifugation at 14,000 rpm and RT for 1 minute. Residual hexane was evaporated *via* argon flux. Subsequently, 450 µL of sonicated and degassed deselenization buffer were added to the reaction mix and the pH-adjusted to 7-7.5, followed by incubation a RT and LC-MS monitoring. After reaching complete deselenization, the product was purified through RP-HPLC and lyophilized, followed by DI-MS evaluation. If the deselenization reaction was conducted on the next day, the reaction mixture was flash-frozen in liquid nitrogen and stored at -20 °C.

Additionally, a test ligation of bvPrP-WT to ubiquitin 46-76 was also performed. Here, 1.5 equiv. ubiquitin 46-76 (0.8 mg, 0.222 µmol) were dissolved in 300 µL sonicated and degassed DSL buffer and added to the reaction. Furthermore, all reactions were conducted at 900 rpm. All other steps were conducted likewise.

Each reaction step was accompanied by LC-MS monitoring. Moreover, samples were taken for analytical SDS-PAGE before advancing to the next reaction step. For the ubiquitin ligation and the final GPI ligation analytical HPLC was also conducted.

Table 5: EPSL buffer compositions and concentrations

Buffer	Component	Concentration
Conversion buffer	GdnHCl	6 M
	HEPES	200 mM
	TCEP	100 mM
	DPDS	50 mM
DSL buffer	GdnHCl	6 M
	HEPES	200 mM
	DPDS	5 mM
Deselenization buffer	GdnHCl	6 M
	HEPES	200 mM
	TCEP	200 mM
	DTT	25 mM

3.4 Copper catalyzed azide alkyne cycloaddition

The copper catalyzed azide alkyne cycloaddition (CuAAC) reaction is an expansion of the Huisgen 1,3-dipolar cycloaddition, which encompasses the cyclization of azide and alkyne containing reagents at high temperatures, leading to triazole formation. CuAAC instead enables the reaction *via* the application of a copper(I)-cation catalyst, affording increased reaction kinetics, regioselectivity and good yields at mild conditions like ambient temperatures.[46,47] Here, CuAAC was employed to conjugate a functionalized fluorophore or mannose glycan to the bvPrP-N181X protein produced through amber codon suppression. The reaction was performed according to an internal protocol, which was continuously adapted during the mannose conjugation process as described in chapter 3.4.2.

3.4.1 NcAA integrity verification

To verify the integrity of the azide or alkyne handle of either the AzK or YnK ncAA within the modified bvPrP-N181X protein, CuAAC with a Fluor 488 alkyne or azide fluorophore was conducted respectively. This reaction was performed twice for bvPrP-N181X-AzK and once for bvPrP-N181X-YnK.

Firstly, the $CuSO_4$, TBTA and sodium ascorbate stock solutions were prepared and degassed thoroughly. Subsequently, 4.8 µL of $CuSO_4$, 10.4 µL of TBTA and 3.2 µL of sodium ascorbate solution per catalyzed reaction were combined into a pre-mix and degassed for 10 additional minutes. For bvPrP-N181X-AzK 0.1 mg (4.3 nmol, 1st reaction) or 0.05 mg (2.2 nmol, 2nd reaction) of lyophilized hydrazide sample were transferred into a 1.5 mL Eppendorf tube and dissolved in 20 µL 6 M GdnHCl (pH=8). Afterwards 2 µL of Fluor 488 alkyne solution were supplemented. If evaluating an uncleaved sample, 20 µL of uncleaved protein in 6 M GdnHCl solution (pH=8) were used directly and likewise supplemented with the fluorophore solution. Then 18.4 µL of the pre-mix were added and the samples incubated at RT in darkness for 45-60 minutes. Samples lacking the catalyzing pre-mix served as negative control. Subsequently, all samples were precipitated (see 3.6.1), and an SDS-PAGE was performed for evaluation.

Similarly, 0.1 mg of lyophilized bvPrP-N181X-YnK hydrazide (4.3 nmol) sample was dissolved in 50 µL 6 M GdnHCl (pH=8). Afterwards, 20 µL were transferred to a new Eppendorf tube and supplemented with 2 µL Fluor 488 azide solution. 20 µL of uncleaved 6 M GdnHCl solution (pH=8) protein solution were supplemented likewise. Subsequently, each reaction was started by the addition of 18.4 µL of degassed pre-mix and treated as mentioned above. Again, samples without the catalyzing pre-mix served as negative control.

Table 6: CuAAC stock solutions and their concentrations

Stock solution	Concentration
$CuSO_4 \cdot 5\ H_2O$	200 mM
TBTA (in DMF)	100 mM
Sodium ascorbate	500 mM
Fluor 488 alkyne	20 mM
Fluor 488 azide	21 mM

3.4.2 Glycan conjugation reaction

To functionalize the bvPrP-N181X-YnK hydrazide at position 181 with a glycan, CuAAC was performed with 2,3,4,6-tetra-O-acetyl-*α*-D-mannopyranosyl azide (azidomannose). The reaction was conducted a total of five times with varying reagent amounts, equivalents and solvent conditions, as depicted in **Table 7**.

For each reaction, the relevant mass of bvPrP-N181X-YnK hydrazide was transferred to a 1.5 mL Eppendorf tube, dissolved in dH_2O (#1,4) or 75 % DMF (#2,3,5) and combined with the relevant azidomannose aliquot, previously prepared in 75 % (#2-5) or 100 % DMF (#1). Simultaneously, a catalytic pre-mix (dH_2O: #4,5; 57 % DMF: #1; 75 % DMF: #2,3) with respective equiv. was assembled from degassed stock solutions and degassed for 10 additional minutes. The reaction was initiated by the addition of the pre-mix, and incubated at RT for up to 4 h 30 minutes, and sampled hourly for LC-MS. Moreover, reactions #3-#5 were incubated in shakers. Reaction #3 was restarted the next day with fresh pre-mix and 50 additional equiv. of azidomannose. Moreover, 9 equiv. of sodium ascorbate were freshly added to reaction #5 after 3 h. All reactions were analyzed with SDS-PAGE and for reactions #2-5 analytical HPLC was also conducted. In addition, for reaction #5 the remaining solution (~17 µL) was combined with 50 µL 50 % ACN and the remaining undissolved precipitate treated with 50 µL dH2O, DMF, 1M HCl and 6 M GdnHCl (pH=8) in this order, with each supernatant evaluated using analytical HPLC.

Table 7: Respective CuAAC reaction reagent amounts, equivalents and solvent conditions.* denotes where the same equiv. of CuSO4, THPTA and sodium ascorbate as well as 51 equiv. azidomannose were added the next day.° denotes where 9 equiv. were additionally added after 3 h.

#	bvPrP-N181X-YnK hydrazide	Azidomannose	$CuSO_4$	TBTA	THPTA	Sodium ascorbate	Solvent
1	0.25 mg	51 equiv.	444 equiv.	481 equiv.	-	740 equiv.	31 % DMF
2	0.25 mg	12 equiv.	222 equiv.	240 equiv.	-	370 equiv.	75 % DMF
3	0.25 mg	10 equiv.*	11 equiv.*	-	12 equiv.*	19 equiv.*	75/58 % DMF
4	0.25 mg	51 equiv.	22 equiv.	-	24 equiv.	37 equiv.	40 % DMF

5	1 mg	13 equiv.	11 equiv.	-	12 equiv.	18 equiv.°	53/52 % DMF

3.5 N-*ε*-(prop-2-ynyloxycarbonyl)-L-lysine synthesis

N-*ε*-(prop-2-ynyloxycarbonyl)-L-lysine (YnK) was synthesized as a hydrochloride salt according to a procedure published by Lemke *et al*. (1st supplement).[48]

2.79 g of Boc-L-Lys-OH (11.35 mmol, 1.2 equiv.) were dissolved in 31.5 mL 1 M NaOH/THF (1:1, v/v) and cooled to 0 °C. Then, 0.925 mL propargyl chloroformate (1.12 g, 9.95 mmol) were added dropwise over 30 minutes while keeping the temperature at 0 °C. After removing the cold source and reaching RT, the reaction was stirred overnight. The next day, 50 mL of EtOAc were added to the reaction mixture. Subsequently, the pH of the aqueous phase was brought to a value of 2 using concentrated HCl, followed by phase separation and extracting the aqueous phase thrice with 40 mL of EtOAc each. Following drying the collected organic phase with $MgSO_4$ and solvent removal *via* rotavapor at 40 °C, a yellow oil was received. After dissolving the yellow oil in 31 mL 1,4-dioxane/concentrated HCl (1:1,v/v) the mixture was reacted for 3 h at RT while stirring. Then, solvents were distilled off using a rotavapor and the resulting residue dissolved in 1 M HCl and lyophilized. The product was received as a brown, waxy substance and was directly used for protein expression. Product identity was evaluated with ^{1}H- and ^{13}C-NMR in DMSO-d6 as well as LC-MS.

3.6 Gel electrophoresis

3.6.1 Sample preparation

Equation 1: Equation for medium taken for normalized bacterial samples. x denotes the sample volume.

$$\frac{1}{OD_{600}} \times 200\ \mu L\ = x\ \mu L$$

Normalized bacterial samples were taken from the growth medium during protein expression according to **Equation 1**. Subsequently, the samples were centrifuged at 14,000 rpm at RT for 30 seconds, the supernatant removed and stored at -20 °C until further use. For SDS-PAGE analysis, the pellets were resuspended in 25 µL dH_2O and 25 µL of 2x SDS Buffer and incubated at 95 °C for 3 minutes followed by vortexing. After centrifugation at 14,000 rpm for 1 minute 10 µL were loaded onto SDS-PAGE. Similarly, for liquid samples in 8 M urea, 25 µL were combined 1:1 with 2x SDS buffer and heat-treated as previously described.

6 M GdnHCl protein samples were first precipitated to remove the chaotropic salt. Thereby 20 µL of sample solution were combined with 180 µL 99.8 % ethanol, vortexed and centrifuged at 14,000 rom for 5 minutes. Following supernatant removal, the pellet was washed with 200 µL 70 % ethanol, vortexed and centrifuged at 14,000 rpm for 5 minutes. After discarding the supernatant, the sample was centrifuged at 14,000 rpm for 1 minute and any excess supernatant removed. The protein pellet was then left to dry at RT and subsequently redissolved in 25 µL dH2O, followed by the addition of 25 µL of 2x SDS buffer and prepared according to the heating scheme mentioned above.

Alternatively, 6 M GdnHCl samples taken during selected CuAAC reactions were also precipitated by adding 360 µL of ice-cold 99.8 % ethanol to 40 µL reaction mixes, followed by vortexing, incubation at -20 °C for 10 minutes and centrifugation at 14,000 rpm for 2 minutes. After supernatant removal and the addition of 400 µL ice-cold 99.8 % ethanol, the protein sample was vortexed, incubated and centrifuged according to the previous conditions. Then the resulting protein pellet was left to dry, dissolved in a 1:1 dH_2O 2x SDS buffer mix and heated according to the procedure above.

Table 8: 2x SDS buffer components and their concentration

Component	Concentration
Tris	500 mM (pH=6.8)
SDS	6 % (w/v)
Glycerol	35 % (v/v)
β-Mercaptoethanol	3.55 (v/v)
Bromophenol blue	0.05 (w/v)

3.6.2 SDS-PAGE

The SDS-PAGE was initiated by casting a 15 % discontinuous acrylamide gel. Thereby the separating gel solution was first added into a multi-casting chamber, enabling the simultaneous generation of up to 12 gels, and each subunit covered by 1 mL of 70 % isopropanol. After polymerizing for 30 minutes, the isopropanol was removed and the stacking gel poured on top and left to harden for 30 minutes after the addition of plastic combs. Subsequently, a gel was transferred into a running chamber, submerged in 1x Laemmli buffer, loaded with 5 µL low molecular weight protein marker (Cytiva) as well as the relevant samples, and was run at constant 200 V at ~60 A for approximately 45 minutes. Afterwards the gel was immersed in Coomassie staining solution for 1 h and then washed

twice with fresh dH_2O for 15 minutes respectively. Subsequently, the gel was destained in newly added dH_2O overnight and visualized with a ChemiDoc system (BioRad).

Table 9: Composition of the separating and stacking gel solutions for a 15 % acrylamide gel (12 gels)

Component		Separating gel	Stacking gel
dH_2O		12.5 mL	12.5 mL
Separating gel buffer (pH=8.8)	1.5 M TrisHCl	13.5 mL	-
	0.4 % (w/v) SDS		
Stacking gel buffer (pH=6.8)	0.5 M TrisHCl	-	2.5 mL
	0.4 % (w/v) SDS		
30 % Acrylamide		26 mL	3.5 mL
10 % SDS		550 µL	185 µL
10 % APS		550 µL	185 µL
TEMED		18 µL	18 µL

Table 10: 1x Laemmli buffer components and their concentration

Component	Concentration
Tris	25 mM
Glycerol	200 mM
SDS	0.1 % (w/v)

Table 11: Coomassie staining solution components and their concentration

Component	Concentration
Coomassie R250	0.1 % (w/v)
Acetic acid	10 % (v/v)
Methanol	45 % (v/v)

3.7 HPLC and NMR

3.7.1 Preparative and semi-preparative RP-HPLC

During this thesis preparative and semi-preparative RP-HPLC purifications were conducted using Shimadzu Prominence or Varian ProStar HPLC devices. Semi-preparative RP-HPLC was performed with two identical columns (PerfectSil, MZ Analysetechnik) with the following specifications: 300 Å 10 µM C4, 250 x 10 mm. Preparative RP-HPLC was carried out using

a Kromasil column (Nouryon) with these specifications: 300 Å 10 µM C4, 21.2 x 250 mm. All samples were solubilized and acidified with 2-5 mL of 6 M GdnHCl (pH=4.7) and any impurities removed using syringe filters with a PES membrane and 0.2 µm pore size (Macherey-Nagel) or through centrifugation at 14,000 rpm for 4-10 minutes and subsequent supernatant transfer to a new 15 mL Falcon tube or 2 mL Eppendorf tube prior to purification. Samples purified by the Varian system were also concentrated to approximately 8 mL using 3 kDa Amicon centrifugal filters (Merck Millipore) prior to injection. The bvPrP hydrazides were purified at the following conditions: Prep: 60 °C, 10 mL/min, 15 minutes desalting, 5 minutes from 5 % to 30 % solvent B, 40 minutes from 30 % to 70 % solvent B. For semiprep purifications the flow rate was reduced to 5 mL/min. The deselenized PrP-WT post EPSL reactions samples were solely purified on the Shimadzu system using these conditions with the flow rate reduced to 3 mL/min.

All fractions generated were evaluated by DI-MS and pooled depending on product content. Fractions containing the purified product were lyophilized.

Table 12: HPLC buffers and their composition. All buffers were degassed prior to use.

Buffer	Composition
Solvent A	0.1 % TFA in filtered dH_2O
Solvent B	0.08 % TFA in ACN
Storage buffer	7:3 ACN:dH_2O

3.7.2 Analytical HPLC

Analytical HPLCs were performed to assess reactant concentrations or reaction progress. The columns had the following specifications: 300 Å 5 µM C4/C18, 4.6 x 150 mm (Kromasil). The respective analysis conditions are displayed in **Table 13**. Condition 1 was used to evaluate the glycan conjugation reactions (3.4.2) and the EPSL of bvPrP-WT to ubiquitin 46-76 (3.3), condition 2 to study the EPSL of bvPrP-WT to the GPI-anchor (3.3), and condition 3 for the analysis of the solubility of the remaining precipitate of the final glycan conjugation reaction in various solvents (3.4.2).

Table 13: Analytical HPLC analysis conditions

Condition	Elution profile	Flow rate	Duration	Temperature	Column type
1	5 % to 65 % B	1 mL/min	30 min	RT	C4
2	5 % to 95 % B	1 mL/min	40 min	60 °C	C4

3	5 % to 65 % B	1 mL/min	60 min	RT	C18

Table 14: Analytical HPLC buffers and their composition. All buffers were degassed prior to use.

Buffer	Composition
Buffer A	0.1 % TFA in filtered dH_2O
Buffer B	0.08 % TFA in ACN
Buffer D	0.1 % TFA in 6:3:1 isopropanol:ACN:dH_2O
Storage buffer	7:3 ACN:dH_2O
Rear seal wash	10 % isopropanol in filtered dH_2O

3.7.3 LC-MS and DI-MS

LC-MS and DI-MS evaluations were conducted using the following devices: an Auto Purification HPLC/MS system (Waters), an Arc LC system (Waters) connected to a SQD2 mass detector and a MSQ Plus HPLC/MS system (Thermo Scientific). All samples were ionized *via* ESI in positive ion mode.

Table 15: LC-MS buffers for LC-MS systems and their composition

Buffer	Composition
Buffer A	0.05 % TFA in filtered dH_2O
Buffer B (Waters)	0.05 % TFA in ACN
Buffer B (Thermo Scientific)	0.08 % formic acid in ACN
Buffer C	0.05 % TFA in 6:3:1 isopropanol:ACN:dH_2O
Buffer D	0.05 % TFA in 6:3:1 isopropanol:ACN:dH_2O
Storage buffer	7:3 ACN:dH_2O

3.7.4 NMR

^{1}H-NMR and ^{13}C-NMR were performed with a Bruker 600 MHz NMR system, at 600 MHz and 151 MHz respectively, using an approximate sample concentration of 14.3 mg/mL. The solvent used was DMSO-d6. Both NMR spectra were evaluated with the help of a PhD student (H. Weißinger).

4. Results and Discussion

4.1 bvPrP-WT hydrazide generation

The focus of this work lies on developing a semi-synthesis route for modified bvPrP through a combination of GCE, EPSL and CuAAC approaches. The generation of the bvPrP-WT hydrazide served as a starting point to learn and optimize the workflow to reliably obtain sufficient amounts of protein hydrazides for EPSL.

Firstly, expression of the bvPrP-WT(23-231)-*Mxe*GyrA-7xHis-CBD fusion protein was conducted in *E. coli* using M9 minimal medium to generate the recombinantly produced bvPrP-WT segment. Protein expression was accidentally induced too early due to a personal error at an OD_{600} of 0.2 through IPTG supplementation and the cells were harvested after 4 h at 37 °C *via* centrifugation. Samples for analytical SDS-PAGE were taken at 0 h, 2 h and 4 h of IPTG induction and are depicted in **Figure 8**, together with samples from the cell pellet solubilized in a buffer containing 6 M GdnHCl (crude) as well as the supernatant following cell lysis.

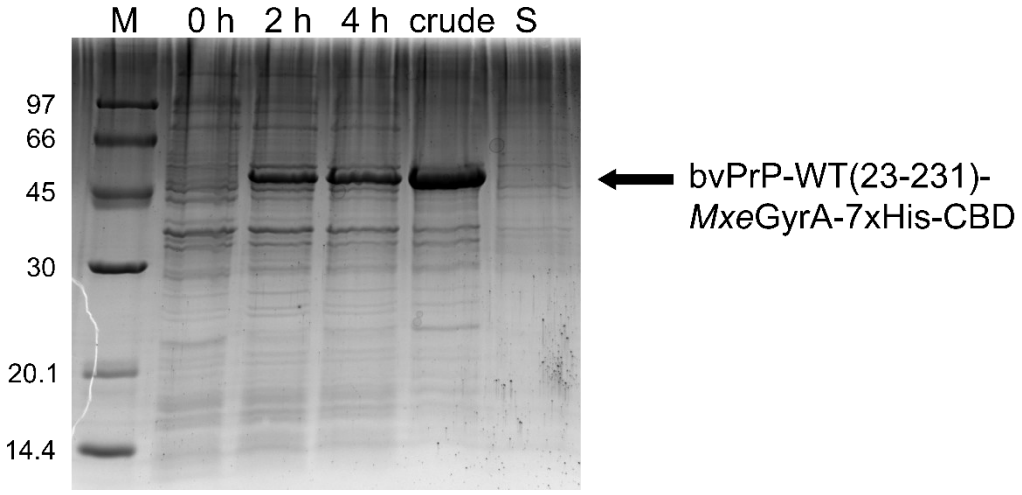

Figure 8: SDS-Page of normalized bvPrP-WT protein expression samples after 0 h, 2 h and 4 h of IPTG induction. Samples taken from the supernatant after cell lysis and centrifugation (S) and subsequent inclusion body solubilization (crude) are also depicted. Masses of the low molecular weight protein marker (M) are displayed in kDa.

When comparing samples from 0 h and 2 h it is visible that the POI, with an expected size of 52,059 Da, was only generated after IPTG induction. Additionally, no significant change in band thickness is visible between the 2 h and 4 h samples. These minimal changes may have been a result of premature IPTG induction and may have had an impact on the overall amount of bvPrP-WT generated. Furthermore, the POI band visible in the crude protein solution and the lack thereof in the cell lysis supernatant clearly indicates the deposition of recombinantly produced PrP in inclusion bodies, as described in literature.[45] bvPrP-WT

expression was also validated by LC-MS following cell harvest and subsequent inclusion body solubilization in 6 M GdnHCl, with the spectrum visible in **Figure 9**.

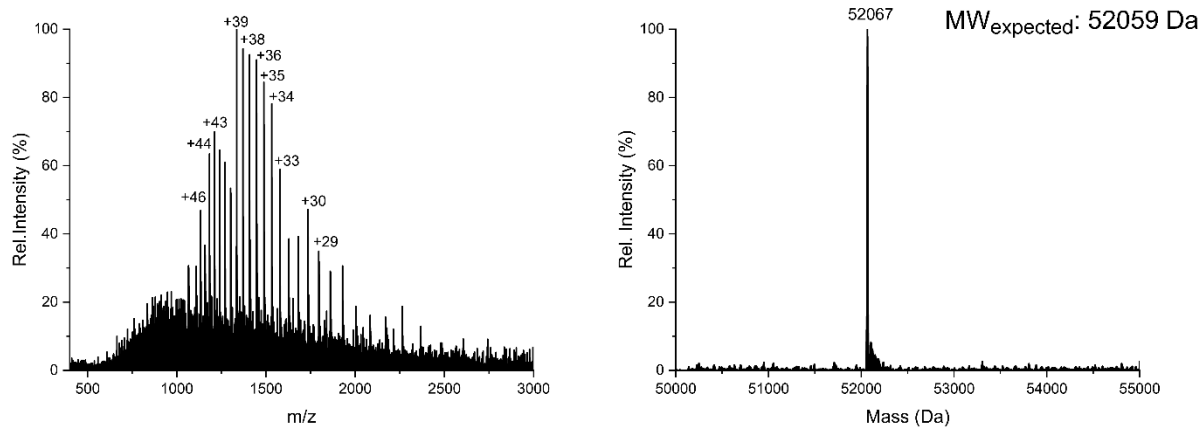

Figure 9: LC-MS spectrum of bvPrP-WT intein fusion protein. The right panel depicts the deconvoluted mass in Da.

This graph shows that the measured molecular weight of bvPrP-WT(23-231)-*Mxe*GyrA-7xHis-CBD, 52,067 Da, does not significantly differ from the expected value, 52,059 Da (+8). While the mass accuracy of the detector used only accounts for mass deviations of approximately 0.5 Da higher deviations can occur for a protein of this size, its denatured state and the ionization method used.[49] Moreover, not only the detector mass accuracy or sample mass, but also the parameters applied during deconvolution may impact the measured masses, leading to deviations from the expected values. Following protein expression, cell lysis and bvPrP-WT solubilization in 6 M GdnHCl, the crude protein solution was purified by Ni-NTA affinity chromatography.

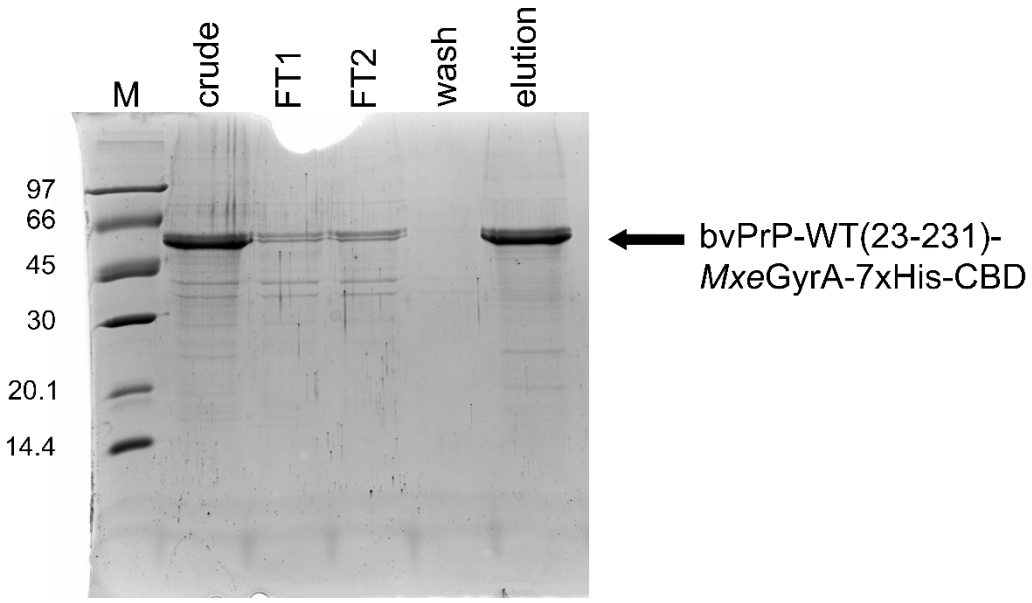

Figure 10: SDS-PAGE of crude bvPrP-WT solution undergoing Ni-NTA purification. The samples evaluated were 6 M GdnHCl solution (crude), the first and second flow-through (FT1/FT2), the wash and the final 6 M GdnHCl 500 mM imidazole eluate (elution). Masses of the low molecular weight protein marker (M) are displayed in kDa.

As shown in **Figure 10**, some impurities, ranging in size between 30 and 45 kDa, were removed during this process while very minor amounts of other proteins were still present in the eluate. Furthermore, the presence of faint POI bands in both flow-through samples indicates some product loss, most probably due to incomplete binding to the Ni-NTA beads. This problem could have been avoided through extended incubation times or a higher bead amount. The double band visible in all but the wash sample at the expected POI size (52,067 Da) is an undetermined contamination from the expression. Interestingly, it was induced by IPTG and bound to the Ni-NTA beads. However, it could not be detected *via* LC-MS measurement.

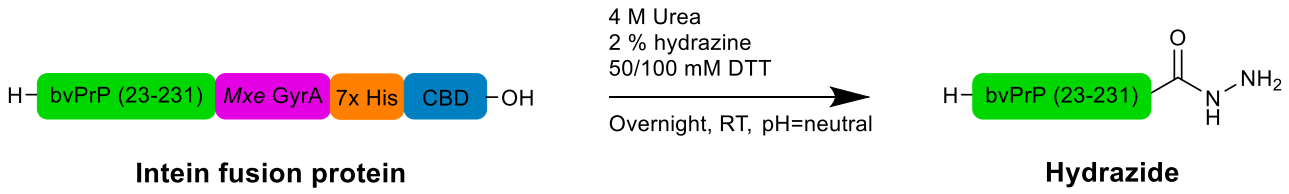

Figure 11: Scheme of the intein cleavage reaction *via* hydrazinolysis.

A buffer exchange to 8 M urea was then conducted to prepare the purified protein solution for intein cleavage with hydrazine to generate the bvPrP-WT hydrazide (**Figure 11**). The cleavage reaction was performed after a 1:1 dilution with the cleavage solution, and at a final concentration of 4 M urea, 50 mM DTT and 2 % hydrazine. This reaction mixture was stirred overnight at RT. For this cleavage reaction the pH was not evaluated or adjusted.

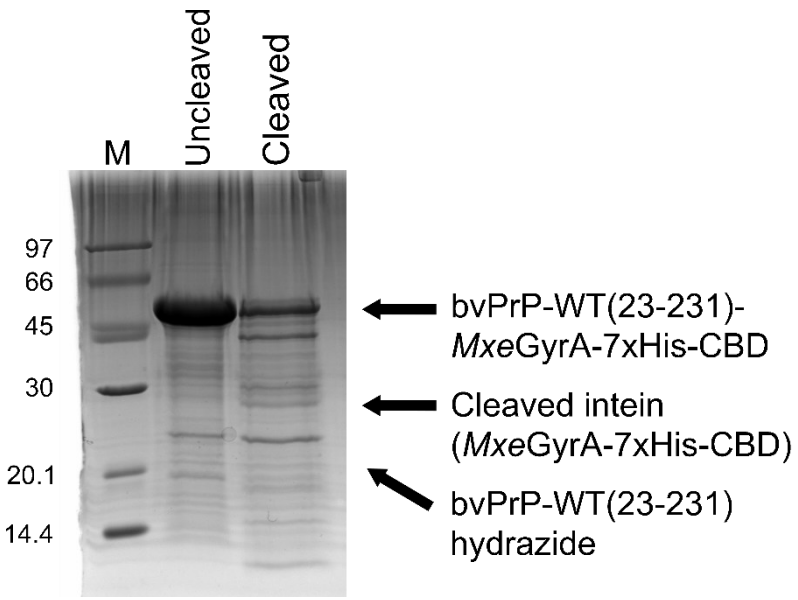

Figure 12: SDS-Page of the first bvPrP-WT intein hydrazinolysis. The unreacted 8 M urea sample is denoted by “Uncleaved”, the post-cleavage sample as “Cleaved”. Masses of the low molecular weight protein marker (M) are displayed in kDa.

Figure 12 shows the cleaved bvPrP-WT hydrazide at the expected size of ~23 kDa and the accompanying cleaved intein at ~29 kDa. Moreover, a significant amount of non-cleaved bvPrP-WT intein fusion protein is also visible, indicating incomplete hydrazinolysis. This may have been caused by insufficient reaction time, insufficient folding of the intein, low DTT amount or the pH conditions, as the cleavage solution was not pH-adjusted beforehand.

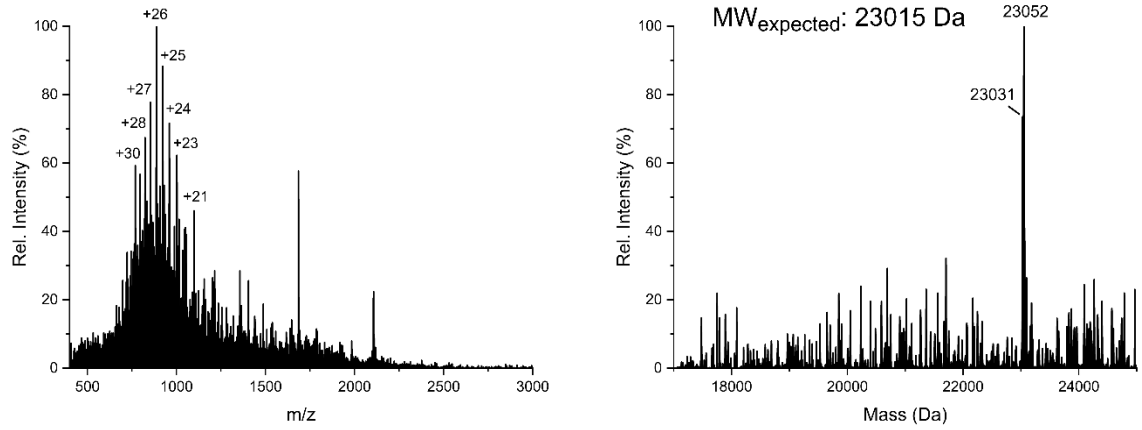

Figure 13: LC-MS spectrum of bvPrP-WT hydrazide. The right panel depicts the deconvoluted masses in Da.

LC-MS indicated two masses, 23,052 Da (+37) and 23,031 (+16), corresponding to an additional sodium atom and hydrazide group and an additional hydrazide group respectively (**Figure 13**). Alternatively, a single and double oxidation of the PrP hydrazide may also lead to these mass changes. Following subsequent RP-HPLC purification, the purified and lyophilized bvPrP-WT hydrazide gave a final yield of 6 mg, or 5 mg/L of growth medium. Additionally, a significant amount of bvPrP-WT fusion protein did not undergo cleavage, as

mentioned above, and was also collected during RP-HPLC, amounting to 122 mg, or 102 mg/L, and was reprocessed with adapted reaction conditions as described later in this chapter.

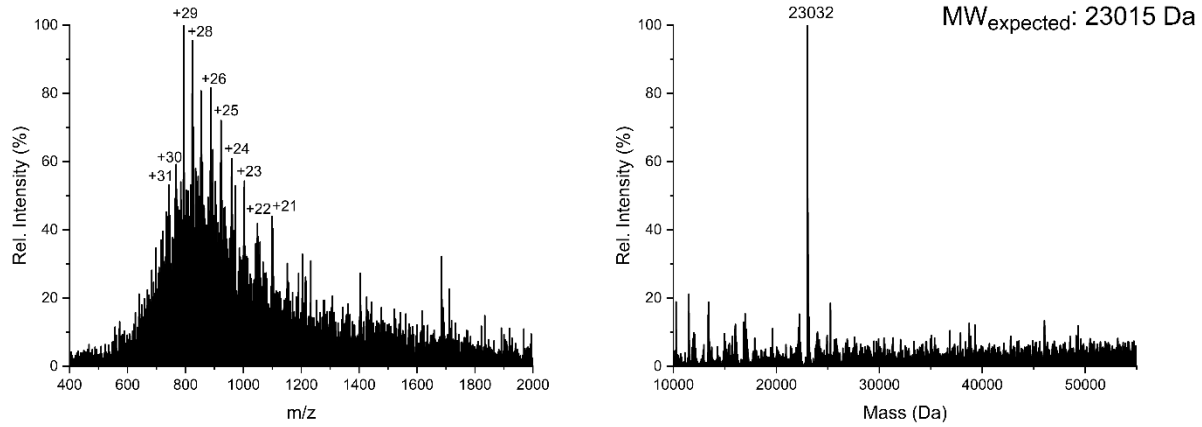

Figure 14: DI-MS spectrum of purified and lyophilized bvPrP-WT hydrazide. The right panel depicts the deconvoluted mass in Da.

During the final MS analysis of the lyophilized bvPrP-WT hydrazide only a 23,032 Da (+17) species was detected (**Figure 14**). Again, it is suggested that the molecule contains a second, additional hydrazide functionality. Structurally, a change of +14 Da in mass is associated with the replacement of the acidic hydroxide with a hydrazide moiety within an aspartic acid sidechain.[50] This side-reaction may have been caused by the previous reaction conditions. However, it also must be mentioned that the spectrum indicates product impurity, possibly affecting the detected mass, which could be alleviated by adjusting the RP-HPLC conditions. Nevertheless, we suspected that the +14 Da mass increase may have been caused by the previous reaction conditions. Due to this result and the low product yield from the previous cleavage reaction the unreacted sample collected earlier was redissolved in 8 M urea and combined 1:1 with an adapted cleavage solution. For this repetition the cleavage solution was neutralized prior to addition and the DTT content increased to a final concentration of 100 mM DTT. The hydrazine content was left at 2 %. The accompanying analytical SDS-Page is depicted in **Figure 15**.

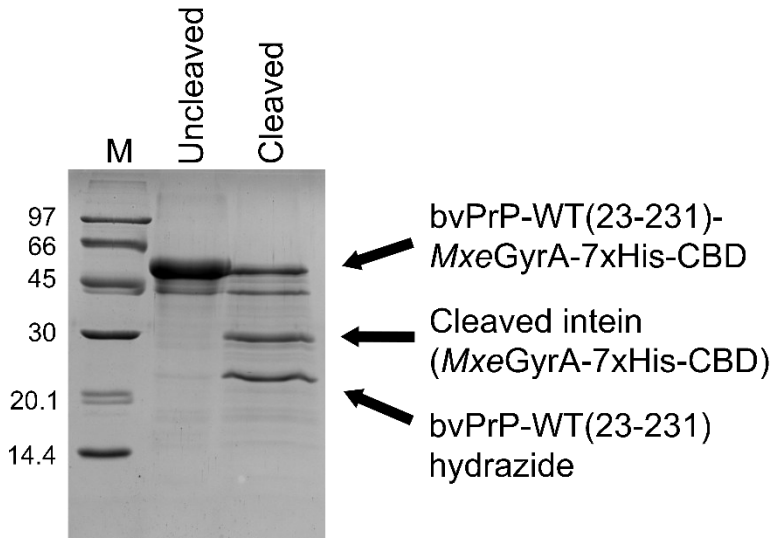

Figure 15: SDS-Page of the second bvPrP-WT intein hydrazinolysis. The unreacted 8 M urea sample is denoted by “Uncleaved”, the post-cleavage sample as “Cleaved”. Masses of the low molecular weight protein marker (M) are displayed in kDa.

Here, it is clearly visible that a higher fraction of the bvPrP intein fusion protein did undergo cleavage when compared to the previous hydrazinolysis reaction. Nevertheless, no work-up was carried out as the focus was shifted to the generation of modified PrP hydrazides including a ncAA through GCE.

4.2 bvPrP-N181X-AzK and bvPrP-N197X-AzK hydrazide generation

Following bvPrP-WT hydrazide generation, expressions of the mutant protein variants bvPrP-N181X and bvPrP-N197X in the presence of 5 mM AzK in M9 minimal medium were performed. These two positions are the native N-glycosylation sites of the PrP protein where the native asparagine amino acids were replaced with an amber stop codon in the respective mutant sequences to enable amber codon suppression.

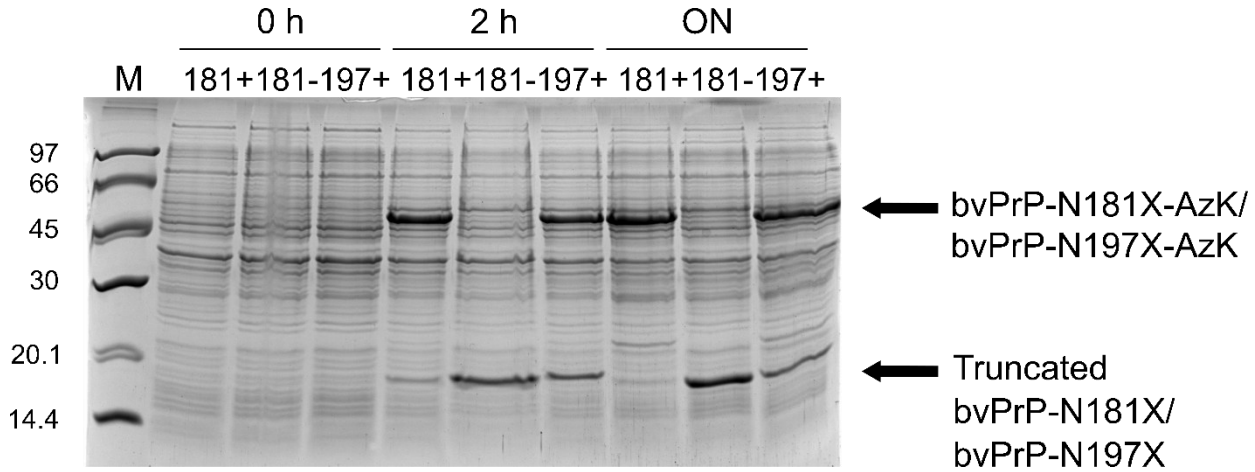

Figure 16: SDS-Page of normalized bvPrP-N181X-AzK (181+) and bvPrP-N197X-AzK (197+) protein expression samples after 0 h, 2 h and overnight (ON) following IPTG induction. Uninduced samples grown using the bvPrP-N181X mutant *E. coli* strain served as negative control (181-). Masses of the low molecular weight protein marker (M) are displayed in kDa.

As shown in **Figure 16**, no POI was generated prior to IPTG induction. Moreover, when comparing the bvPrP-N181X-AzK and bvPrP-N197X-AzK expression 2 h and 14 h after induction, the expected POI with a mass of 52,186 Da (bvPrP-N181X-AzK fusion protein) is produced more efficiently as evidenced by a slightly stronger product band and a lower amount of truncated protein present. The truncated proteins, resulting from premature translation termination, have expected sizes of 17,069 Da and 18,823 Da for bvPrP-N181X-AzK and bvPrP-N197X-AzK respectively. In contrast, the induced control in absence of AzK only led to the generation of truncated protein, as expected. Following cell lysis and inclusion body solubilization in 6 M GdnHCl, the crude protein solutions were evaluated by LC-MS (**Figure 17**).

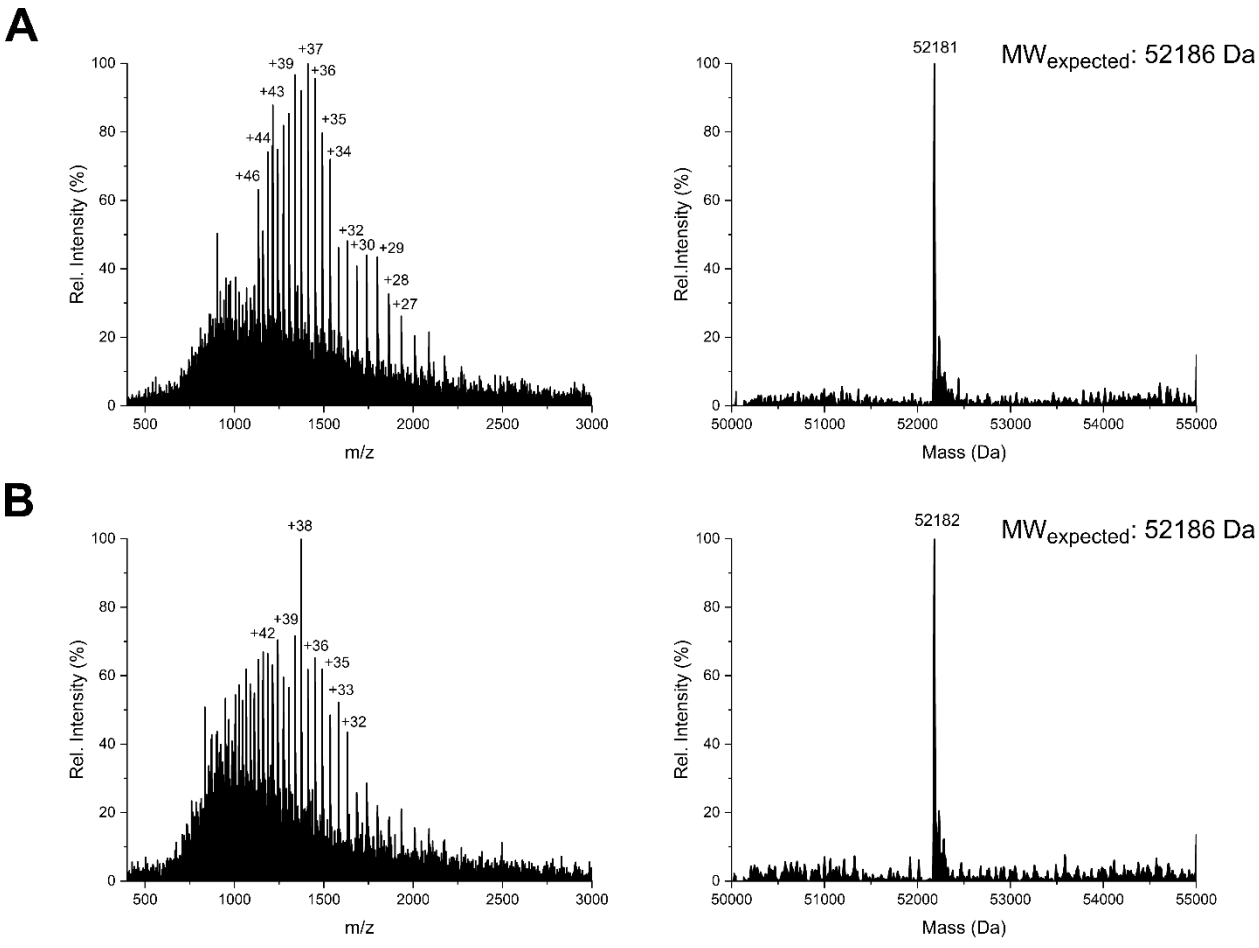

Figure 17: LC-MS spectra of bvPrP-N181X-AzK (A) and bvPrP-N197X-AzK (B) intein fusion proteins. The right panels depict the deconvoluted masses in Da.

The measurements are in accordance with the expected mass of 52,186 Da and show that both protein variants were produced successfully, with the bvPrP-N181X-AzK intein fusion protein measured at 52,181 Da (-5) and the bvPrP-N197X-AzK intein fusion protein at 52,182 Da (-4). These negative mass deviations are acceptable based on the reasons stated

above. Ni-NTA purification was then performed to obtain the bvPrP variants for subsequent experiments.

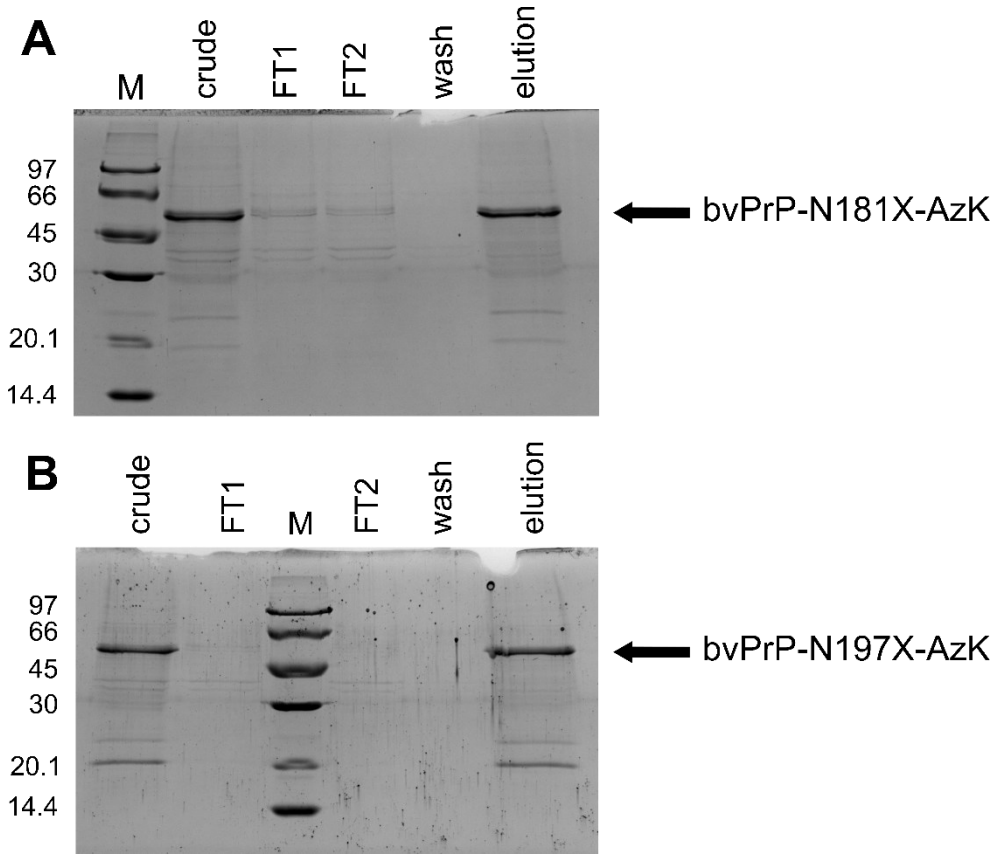

Figure 18: SDS-PAGE of crude bvPrP-N181X-AzK (A) and bvPrP-N197X-AzK (B) solutions undergoing Ni-NTA purification. The samples evaluated were 6 M GdnHCl solution (crude), the first and second flow-through (FT1/FT2), the wash and the final 6 M GdnHCl 500 mM imidazole eluate (elution). Masses of the low molecular weight protein marker (M) are displayed in kDa.

As shown in **Figure 18**, mainly impurities in the 30 kDa to 45 kDa range were removed, corresponding to the previous Ni-NTA purification results. However, during the current purification steps only very minor bands of the POIs are visible in the flow-through samples, indicating a higher degree of binding to the Ni-NTA beads compared to the previous experiment. This may have been caused by individual differences in preparation of the Ni-NTA beads or the decreased storage time of the beads in between uses. Alternatively, a lower amount of POI to be purified may also explain this finding. Furthermore, both truncated protein variants, with molecular weights of 17,069 Da and 18,823 Da for bvPrP-N181X-AzK and bvPrP-N197X-AzK respectively, were not removed during this purification step. This may have been caused by unspecific interaction with Ni-NTA beads, leading to co-elution and incomplete purification, as the N-terminal domain of PrP tends to interact with divalent metal cations.[51] However, as discovered later on for the bvPrP-N181X-YnK sample, this problem could be alleviated by a low-concentration imidazole wash prior to elution.[41] It also must be noted that the crude and elution samples of both protein variants exhibit a band at

~23 kDa, which may correspond to prematurely cleaved protein. Nevertheless, its identity was not determined further and could therefore also be caused by contamination with protein binding unspecifically to Ni-NTA.

After the Ni-NTA purification and subsequent buffer exchange to 8 M urea the protein solutions were combined 1:1 with neutralized cleavage solutions containing 200 mM DTT and 4 % hydrazine to generate the respective protein hydrazides. **Figure 19** shows the corresponding analytical SDS-PAGE.

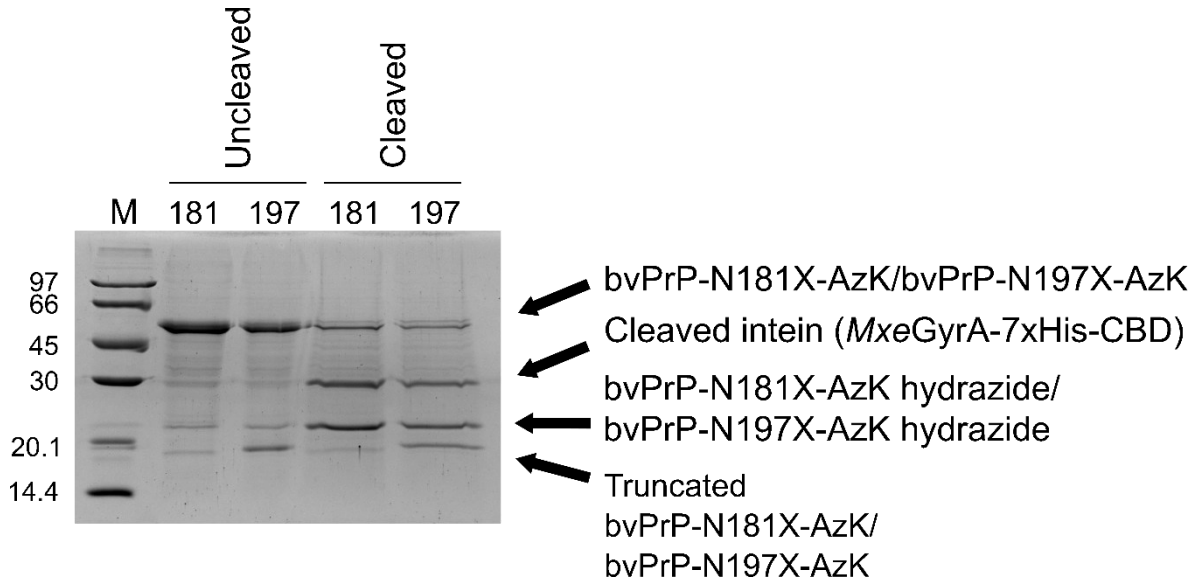

Figure 19: SDS-PAGE of bvPrP-N181X-AzK (181) and bvPrP-N197X-AzK (197) intein hydrazinolyses. The unreacted 8 M urea samples are denoted by “Uncleaved”, the post-cleavage samples as “Cleaved”. Masses of the low molecular weight protein marker (M) are displayed in kDa.

Both samples were almost completely cleaved after reacting overnight at RT. The bands of the cleaved-off intein at ~29 kDa as well as the produced protein hydrazides at ~23 kDa are clearly visible. However, inconsistencies regarding the expected protein mass, 23,142 Da, are encountered when evaluating the accompanying LC-MS analyses (**Figure 20**).

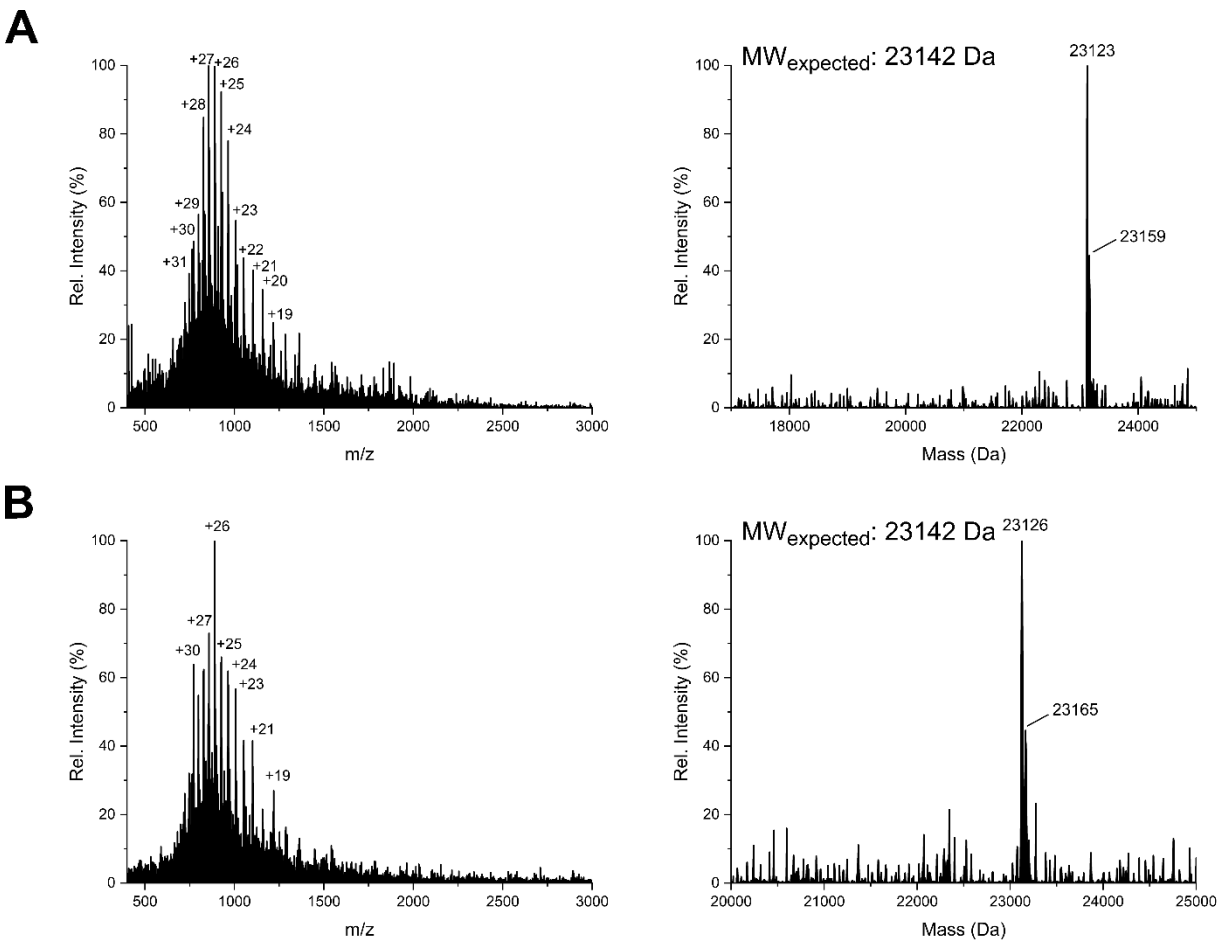

Figure 20: LC-MS spectrum of bvPrP-N181X-AzK (A) and bvPrP-N197X-AzK (B) hydrazides. The right panel depicts the deconvoluted masses in Da.

The measured spectra for both the bvPrP-N181X-AzK and bvPrP-N197X-AzK hydrazides do not correspond to the expected molecular weight. Instead, a 23,123 Da (-19) and 23,159 Da (+17) species for bvPrP-N181X-AzK, and a 23,126 Da (-16) and 23,165 Da (+23) species for bvPrP-N197X-AzK were detected. The latter two samples would correspond to the POIs with an additional hydrazide or sodium atom respectively. However, the -16 Da and -19 Da masses could not be assigned accurately without further evaluation. Subsequent MS analysis of the RP-HPLC purified and lyophilized bvPrP-N181X-AzK hydrazide, with a final yield of 25 mg/L, again showed that two species, with 23,123 Da and 23,159 Da, were measured, with the spectra visible in **Figure 21**.

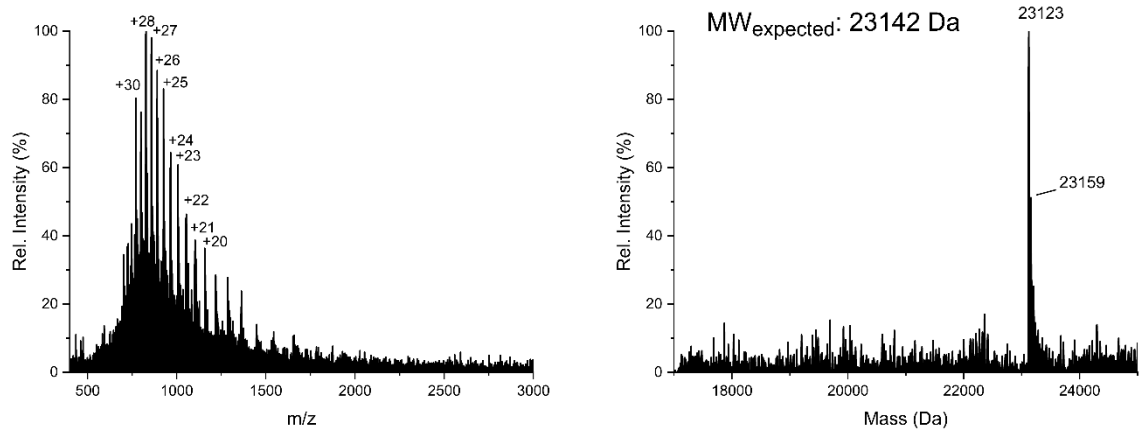

Figure 21: DI-MS spectrum of purified and lyophilized bvPrP-N181X-AzK hydrazide. The right panel depicts the deconvoluted mass in Da.

We suspected that the azide moiety of the AzK within the protein was reduced by DTT to an amine group during hydrazinolysis, which has been reported in the literature for variety of azide containing compounds in presence of DTT.[52] We therefore conducted test cleavages with DTT concentrations of 50 mM and 100 mM with samples taken at two timepoints, after 3 h and overnight, to evaluate if any change in the DTT concentration has an effect on the masses measured.

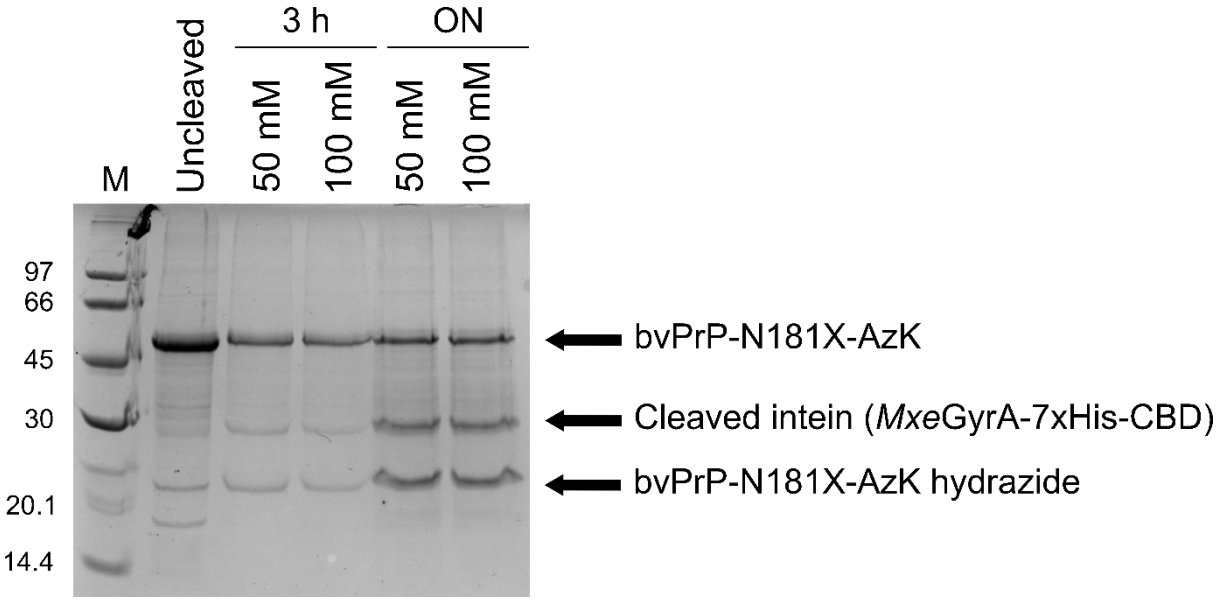

Figure 22: SDS-PAGE of the bvPrP-N181X-AzK test hydrazinolyses. The unreacted 8 M urea sample ais denoted by “Uncleaved”. Sample are also depicted with their relevant DTT concentration (50 mM, 100 mM) and the sampling timepoints (3 h, overnight (ON)). Masses of the low molecular weight protein marker (M) are displayed in kDa.

The analytical SDS-PAGE (**Figure 22**) shows that only a minor portion of the fusion protein underwent hydrazinolysis after 3 h, regardless of DTT concentration. LC-MS measurements showed that the correct mass, 23,144 Da (+2), is detected after 3 h of reaction alongside a

23,117 Da (-25) species. After reacting overnight, more cleavage product was visible in the SDS-PAGE compared to the 3 h sample. Nevertheless, there was still uncleaved protein present. During the accompanying LC-MS measurement a mass of 23,122 Da (-20) was obtained. The expected mass of 23,142 Da was not detected.

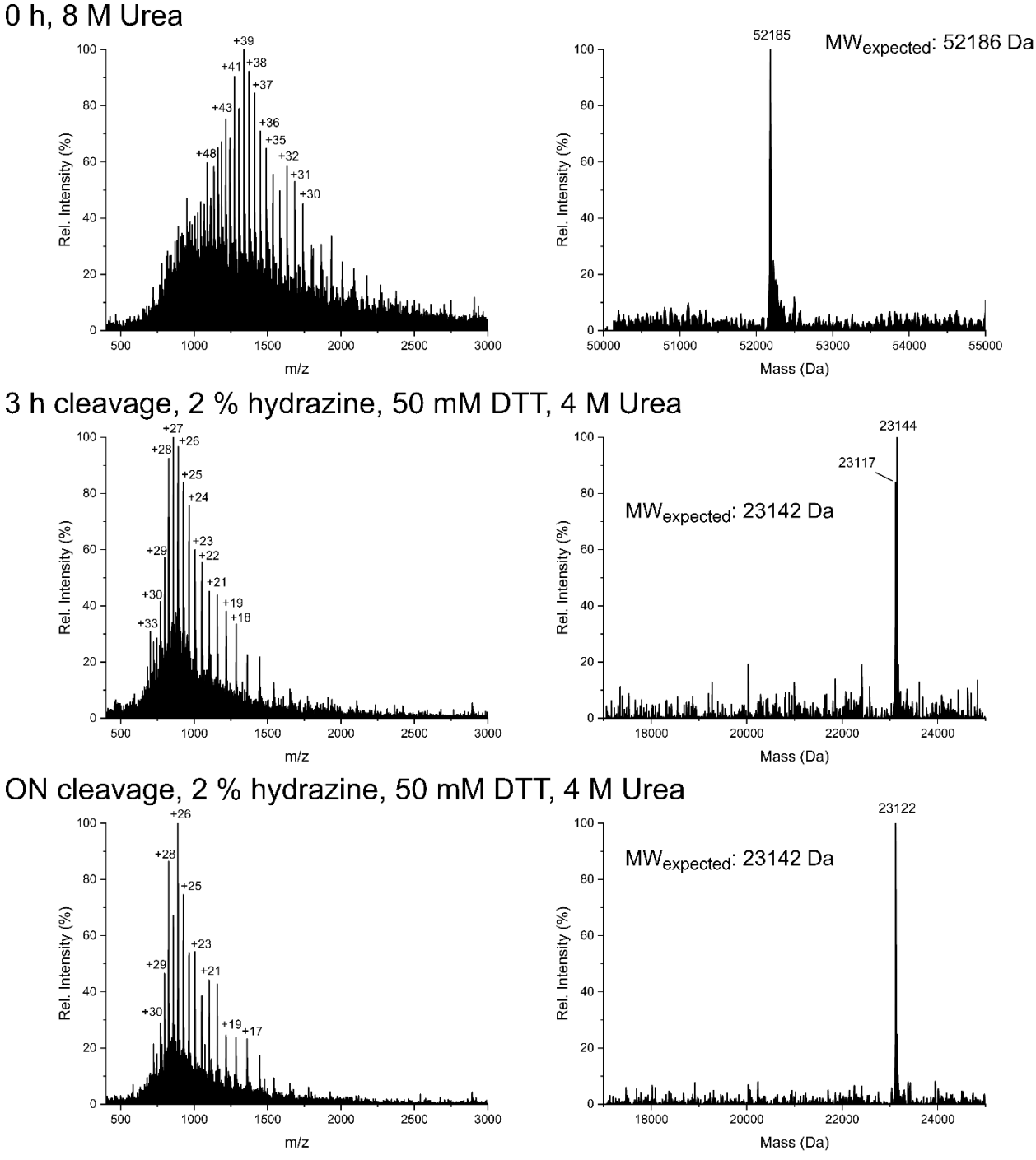

Figure 23: LC-MS spectra of bvPrP-N181X-AzK after 0 h in 8 M urea, 3 h and overnight (ON) at 2 % hydrazine, 50 mM DTT and 4 M urea. The right panel depicts the deconvoluted masses in Da.

Together, these results indicate the importance of cleaving overnight in terms of reaction completion but also suggest that the reaction conditions are responsible for the change in

mass over time. The LC-MS measurements of the sample treated with 100 mM DTT are not exhibited here as these showed comparable results.

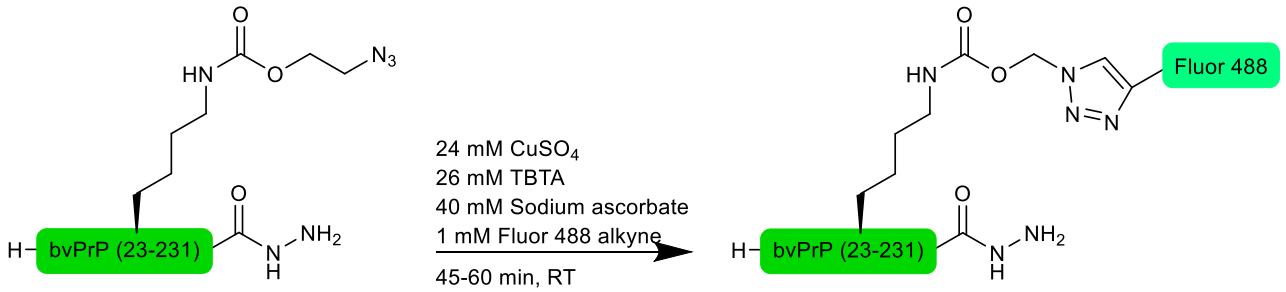

Figure 24: bvPrP-N181X-AzK hydrazide and Fluor 488 alkyne CuAAC reaction scheme.

To further assess AzK integrity, a CuAAC reaction with a Fluor 488 alkyne using a purified and lyophilized hydrazide sample as well as the uncleaved protein solubilized in 6 M GdnHCl was performed (**Figure 24**).

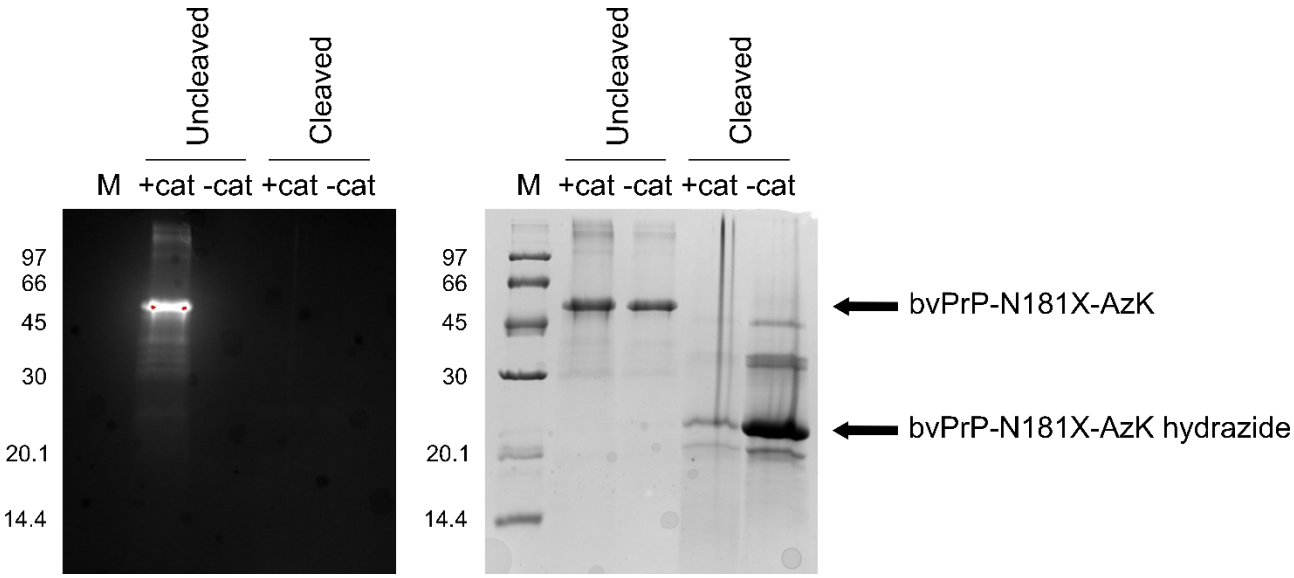

Figure 25: SDS-PAGE of bvPrP-N181X-AzK CuAAC reaction samples. The crude 6 M GdnHCl protein samples are denoted “Uncleaved”, the purified, lyophilized samples by “Cleaved”. Samples supplemented with the catalytic pre-mix are denoted “cat+”, the negative control with “cat-“. The right panel shows the Coomassie stained gel, the left panel the gel under 488 nm light. Masses of the low molecular weight protein marker (M) are displayed in kDa.

As shown in the analytical SDS-PAGE (**Figure 25)**, no signal was obtained for the cleaved sample (23,142 Da), indicating azide decomposition. In contrast, the crude, uncleaved sample (52,186 Da) exhibited a strong signal, displaying CuAAC reaction capability and therefore the presence of an azide moiety. On a sidenote, the clearly visible difference in band thickness of the two cleaved, lyophilized samples (+cat and -cat) may have been caused by insufficient dissolvement of the sample prior to sample transfer, issues caused by the reagents within the catalytic pre-mix, as described in chapter 3.4.1, or its inability to dissolve following SDS-PAGE sample preparation.

Following the interesting observation made with the cleaved sample during the CuAAC reaction, we sought to assess what happened to the azide group in the cleaved, purified sample. Thus, we performed a HRMS measurement to identify the exact mass of the cleaved product. The result of the HRMS analysis shows a main peak at 23,116 Da, as visible in **Figure 26**.

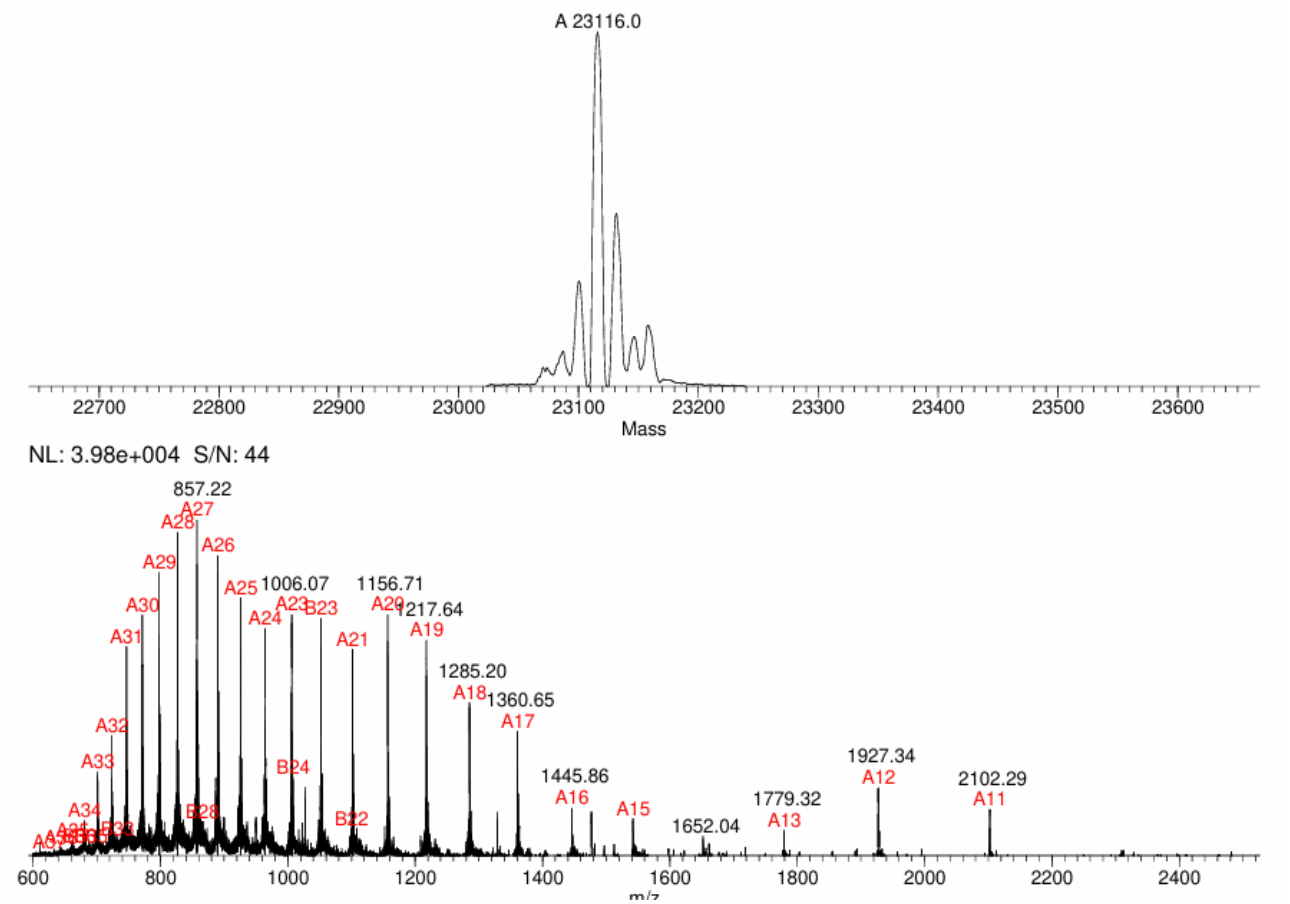

Figure 26: HRMS analysis spectra of the bvPrP-N181X-AzK hydrazide. The upper panel depicts the deconvoluted mass in Da.

This equates to an overall -26 Da loss in molecular weight, compared to the expected mass of 23,142 Da, and directly corresponds to an azide reduction to a primary amine (**Figure 27**).

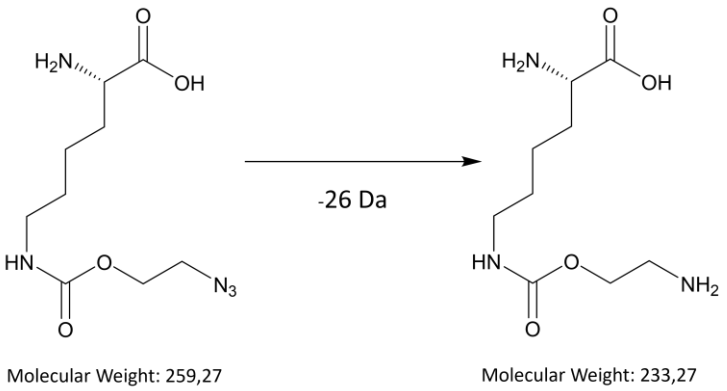

Figure 27: Reduction of the azide group in AzK into an amine.

Overall, the results above indicate that the azide group was reduced, most probably during the cleavage reaction with DTT and hydrazine. With these new insights we shifted our focus on the incorporation of the CuAAC counterpart of AzK, YnK, which contains an alkyne moiety instead, which should be stable to all conditions used here. In the following chapter the YnK containing hydrazide generation of this protein variant is explored.

No final analysis of the bvPrP-N197X-AzK hydrazide regarding its final mass and structural integrity could be conducted due to a personal error during the RP-HPLC fraction collection leading to a complete loss of the sample. Another expression and further assessment of any bvPrP-N197X modification during this thesis was disregarded in favor of the bvPrP-N181X protein variant due to the previously detected comparatively higher expression efficiency of the latter.

4.3 bvPrP-N181X-YnK hydrazide generation

After encountering the azide reduction issues with the bvPrP-N181X-AzK protein variant during hydrazine cleavage with DTT, protein expression was conducted in M9 minimal medium supplemented with 5 mM YnK. We suspected that the *Methanosarcina mazei* amber codon suppression machinery would also be able to recognize this ncAA due to its high structural similarity to AzK, a property also described in literature[22,53], leading to the generation of bvPrP-N181X-YnK. Expression was conducted alongside an AzK sample to validate and compare expression differences.

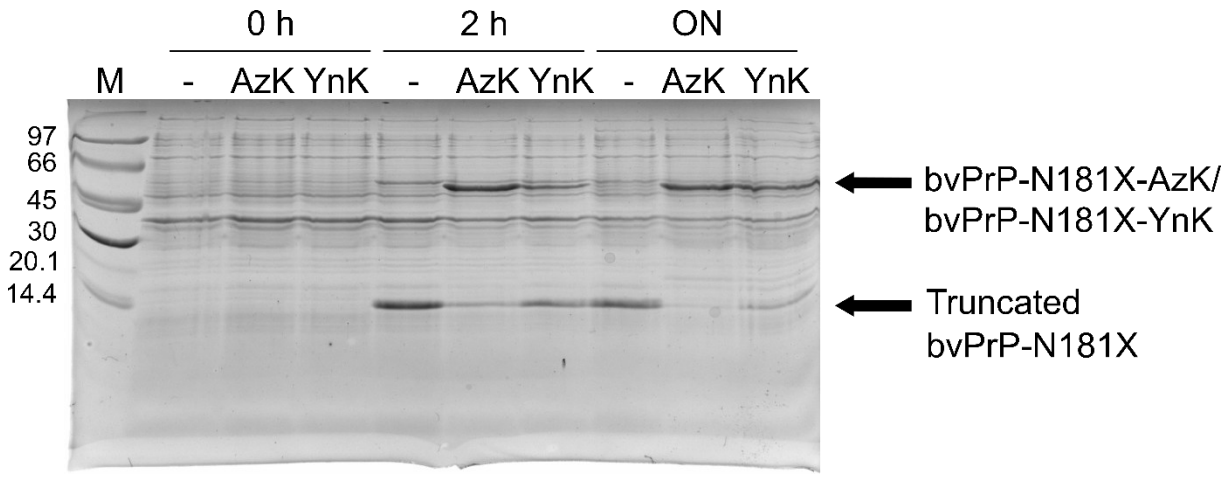

Figure 28: SDS-PAGE of normalized bvPrP-N181X-AzK (AzK) and bvPrP-N181X-YnK (YnK) protein expression samples after 0 h, 2 h and overnight (ON) following IPTG induction. Uninduced samples grown using the bvPrP-N181X mutant *E. coli* strain served as negative control (-). Masses of the low molecular weight protein marker (M) are displayed in kDa.

As visible in **Figure 28**, both modified protein variants were produced following IPTG induction, with the bvPrP-N181X-AzK 2 h and overnight samples exhibiting a lower amount of truncated protein when compared to the full-length bvPrP-N181X-YnK samples. These results indicate an increased affinity of the pyrrolysine aaRS binding pocket to AzK compared to YnK and coincide with findings made by Wiltschi *et al*. Here, EGFP expression was conducted *via* amber codon suppression under growth decoupling conditions, during which approximately 50 % less EGFP was produced when YnK instead of AzK was applied.[53]

Since YnK is rather expensive when sourced commercially, we also synthesized it (see 4.6) in our laboratory to enable up-scaling of the protein production in the future. Additionally, used M9 minimal medium which was left over as the supernatant following cell harvest was recycled and applied a second time for protein expression for economic reasons, as we did not know how much YnK had remained within the medium after the first expression and would be discarded otherwise. Thus, protein expression of bvPrP-N181X-YnK employing 5 mM of this self-made YnK as well as recycled M9 growth medium possibly containing residual YnK was therefore conducted to infer their applicability in comparison to commercial YnK.

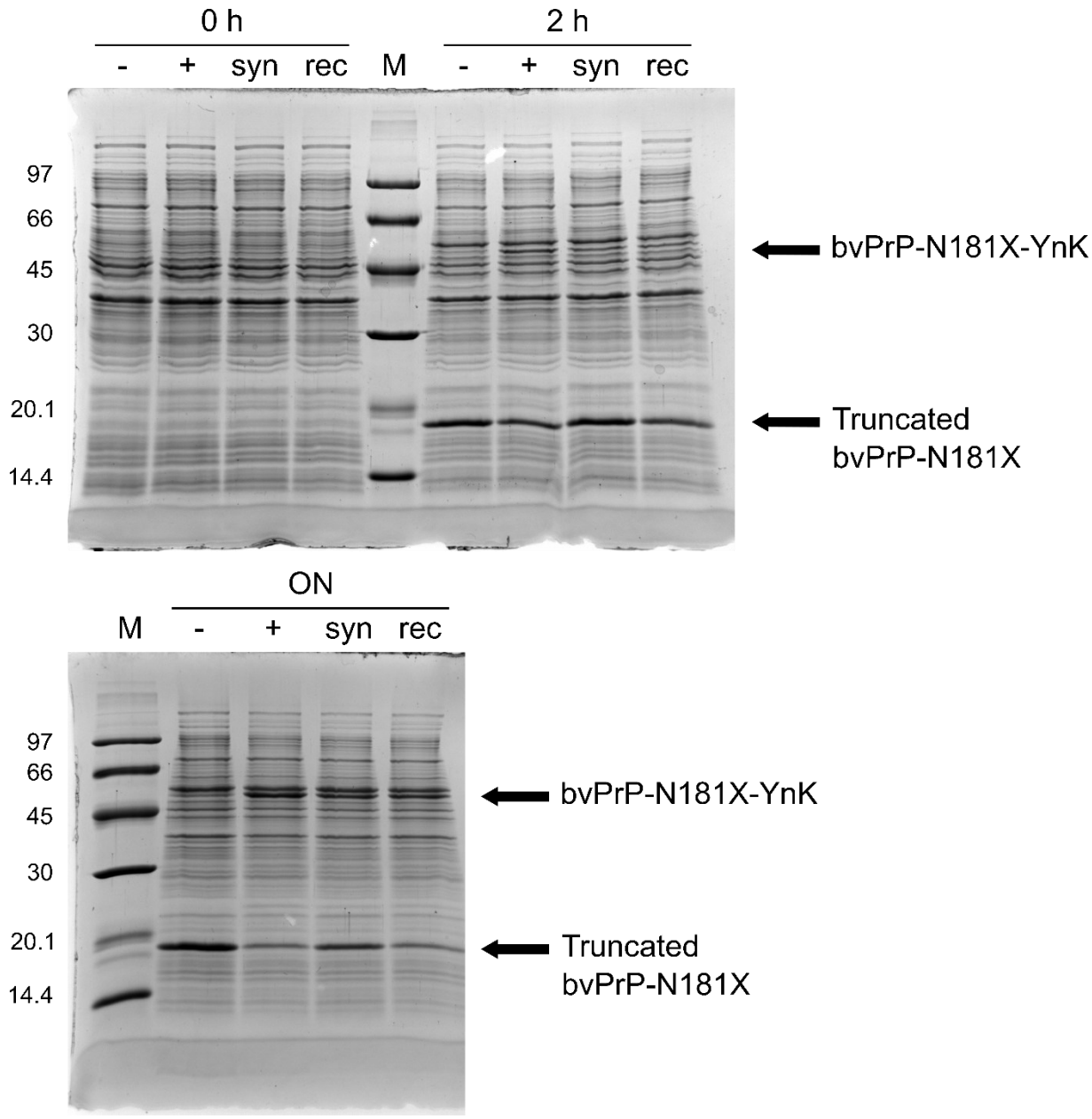

Figure 29: SDS-Page of normalized bvPrP-N181X-YnK (YnK) protein expression samples after 0 h, 2 h and overnight (ON) following IPTG induction. Samples using commercial YnK are denoted by "+", synthesized YnK by "syn" and samples with YnK solely originating from recycled medium by "rec". Uninduced samples grown using the bvPrP-N181X mutant *E. coli* strain served as negative control (-). Masses of the low molecular weight protein marker (M) are displayed in kDa.

Figure 29 again shows that product formation only occurs after IPTG supplementation for all samples evaluated. In both 2 h and overnight samples it is visible that commercial YnK is slightly better incorporated than synthesized YnK, as exhibited by its increased band thickness. Self-made YnK also led to a visibly higher formation of truncated protein, possibly due to a lower amount of usable YnK present in the crude product following its direct application in protein expression after synthesis. On the other hand, recycled YnK samples exhibit a similar amount of truncated protein to the commercial YnK and similar fusion protein formation to the synthesized YnK sample. It is suggested that this is a result of nutrient

deficiency and simultaneous lack of available YnK for protein expression. Nevertheless, these results also indicate that the truncated protein is also produced at excess YnK, as proven by the presence of usable YnK in the recycled sample. As the integration of the ncAA always competes with the natural release factors, leading to the generation of truncated protein[20,21], it also suggested to decrease the expression temperature to slow down the metabolic rate and allow more time for faithful YnK integration.

Following protein expression and solubilization of the bvPrP containing inclusion bodies POI generation was also evaluated using LC-MS.

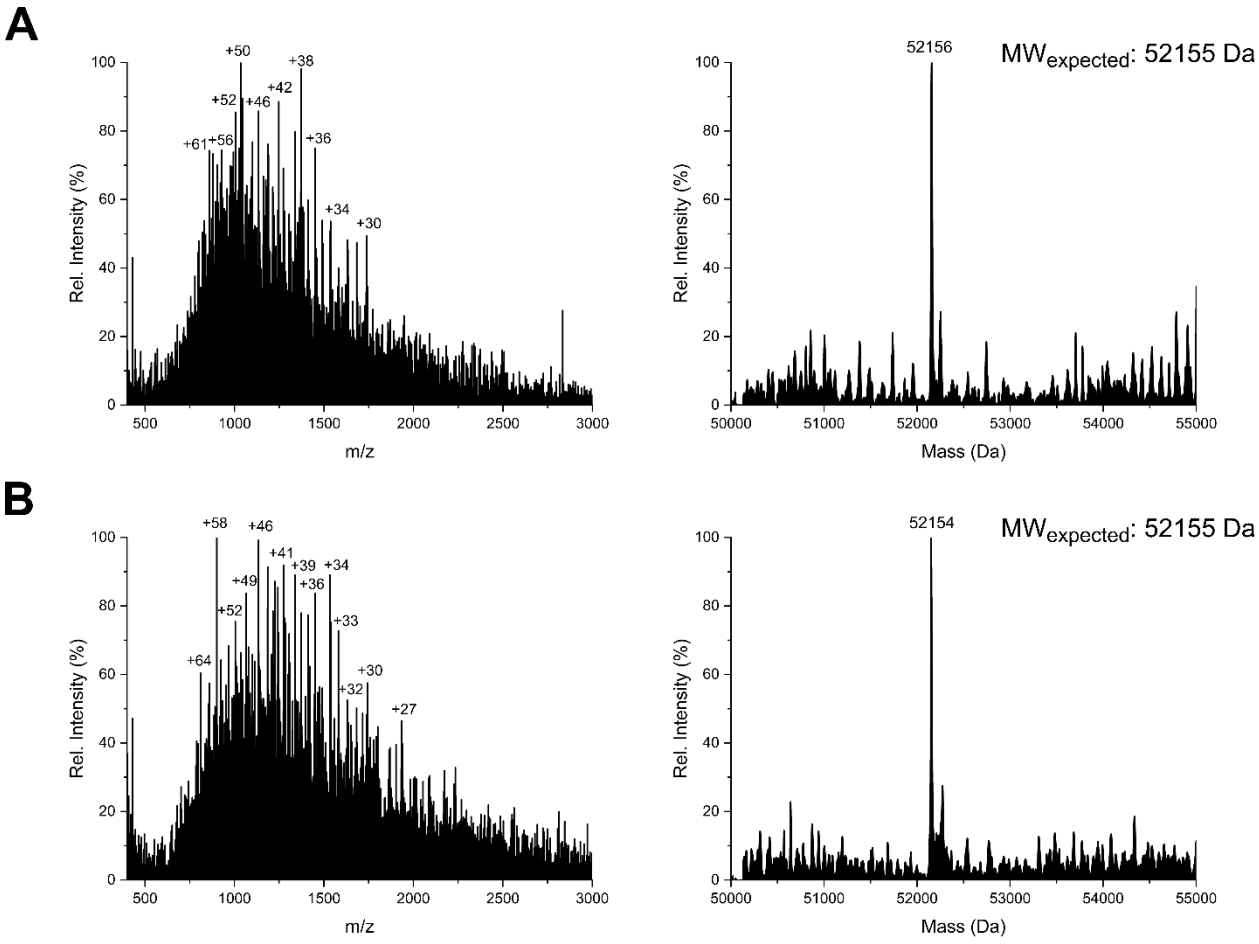

Figure 30: LC-MS spectra of bvPrP-N181X-YnK intein fusion proteins. A shows the crude protein generated using commercial YnK, B the protein produced using self-made YnK. The right panels depict the deconvoluted masses in Da.

As visible in **Figure 30**, both commercial and synthesized YnK led to the generation of bvPrP fusion proteins in accordance with the expected mass of 52,155 Da. However, it has to be mentioned that both of these LC-MS spectra are of low quality. This is possibly a result of lower POI concentration within the crude sample compared to the WT or AzK fusion proteins, resulting in a higher influence of co-elutants during the measurement. Product generated using recycled YnK expression medium was not evaluated separately as it contained YnK

which already had been successfully used for expression previously. After LC-MS evaluation all samples were combined. Next, Ni-NTA purification was conducted. **Figure 31** depicts the corresponding analytical SDS-PAGE.

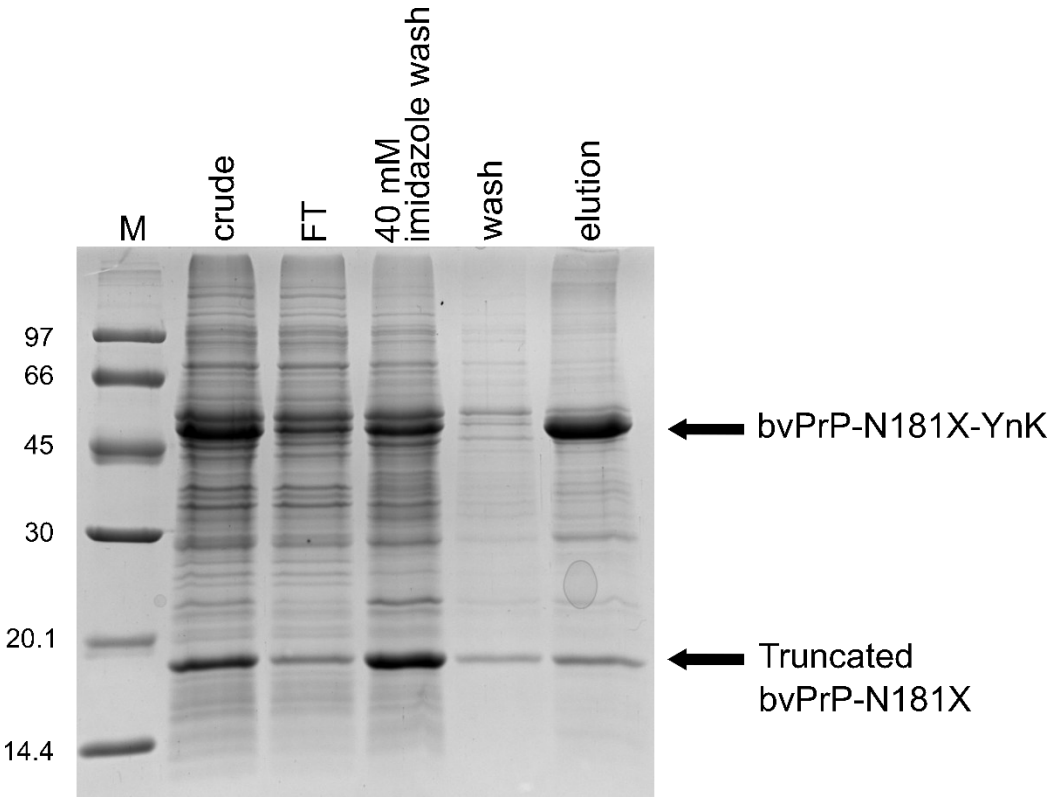

Figure 31: SDS-PAGE of a crude bvPrP-N181X-YnK solution undergoing Ni-NTA purification. The samples evaluated were 6 M GdnHCl solution (crude), the combined flow-throughs (FT), a 40 mM imidazole wash, the wash and the final 6 M GdnHCl 500 mM imidazole eluate (elution). Masses of the low molecular weight protein marker (M) are displayed in kDa.

Similar to the bvPrP-N181X-AzK purification, bands corresponding to the prematurely cleaved protein are visible in all samples at ~23 kDa. During this purification a 40 mM imidazole wash was employed to remove any unspecific binding from the Ni-NTA beads. However, it is clearly visible that alongside contaminants such as truncated protein also a high amount of product co-eluted during this step. Furthermore, a significant number of contaminating proteins is still present in the eluted sample. For another bvPrP-N181X-YnK crude protein solution a 20 mM imidazole wash was conducted during Ni-NTA purification instead. Here, no product was eluted but also barely any contaminants were removed. Therefore, we concluded that an additional imidazole wash is ineffective for this protein during Ni-NTA purification, possibly due to previously mentioned divalent cation affinity, and can be disregarded.[51] Moreover, the contaminants mentioned above are usually removed during the final RP-HPLC purification. Following Ni-NTA purification and subsequent buffer exchange to 8 M urea, hydrazinolysis was performed at a final concentration of 4 M urea, 50 mM DTT and 2 % hydrazine.

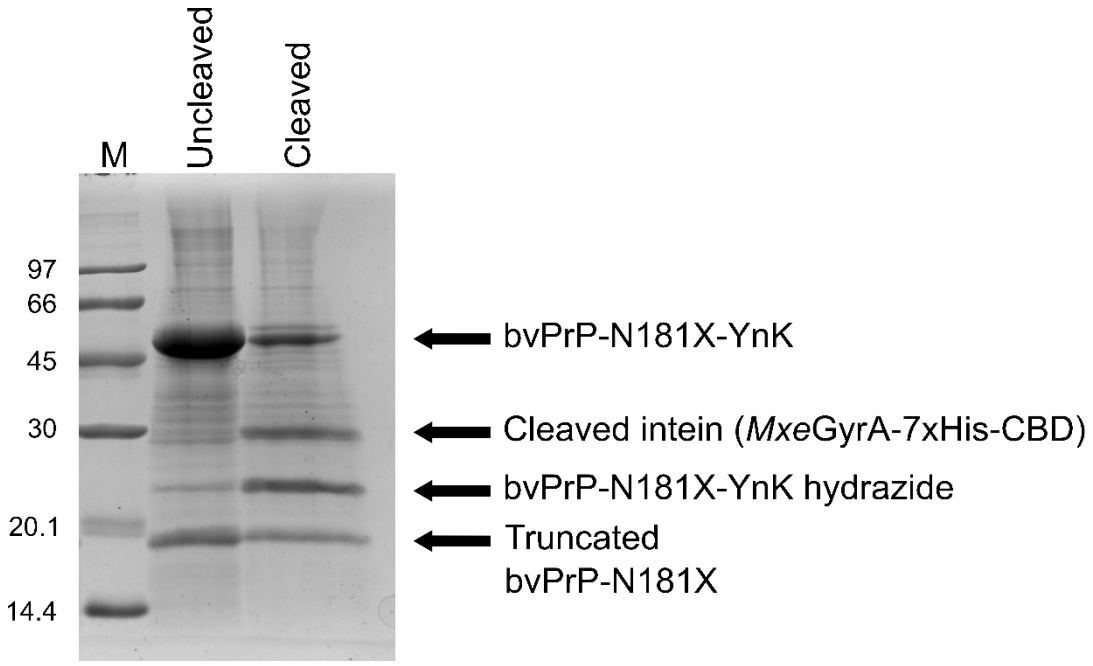

Figure 32: SDS-Page of bvPrP-N181X-YnK intein hydrazinolysis. The unreacted 8 M urea sample is denoted by “Uncleaved”, the post-cleavage sample as “Cleaved”. Masses of the low molecular weight protein marker (M) are displayed in kDa.

As shown in **Figure 32**, bands corresponding to the cleaved-off intein, at ~29 kDa, and the newly formed bvPrP-N181X-YnK hydrazide, with an expected mass of ~23 kDa, are visible in the analytical SDS-PAGE after the cleavage reaction, indicating successful hydrazinolysis. However, a starting material band is also still detectable at ~52 kDa, indicating an incomplete reaction. LC-MS analysis showed one mass peak with 23,118 Da (+7), which corresponds to the expected value of the bvPrP-N181X-YnK hydrazide (**Figure 33**).

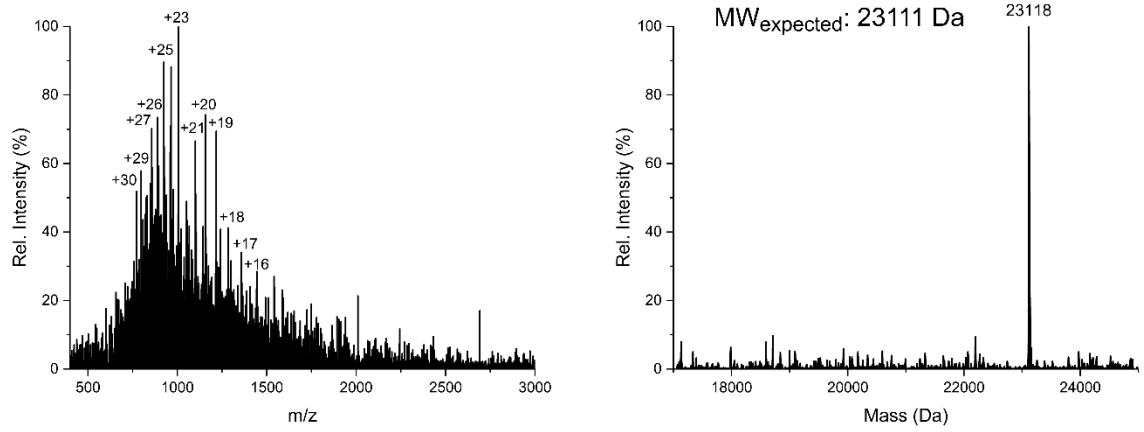

Figure 33: LC-MS spectrum of bvPrP-N181X-YnK hydrazide. The right panel depicts the deconvoluted masses in Da.

Following hydrazinolysis and subsequent RP-HPLC of the cleavage solution, the collected and lyophilized product was obtained at 10 mg/L. This is a 60 % decrease compared to the

AzK hydrazide yield, reinforcing the decreased incorporation and product formation observed using YnK instead of AzK. The lyophilized bvPrP-N181X-YnK hydrazide was then analyzed *via* DI-MS and HRMS to confirm the correct product identity.

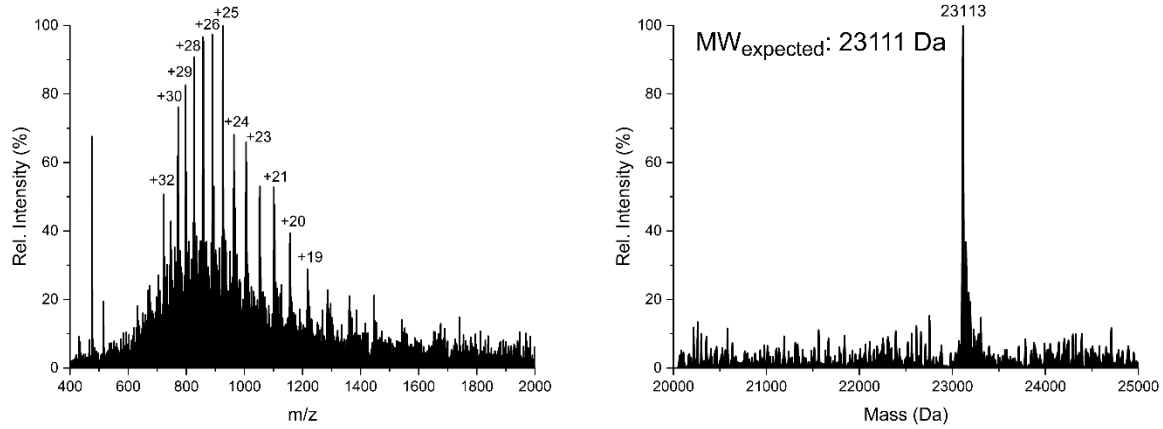

Figure 34: DI-MS spectrum of purified and lyophilized bvPrP-N181X-YnK hydrazide. The right panel depicts the deconvoluted mass in Da.

As shown in **Figure 34**, the final product, measured at 23,113 Da (+2), indeed corresponds to the expected mass of 23,111 Da when taking the acceptable mass deviations into account and, unlike the AzK containing analogue, does not undergo an undesired reaction during intein cleavage. The HRMS analysis further confirms this finding, with an exact mass measurement of 23,111 Da (**Figure 35**).

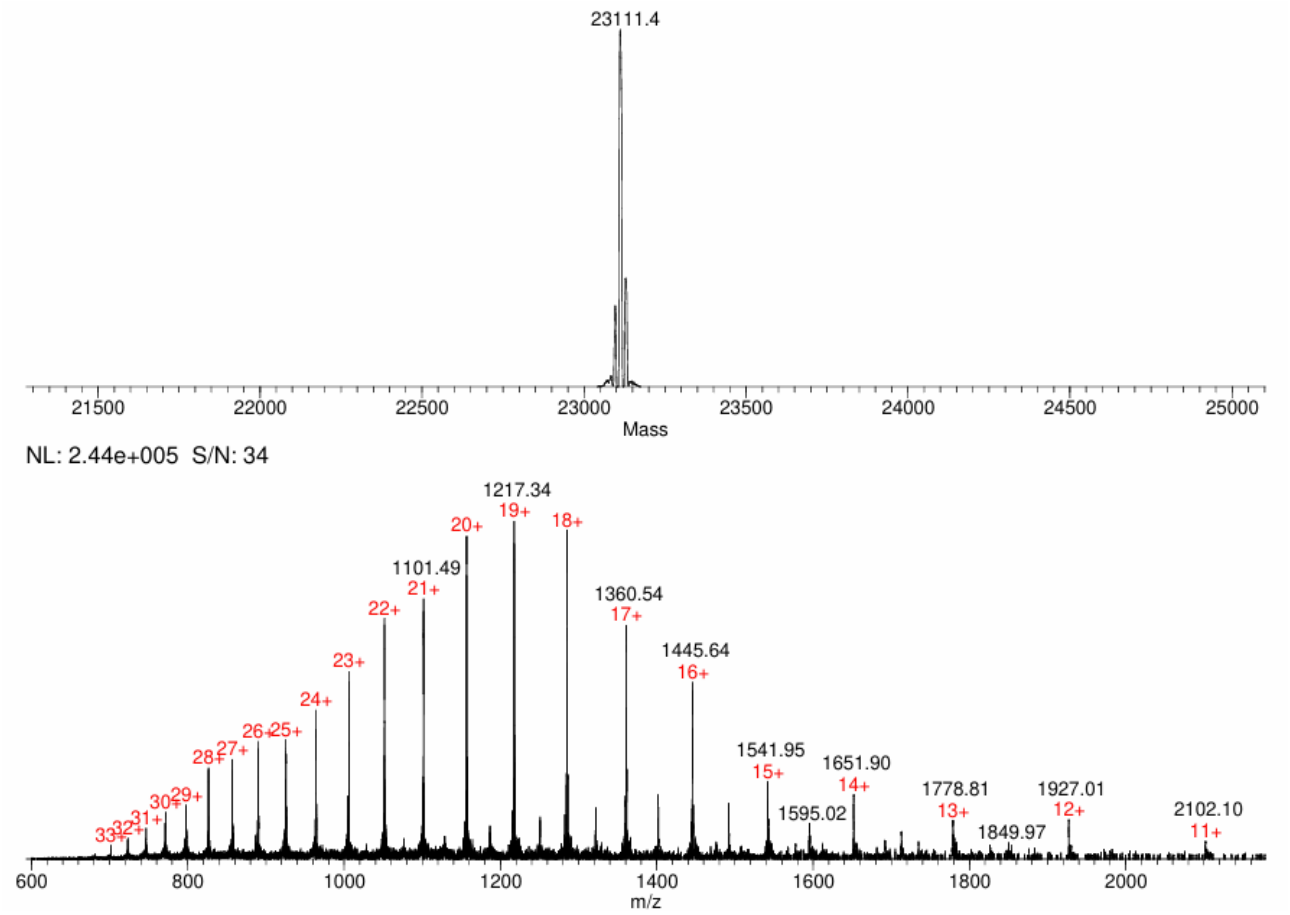

Figure 35: HRMS analysis spectra of the bvPrP-N181X-YnK hydrazide. The upper panel depicts the deconvoluted mass in Da.

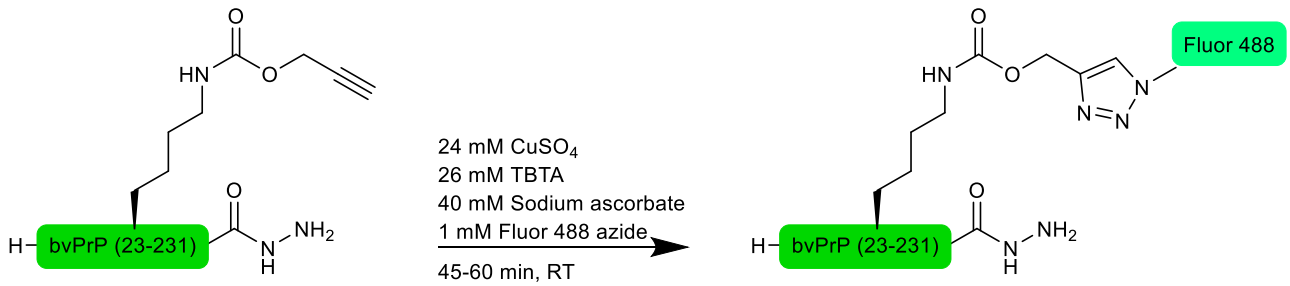

Figure 36: bvPrP-N181X-YnK hydrazide and Fluor 488 alkyne CuAAC reaction scheme

Finally, incorporation of YnK was further tested by conducting a CuAAC reaction with a Fluor 488 azide fluorophore using both a crude, uncleaved protein in 6 M GdnHCl solution as well as a cleaved, lyophilized sample dissolved in the same buffer (**Figure 36**).

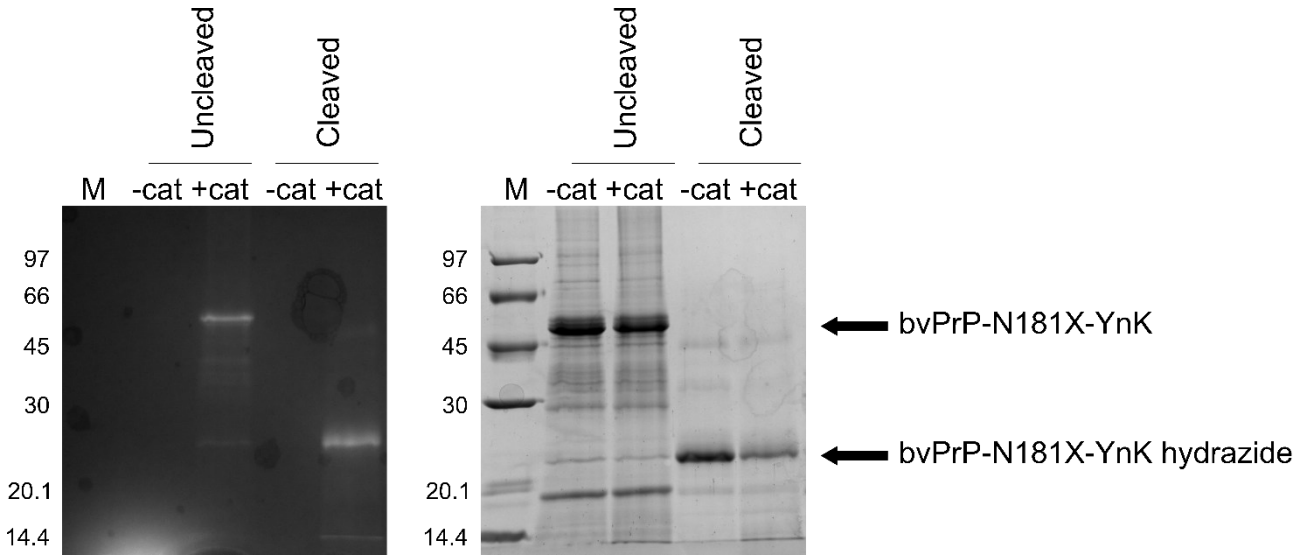

Figure 37: SDS-PAGE of bvPrP-N181X-YnK CuAAC reaction samples. The crude 6 M GdnHCl protein samples are denoted by “Uncleaved”, the purified, lyophilized samples by “Cleaved”. Samples supplemented with the catalytic pre-mix are denoted “cat+”, the negative control with “cat-“. The right panel shows the Coomassie stained gel, the left panel the gel under 488 nm light. Masses of the low molecular weight protein marker (M) are displayed in kDa.

Figure 37 depicts the corresponding analytical SDS-PAGE gel. Here, both the uncleaved and cleaved protein samples exhibit a clear fluorescent signal, indicating that the alkyne moiety within YnK is present in both samples. Nevertheless, it also must be noted that the contradicting band width of the intein fusion protein sample in the Coomassie stained gel and the gel evaluated under 488 nm light excitation suggests that some sample was left unreacted. This could have been alleviated by increased reaction time. The concentration difference of the cleaved samples may indicate re-solubilization issues following precipitation during sample preparation or incomplete dissolvement of the sample prior to transfer to a new Eppendorf tube. However, it may also be connected to the reaction reagents as also a minor difference is noticeable between the uncleaved sample in this regard. Furthermore, white precipitate was also noticed in the cleaved sample supplemented with catalytic pre-mix during the reaction, possibly influencing solubility of this sample. It is possible that precipitation also occurred during the AzK integrity CuAAC, as covered in the previous chapter, and was overlooked due to low visibility while conducting the reaction in dark conditions, explaining the previously detected differences in band width. This finding is further discussed in chapter 4.5.

4.4 bvPrP-WT hydrazide selenoester conversion and EPSL

To ultimately afford modified full-length variants of bvPrP with a C-terminal GPI anchor, selenoester conversion and subsequent EPSL were first performed to assess the standard reaction conditions used in our laboratory, with bvPrP-WT hydrazide serving as the starting

material. This reaction was conducted four times with a SPPS generated GPI anchor mimic (**Figure 38**), and once with a ubiquitin 46-76 fragment.

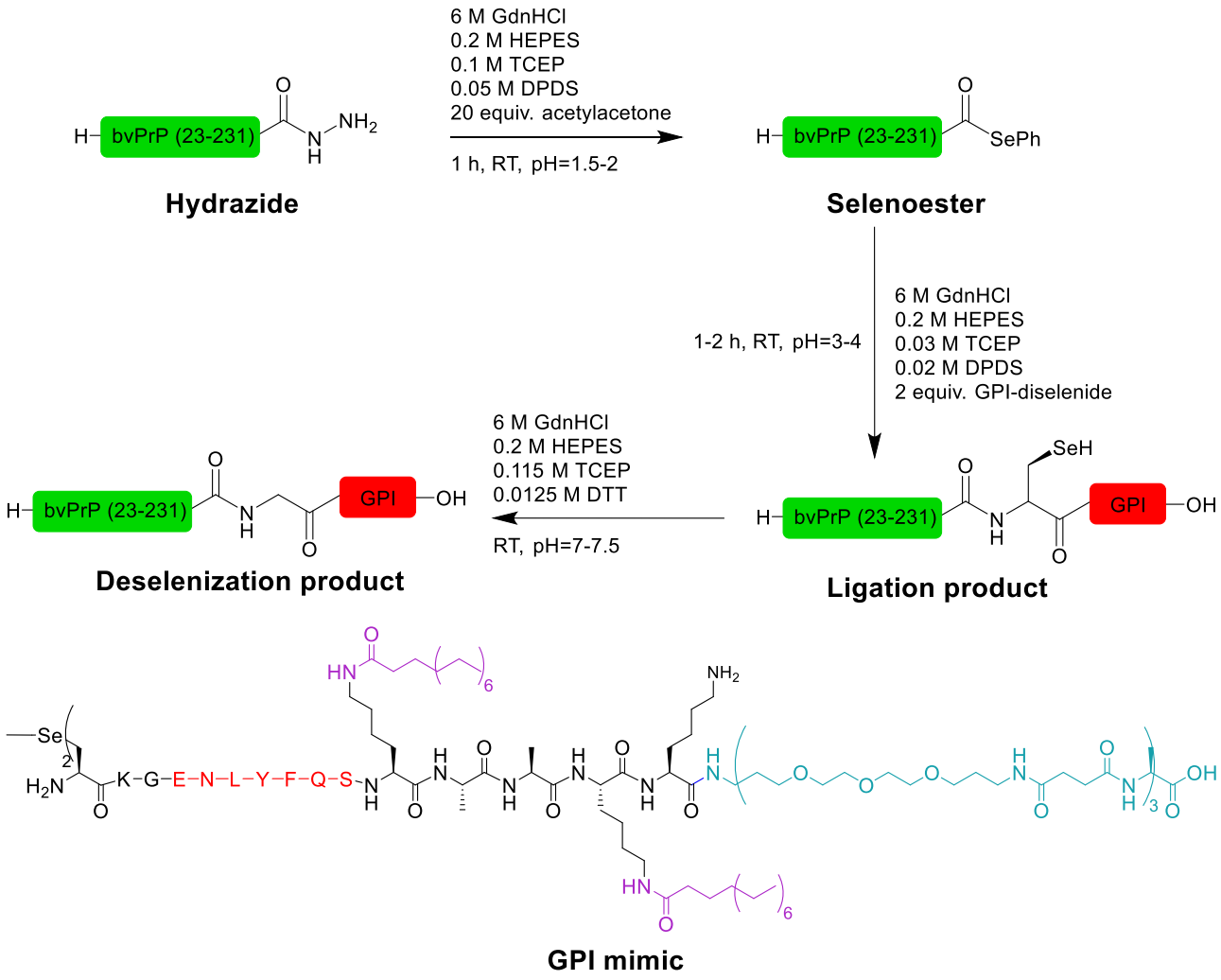

Figure 38: General bvPrP-WT and GPI EPSL reaction scheme with GPI mimic structure, with color-labeled TEV protease cleavage site (red), palmitoyl moieties (magenta) and a polyethyleneglycol polyamide trimer solubility tag (turquoise). The GPI mimic structure was adapted from the published version by Olschewski *et al.*[56]

Synthetic GPI anchor mimics have been used in previous works by Becker and co-workers to semi-synthetically produce PrP variants with and without additional N-glycosylation mimics through EPL or protein *trans*-splicing for a variety of subsequent evaluations.[54–56] The first two ligation reactions were executed in cooperation with a PhD student (A. Mägde).

During the initial EPSL performed using the GPI anchor two mistakes were made during selenoester conversion. First, the conversion buffer was not degassed prior to bvPrP-WT hydrazide dissolution. Secondly, the reaction mixture did undergo extreme pH changes during adjustment. Together these mistakes possibly affected the bvPrP-WT hydrazide or the generated protein selenoester by creating an oxidative environment facilitating unwanted side reactions, as evidenced by the mass changes below.

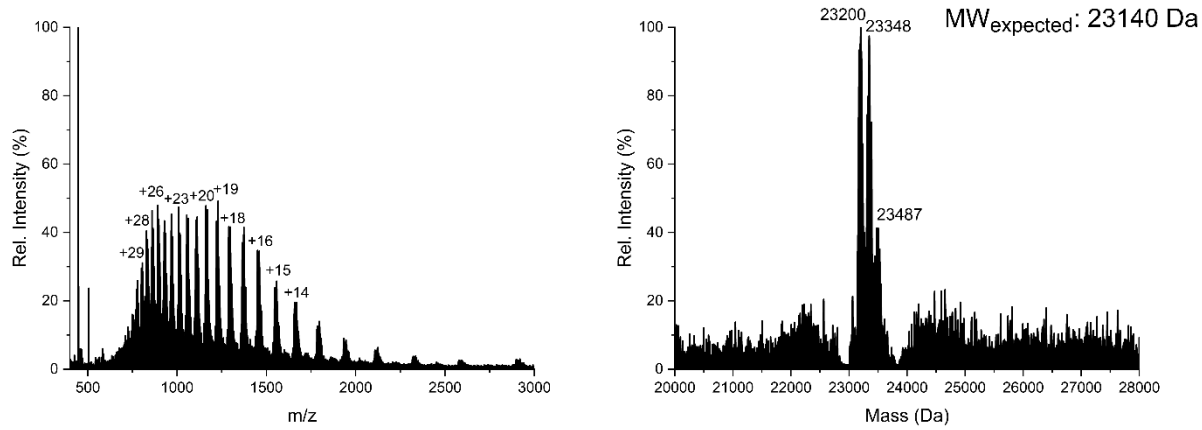

Figure 39: LC-MS spectrum of the first EPSL selenoester conversion. The right panel depicts the deconvoluted masses in Da.

During the selenoester conversion step the accompanying LC-MS measurement exhibited two main mass peaks at 23,200 Da (+60) and 23,348 Da (+208) and a minor 23,487 Da (+347) peak (**Figure 39**), which vary significantly from the expected mass of 23,140 Da. These masses also do not match single (23,296 Da) or double additions (23,452 Da) of selenophenol, which corresponds to +156 Da per moiety. Nevertheless, two equiv. of GPI-diselenide were dissolved in degassed DSL buffer and added to the reaction as we were unsure if these changes would affect the overall reaction progress.

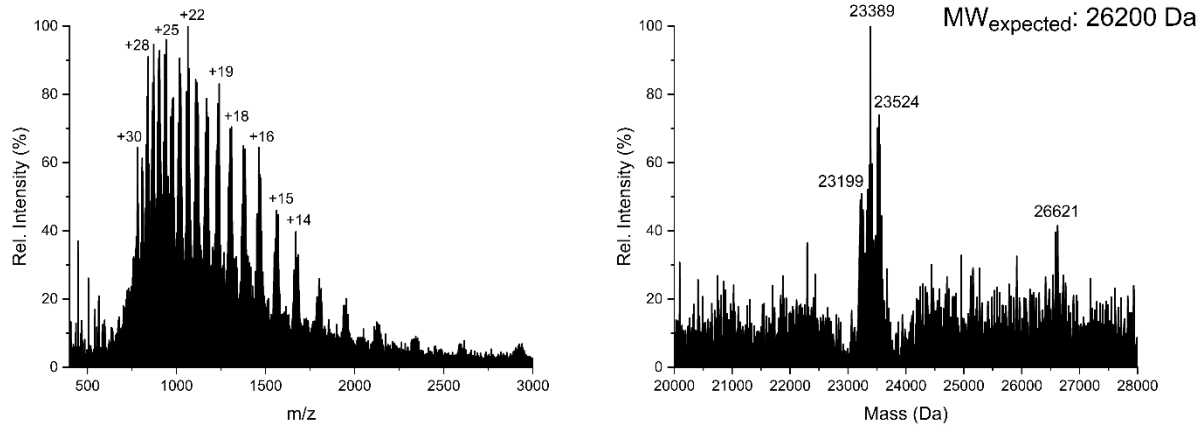

Figure 40: LC-MS spectrum of the first EPSL dieselenide-selenoester ligation to the GPI anchor. The right panel depicts the deconvoluted masses in Da.

The expected mass of the bvPrP-WT-GPI ligation product, 26,200 Da, was not detected (**Figure 40**). Instead, a peak at 26,621 Da (+421) was measured. Additionally, peaks at 23,199, 23,389 and 23,524 Da were found, which may correspond to the masses detected during selenoester conversion, indicating incomplete reaction. However, all detected masses still vary greatly from the expected masses for the selenoester or the ligation

product, and these deviations could not be assigned. Due to the extreme mass differences recorded during both reaction steps, possibly as a result of the errors made during the preparation of the selenoester conversion, the reaction was repeated.

As shown in **Figure 41**, the repetition did encompass the successful generation of the bvPrP-WT selenoester after approximately one hour, measured at 23,144 Da (+4). Additionally, a 23,296 Da (+156 Da) species was detected, which corresponds to an additional selenophenol moiety.

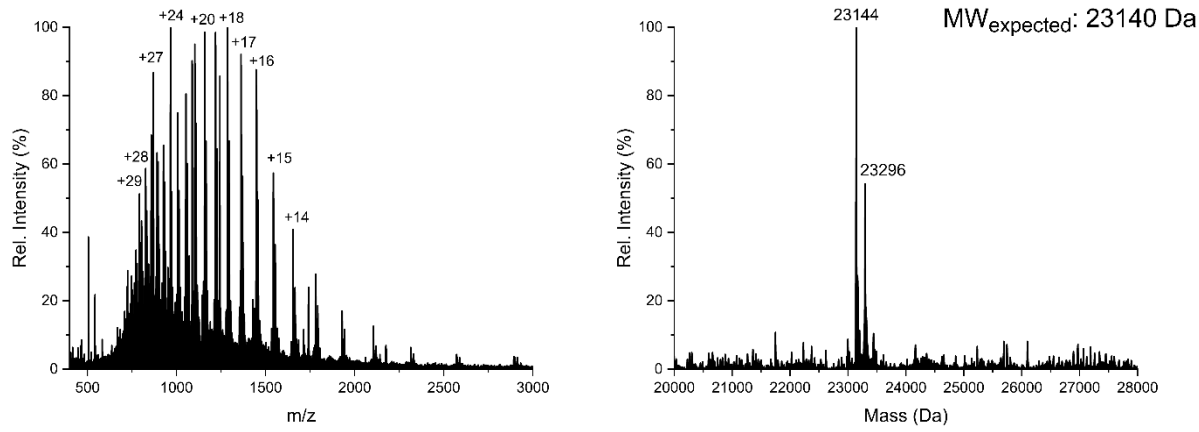

Figure 41: LC-MS spectrum of the second EPSL selenoester conversion. The right panel depicts the deconvoluted masses in Da.

The subsequent ligation of the selenoester to the GPI anchor only yielded minor product formation after 1.5 hours, with one or two additional selenophenols present, measured at 26,368 Da (+168), possibly with an additional hydrazide, and 26,535 Da (+335), with an additional sodium atom, respectively (**Figure 42**).

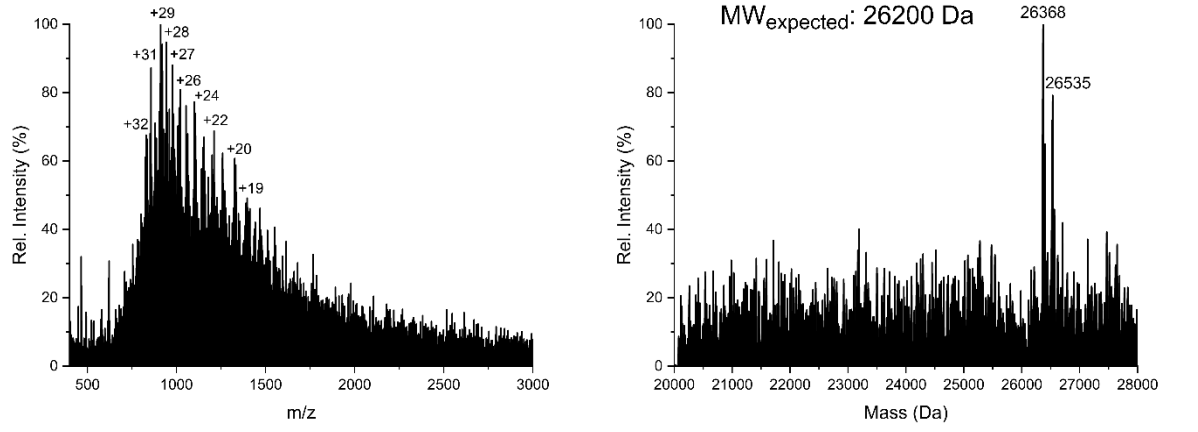

Figure 42: LC-MS spectrum of the second EPSL dieselenide-selenoester ligation to the GPI anchor. The right panel depicts the deconvoluted masses in Da.

However, significant amounts of starting material were left unreacted and detected with various excess masses. Furthermore, the following deselenization was unsuccessful and did not yield the desired product. As a 23,160 Da mass was detected here, which may correspond to the selenoester (+20), it can be speculated that deselenization did not reach completion. Nevertheless, the exact reason for deselenization failure during the deselenization reaction could not be determined.

To assess possible issues connected to the reaction conditions, EPSL was performed using a ubiquitin 46-76 fragment carrying an N-terminal selenocystein instead of the GPI-diselenide. It has to be noted that the reaction mixture was incubated at RT and 900 rpm throughout the experiment, as the solution exhibited increased viscosity following bvPrP-WT dissolvement in the conversion buffer. Following bvPrP-WT hydrazide dissolution in the conversion buffer, selenoester generation was detected after approximately 45 min of reaction time, as visible in **Figure 43.**

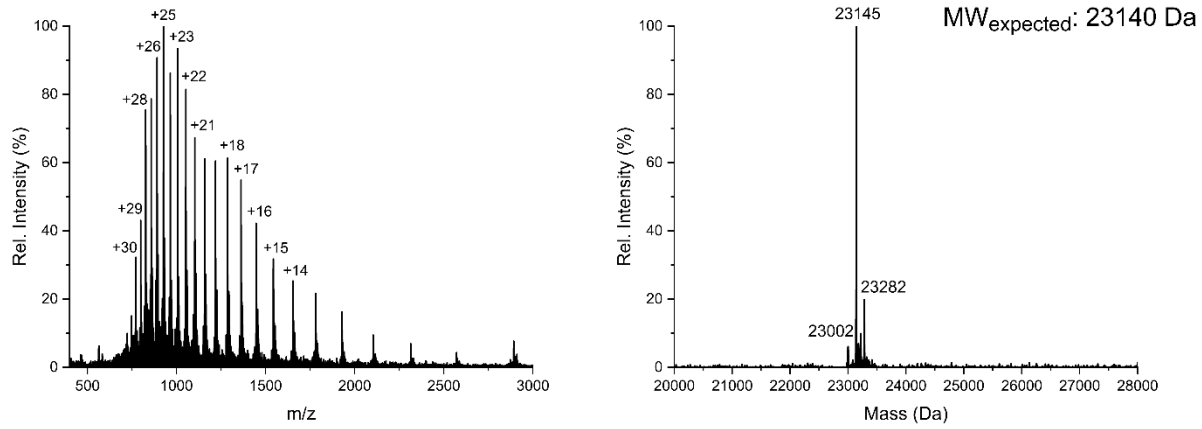

Figure 43: LC-MS spectrum of the third EPSL selenoester conversion. The right panel depicts the deconvoluted masses in Da.

In addition to the selenoester mass, at 23,145 Da (+5), a second and third mass, with 23,282 Da (+142) and 23,002 Da (-138) respectively, was detected. The second peak may correspond to a simultaneous loss of the C-terminal hydrazide and an additional bound phenylselenide functionality, while the third indicates the loss of the hydrazide moiety of the educt. The hydrazide loss may have occurred due to TCEP induced reduction. Next, 1.5 equiv. of ubiquitin 46-76 were dissolved in degassed DSL buffer and added to the reaction.

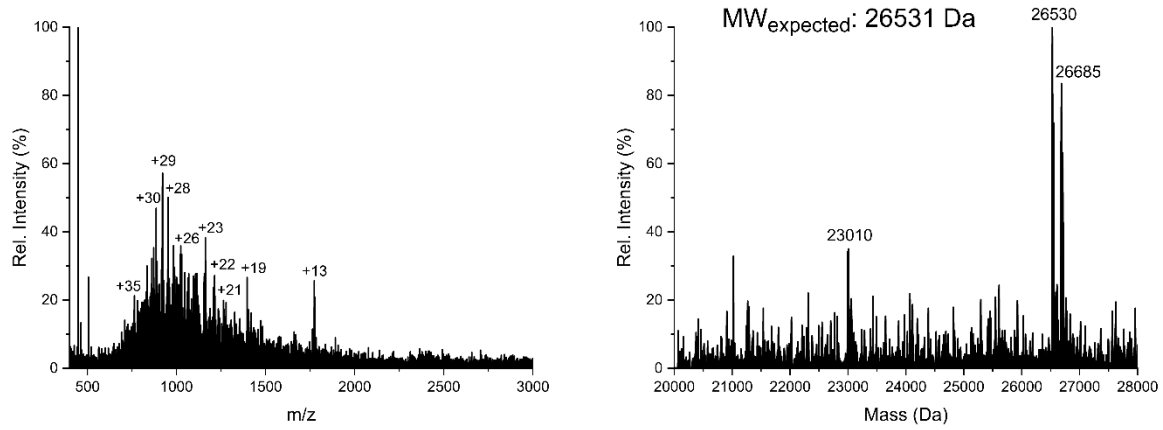

Figure 44: LC-MS spectrum of the third EPSL dieselenide-selenoester ligation to the ubiquitin 46-76 fragment. The right panel depicts the deconvoluted masses in Da.

Figure 44 depicts the LC-MS results after approximately one hour of reaction time. The expected mass, 26,531 Da, was detected as 26,530 Da (-1). Additionally, a second mass, at 26,685 Da (+154), was measured, coinciding with a second bound selenophenol moiety. A 23,010 Da (-5) mass corresponding to the bvPrP-WT hydrazide was also measured. After LC-MS evaluation of the DSL reaction, the reaction solution was flash frozen in liquid nitrogen and stored at -20 °C. The next day, following selenium extraction, approximately 60 % of the reaction volume was lost by accident during hexane removal *via* argon stream. Therefore, only 150 µL of deselenization buffer were added, and the reaction was run for three hours.

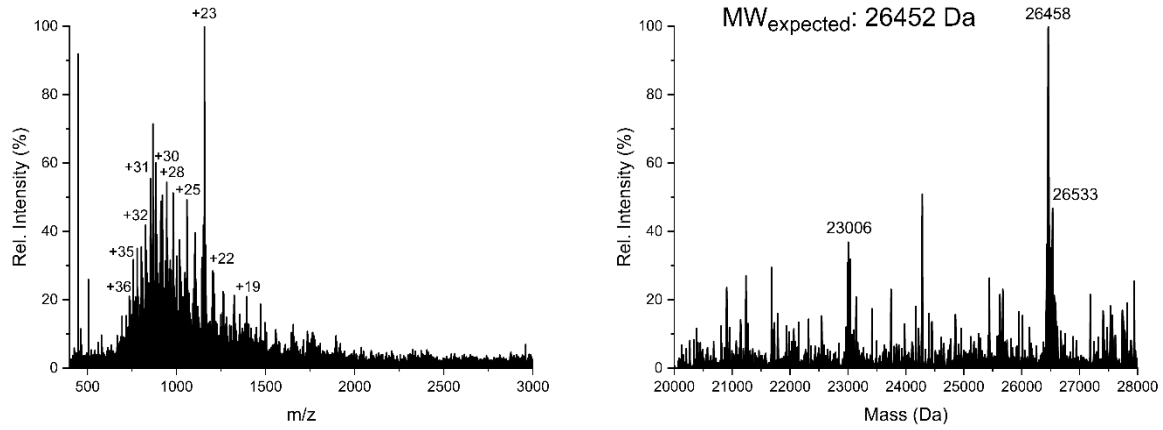

Figure 45: LC-MS spectrum of the third EPSL deselenization reaction. The right panel depicts the deconvoluted masses in Da.

As shown in **Figure 45**, the main mass corresponds to the expected product, 26,452 Da, measured at 26,458 Da (+6). The second highest peak, at 26,533 Da (+81), corresponds to an additional selenium atom. The 23,006 Da mass again coincides with the hydrazide educt.

Several unassignable mass peaks are also depicted, suggesting protein decomposition. Subsequent RP-HPLC purification and lyophilization yielded 2.2 mg (0.083 µmol), resulting in a 56 % yield. However, this result includes both a significant accidental loss as well as impurities, as the final analysis exhibited several non-product masses (**Figure 46**).

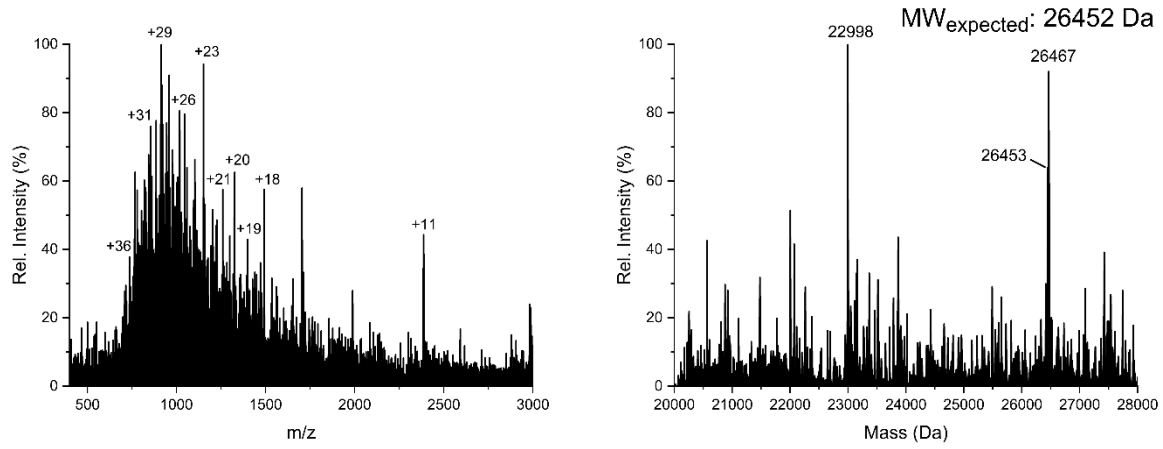

Figure 46: LC-MS spectrum of the third EPSL final analysis. The right panel depicts the deconvoluted masses in Da.

Higher product purity may be achieved through altering the RP-HPLC conditions. Nevertheless, this was not conducted for this reaction.

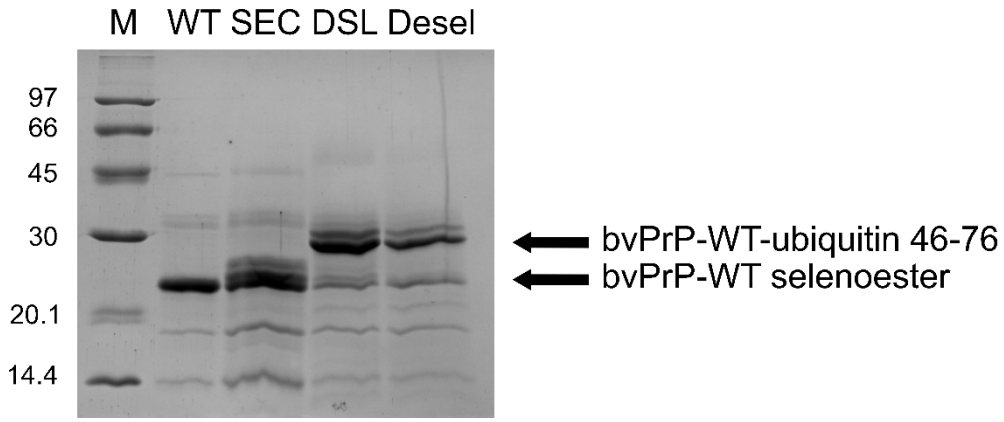

Figure 47: SDS-PAGE of bvPrP-WT and ubiquitin 46-76 EPSL samples. The bvPrP-WT hydrazide educt is denoted by “WT”, the selenoester conversion sample by “SEC”, the diselenide-selenoester ligation sample by “DSL” and the deselenization sample by “Desel”. Masses of the low molecular weight protein marker (M) are displayed in kDa.

The analytical SDS-PAGE conducted for this EPSL reaction also shows that the bvPrP-WT hydrazide to ubiquitin 46-76 ligation was successful (**Figure 47**). Moreover, the additional band above the bvPrP-WT-ubiquitin 46-76 ligation product, as seen in the DSL and deselenization samples, may indicate a second instance of bound ubiquitin 46-76 which was not removed during deselenization. This might have been alleviated by TCEP addition during sample preparation. The analytical HPLC runs performed for this reaction were conducted

with insufficient sample amounts and yielded poor results. Therefore, they could not be assessed.

As the preceding reaction showed that EPSL was possible at the conditions given, the reaction was repeated with the GPI-diselenide. The fourth reaction did yield the selenoester, however, due to a personal error, the GPI was not added during the DSL step, rendering the reaction unsuccessful. During the fifth reaction, the selenoester was obtained after one reaction hour, as shown in **Figure 48**.

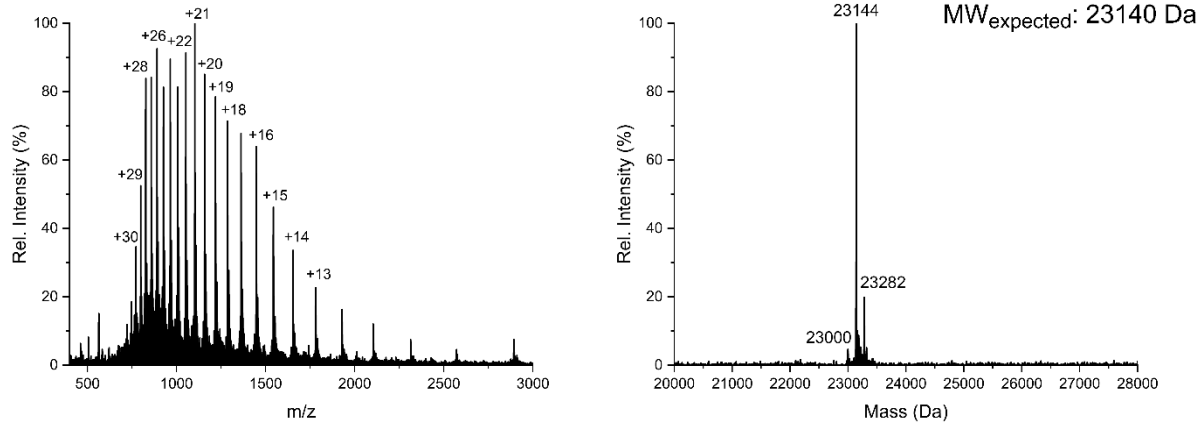

Figure 48: LC-MS spectrum of the fifth EPSL selenoester conversion. The right panel depicts the deconvoluted masses in Da.

Alongside the desired selenoester, the educt without its hydrazide at 23,000 Da (-15) and the product with a second selenophenol and simultaneous loss of a hydrazide, at 23282 Da (+142), were detected. The subsequent ligation to the GPI-anchor was also performed successfully, as exhibited by **Figure 49**.

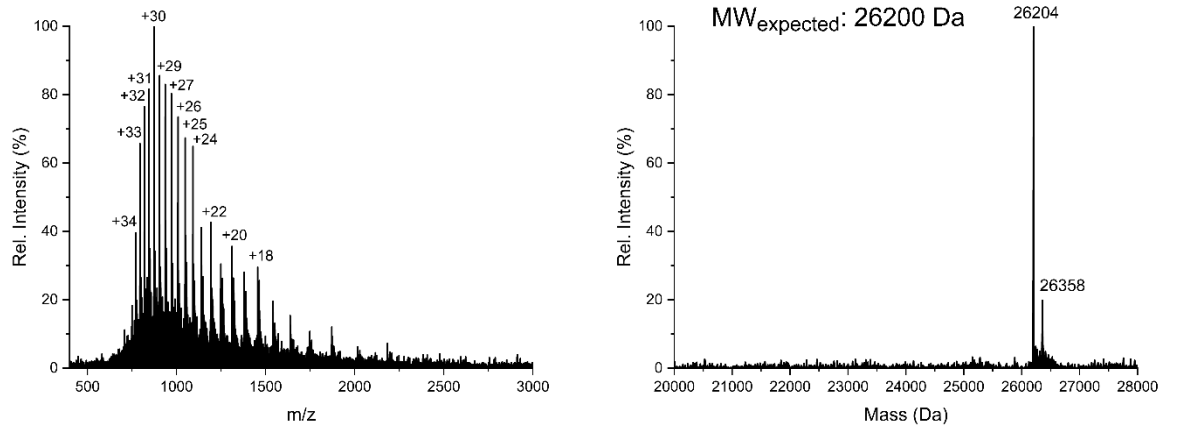

Figure 49: LC-MS spectrum of the fifth EPSL dieselenide-selenoester ligation to the GPI anchor. The right panel depicts the deconvoluted masses in Da.

Here, both the expected mass of 26,200 Da of the ligation product as well as the product with a second selenophenol moiety were found after two reaction hours. However, it must be noted that the GPI amount added may vary between 1.6 and 2.3 mg (1.7 – 2.4 equiv.) compared to the 1.9 mg (2 equiv.) normally used as the balance did change values extensively over time during weighing without further addition of material. Reweighing was disregarded due to the low GPI-diselenide amount remaining in storage and the possibility of material loss caused by electrostatics. Next, the reaction was flash-frozen and stored at -20 °C overnight. The next day, following hexane extraction of unreacted selenium, deselenization was conducted for two hours. During this reaction white precipitate formation was observed. As visible in **Figure 50**, only the deselenized ligation product with an expected mass of 26,121 Da was measured at 26,127 Da (+6) at the relevant chromatogram peak, indicating successful deselenization of the bvPrP-WT-GPI ligation product.

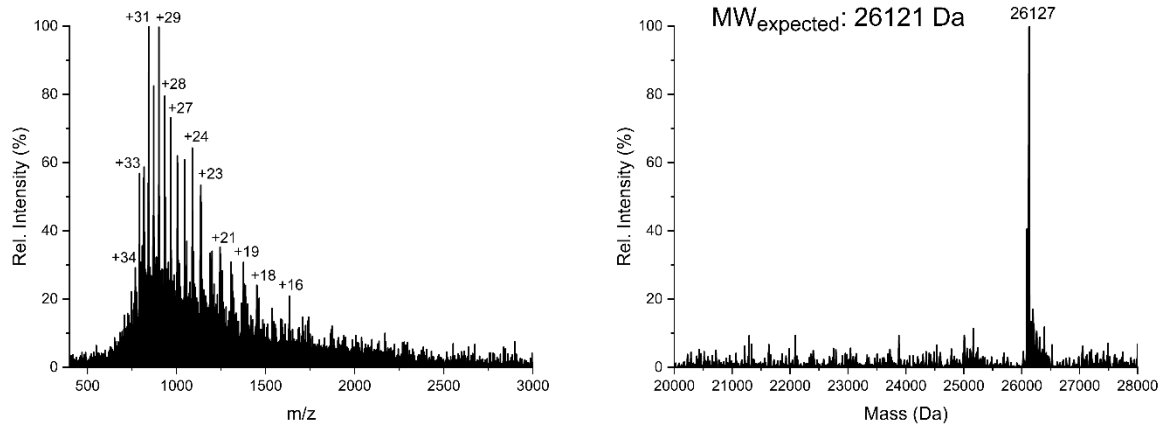

Figure 50: LC-MS spectrum of the fifth EPSL deselenization reaction. The right panel depicts the deconvoluted masses in Da.

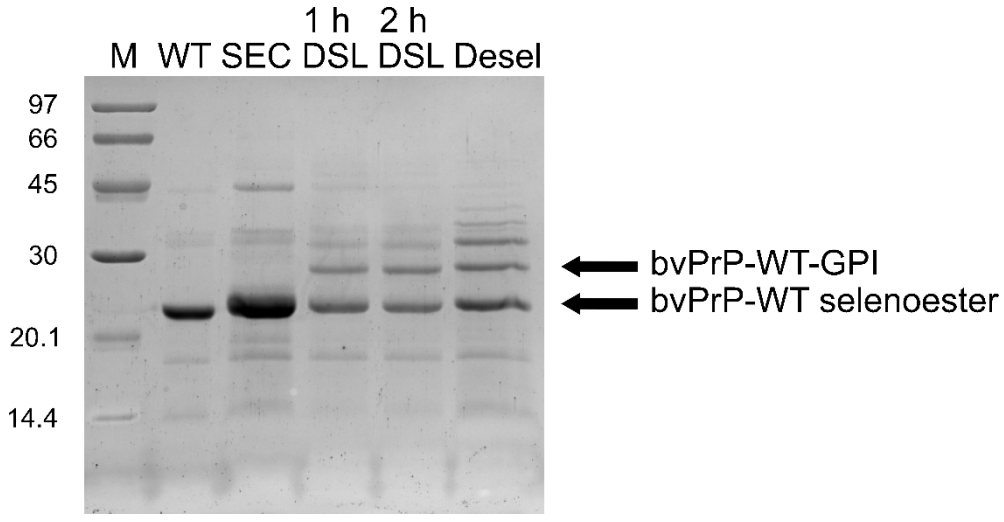

Figure 51: SDS-PAGE of bvPrP-WT and GPI ligation samples from the fifth EPSL. The bvPrP-WT hydrazide educt is denoted by “WT”, the selenoester conversion sample by “SEC”, the diselenide-selenoester ligation

samples by “DSL”, and include the timepoint of their sampling, and the deselenization sample by “Desel”. Masses of the low molecular weight protein marker (M) are displayed in kDa.

The analytical SDS-PAGE conducted for this reaction shows that, despite product formation, a significant amount of educt or selenonester intermediate did not undergo reaction, visualized by a thick band at ~23 kDa (**Figure 51**). Additionally, it is indicated that the additional hour of DSL did not increase reaction progress. Moreover, the bands above 30 kDa suggest the formation of significant byproducts, possibly additional GPIs, which could not be detected during LC-MS. However, as no TCEP was added during sample preparation, mixed selenide products could be expected.

To further assess the overall reaction progress, an analytical HPLC analysis was also conducted. The assignments for the identity of each peak were made based on the accompanying LC-MS measurement.

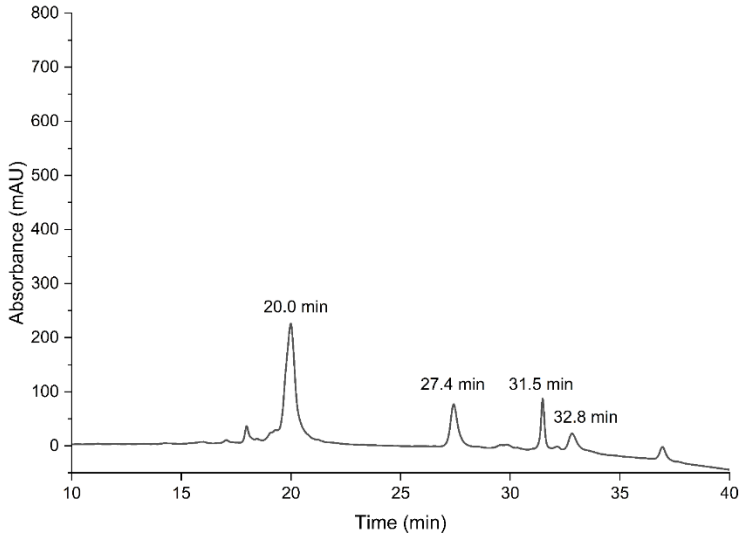

Figure 52: Analytical HPLC chromatogram of the fifth EPSL reaction following deselenization.

Figure 52 shows that approximately 70 % of the educt were converted into the selenoester (20.0 min) and did not undergo further reaction, whereas about 20 % correspond to the final bvPrP-WT-GPI product (27.4 min). The small peak to the left of the selenoester peak may coincide with the unreacted hydrazide, however, as it could not be detected during LC-MS, it was not assigned further. Nevertheless, this peak would correspond to the remaining 10 %. The two peaks at 31.5 and 32.8 min correspond to the GPI monomer and GPI-diselenide respectively. Strangely, in contrast to the SDS-PAGE, no mixed selenides could be detected.

Following RP-HPLC purification and freeze-drying, the bvPrP-WT-GPI product was received with a yield of 0.74 mg (0.028 µmol, 19 %). This percentage reflects the results obtained during HPLC and SDS-PAGE analyses. Due to time constraints no final analysis was performed for this product. Therefore, no exact conclusion about its final purity can be made.

Nevertheless, the overall yield is approximately 1.5-3 times lower than the yields mentioned in literature.[40]

Based on the successful bvPrP-WT hydrazide GPI-diselenide reaction it was concluded that no changes are made to the selenoesterification procedure, as it leads to almost complete conversion to the desired intermediate product. In contrast, changes to the DSL reaction conditions should be made, such as elevated TCEP concentration or raised reaction temperature, to increase the ligation efficiency. On a side note, and based on the first two unsuccessful reactions, it is suggested that EPSL is a delicate reaction that needs to be carried out carefully to avoid mistakes that significantly impact the reaction in terms of yield and overall success.

4.5 Glycan conjugation reactions

To evaluate the feasibility of successfully conjugating an azido-glycan to bvPrP-N181-YnK-GPI *via* CuAAC to obtain a glycosylated full-length bvPrP variant, the reaction was first explored using the bvPrP-N181-YnK hydrazide as well as acetyl-protected 1-azidomannose (**Figure 53**).

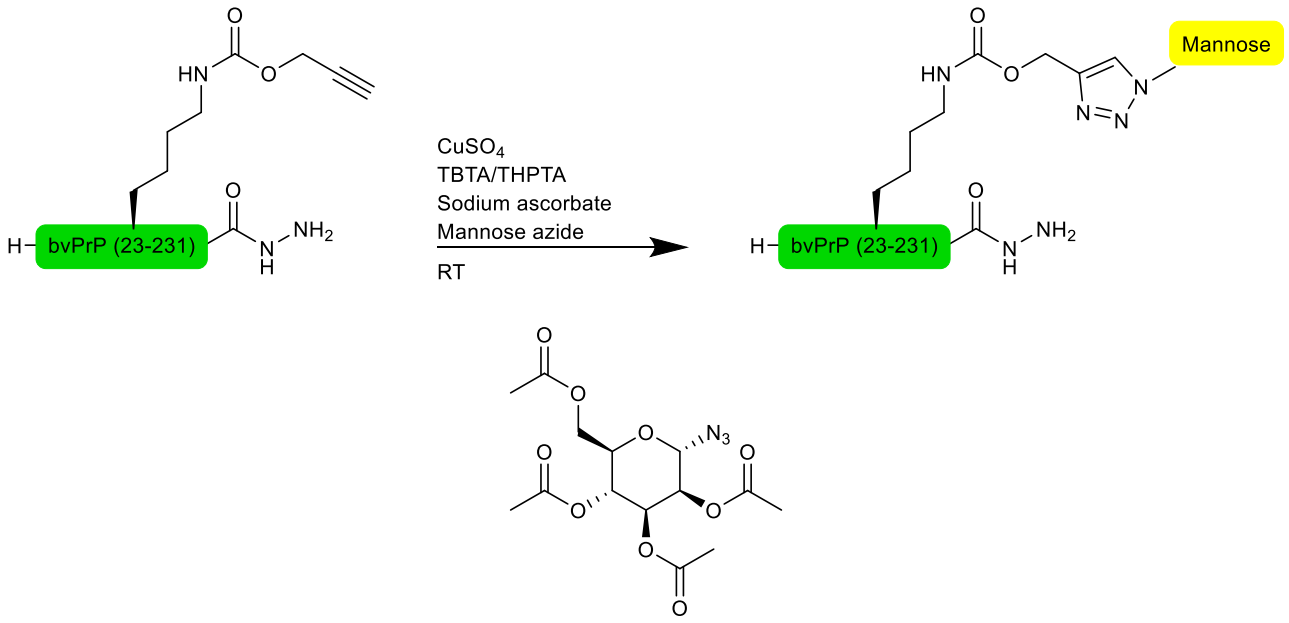

2,3,4,6-tetra-O-acetyl-α-D-mannopyranosyl azide

Figure 53: bvPrP-N181X-YnK hydrazide and azidomannose CuAAC reaction scheme. The structure of 2,3,4,6-tetra-O-acetyl-*α*-D-mannopyranosyl azide (azidomannose) is also depicted.

During the preparation of the pre-mix for reaction #1 (see **Table 7**) a small amount of precipitate formed following the addition of sodium ascorbate to the $CuSO_4$ and TBTA solutions already present in the Eppendorf tube. Further precipitation of a white solid was noticed following addition of the pre-mix to the dissolved bvPrP-N181X-YnK hydrazide and

azidomannose, which worsened after the addition of small amounts of dH_2O and 6 M GdnHCl (pH=8). The LC-MS spectra taken after one and two hours of reaction time did not yield any signals assignable to the hydrazide starting material, however a signal at 531 m/z, fitting to TBTA (MW=530), was detected in the main chromatogram peak. Thus, a sample was taken and precipitated with the ethanol procedure mentioned above to remove TBTA. The LC-MS analysis of this sample also did not yield any contrasting results. Subsequently, solubility of all reagents was tested at various DMF concentrations, concluding that 75 % DMF reliably dissolves all of them. Following subsequent catalytic pre-mix assembly, reaction #2 was performed using half the equiv. of the click reagents and 75 % less of the glycan compared to reaction #1. Here, also white precipitate formed over the course of the reaction and after 2 hours the LC-MS measurement yielded no assignable results apart from a 531 m/z mass peak. To further assess the reaction, analytical HPLC was conducted.

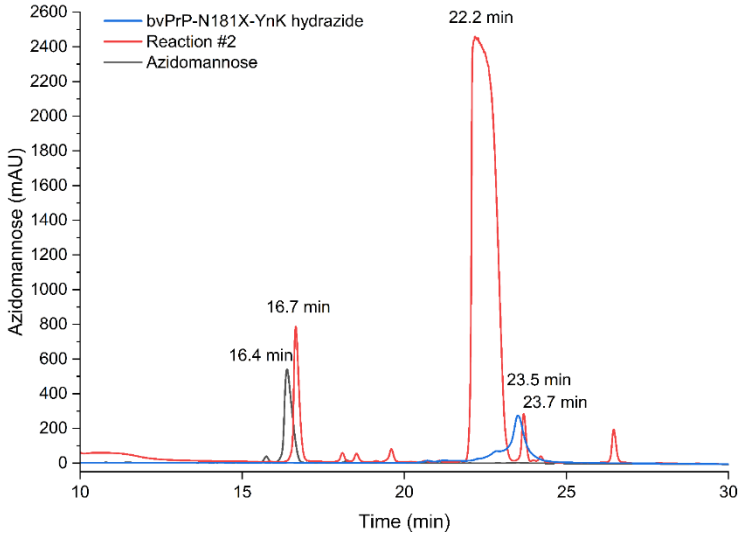

Figure 54: Analytical HPLC chromatograms of reaction #2 (red), azidomannose (black), and the bvPrP-N181X-YnK hydrazide (blue).

When comparing the HPLC chromatograms generated by the two starting materials to the reaction #2 chromatogram (**Figure 54**), peaks at 16.7 and 23.7 min corresponding to the azidomannose and the bvPrP hydrazide respectively, are clearly visible. However, a broad peak at 22.2 min, corresponding to TBTA, masks any potential product formed possibly eluting in this time frame. Therefore, reaction #3 was conducted using THPTA instead of TBTA, which is more water soluble and elutes earlier. Furthermore, the equiv. of the azidomannose as well as the CuAAC reagents was further reduced. As during ascorbate preparation some crystals did not dissolve in 75 % DMF, its DMF concentration was reduced to 32.5 %, leading to complete dissolution. Then, the pre-mix was assembled and the reaction carried out at ~75 % DMF as described above. During the first day of reaction #3,

the bvPrP-N181X-YnK hydrazide was detected throughout, however no product formation was observed. Additionally, crystal formation was observed. Therefore, the next day 50 additional equiv. of azidomannose, 20 µL of dH_2O, as well as the same equiv. of catalytic reagents from the day before were added to restart the reaction. Despite water addition, the crystals persisted in the solution. Furthermore, the solution became very viscous, possibly caused by the high amount of sugar added. The reaction was monitored by LC-MS for two additional hours, however no more starting material or any product formation was detected. Moreover, the accompanying analytical HPLC sample after approximately 6 h of total reaction time did only exhibit a single mannose peak at approximately 16.4 min (**Figure 55**).

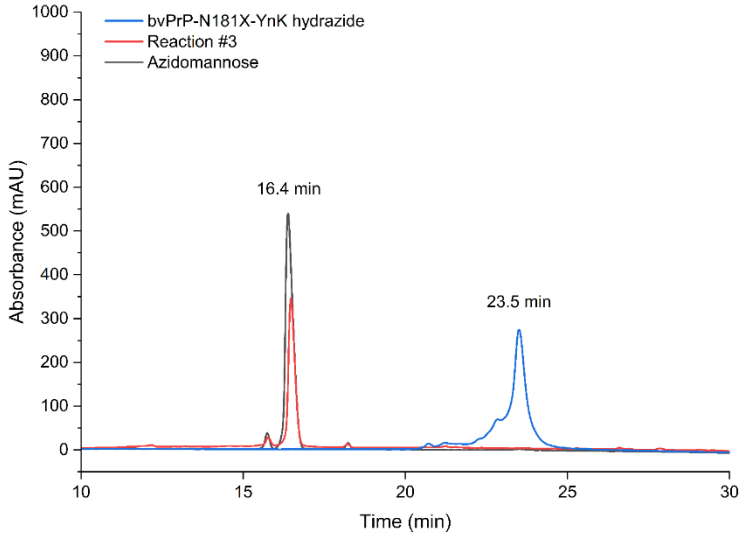

Figure 55: Analytical HPLC chromatograms of reaction #3 (red), azidomannose (black), and the bvPrP-N181X-YnK hydrazide (blue).

Next, reaction #4 was conducted using 51 equiv. of azidomannose, 22 equiv. of $CuSO_4$, 24 equiv. of THPTA and 37 equiv. of sodium ascorbate. After addition of the pre-mix to the reaction, white precipitate formed. Thus, 60 µL dH_2O were added, slightly decreasing the amount of precipitate. Like on the second day of reaction #3, the reaction #4 solution became very viscous, possibly due to the high amount of glycan present. After reacting for one hour, the precipitate had disappeared, however no educt or product were detectable during LC-MS. This did not change over the reaction time, with the final sample evaluated after 3 h 30 min after sample acidification with 0.6 M HCl. Similarly to reaction #3, only the mannose peak was detected at approximately 16.4 min during analytical HPLC (**Figure 56**).

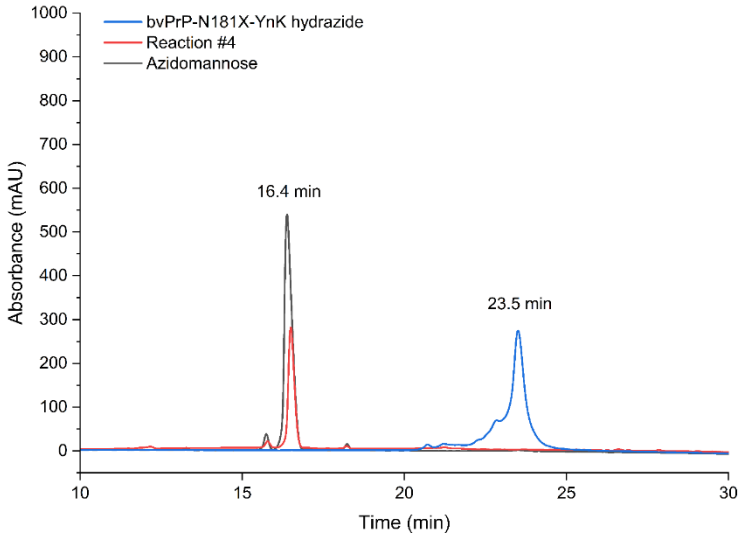

Figure 56: Analytical HPLC chromatograms of reaction #4 (red), azidomannose (black), and the bvPrP-N181X-YnK hydrazide (blue).

Finally, reaction #5 was performed using 13 equiv. of the azidomannose, 11 equiv. of $CuSO_4$, 12 equiv. of THPTA and 18 equiv. of sodium ascorbate. Here, the reaction mixture immediately became cloudy after pre-mix addition, which could not be improved by addition of 20 µL of dH_2O. After three hours of reaction time a blue coloration of the reaction solution was noticed. Therefore, 18 additional equiv. of sodium ascorbate were added, leading to the expected color change to yellow, indicating copper cation re-reduction. However, after approximately one hour the blue color had returned. During 4.5 h of reaction time, no product formation was detected *via* LC-MS. Furthermore, the mass corresponding to the bvPrP-N181X-YnK hydrazide could also not be verified at any time. The accompanying analytical HPLC analysis also did not show any product or educt besides the azidomannose peak at approximately 16.4 min (**Figure 57**).

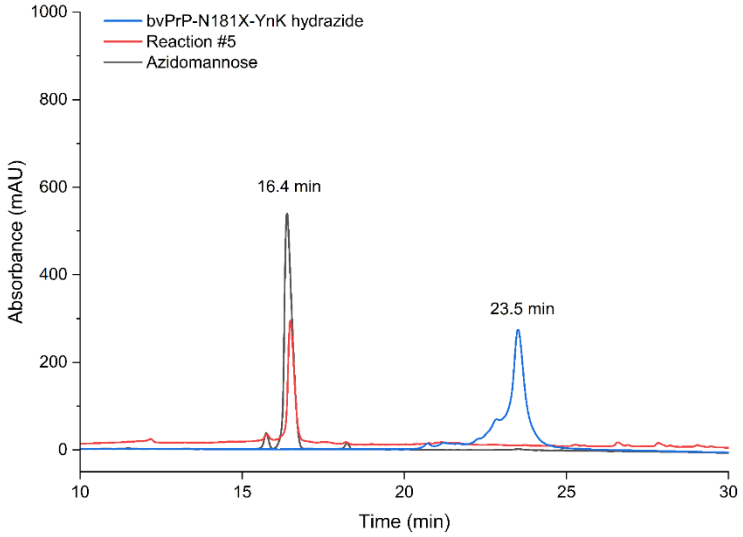

Figure 57: Analytical HPLC chromatograms of reaction #5 (red), azidomannose (black), and the bvPrP-N181X-YnK hydrazide (blue).

Therefore, analytical HPLC of the remaining reaction mixture was conducted using 50 % ACN, dH2O, DMF, 1M HCl and 6 M GdnHCl (pH=8) in this order, to attempt solubilization of any precipitate present. However, it must be mentioned that following 6 M GdnHCl treatment a gelatinous substance remained present, indicating incomplete solubilization. **Figure 58** depicts the corresponding chromatograms.

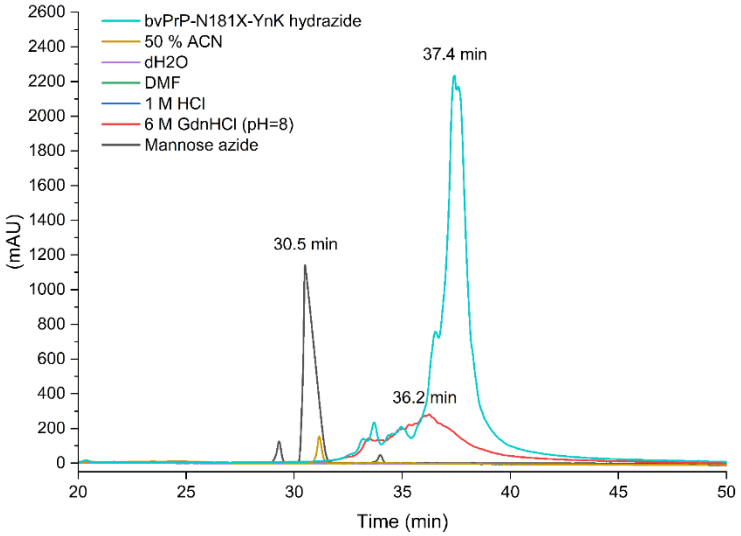

Figure 58: Analytical HPLC chromatograms of reaction #5 solubilization attempts. Sample and their corresponding colors: bvPrP-N181X-YnK hydrazide (cyan), 50 % ACN (yellow), dH_2O (violet), DMF (green), 1 M HCl (blue), 6 M GdnHCl (pH=8) (red), azidomannose (black).

Here, azidomannose can be detected in the 50 % ACN sample, with the small absorbance peak probably corresponding to a high degree of dilution of the sample. Furthermore, a broad peak at 36.2 min is visible in the 6 M GdnHCl sample, which is approximately situated in between the educt elution peaks and could correspond to a potential product peak. No significant peak was detected in the dH2O, DMF or 1 M HCl extracts. Overall, product formation ultimately cannot be deduced from these analyses. As a final attempt to assess product generation, an analytical SDS-PAGE was conducted for all reactions, as shown in **Figure 59**.

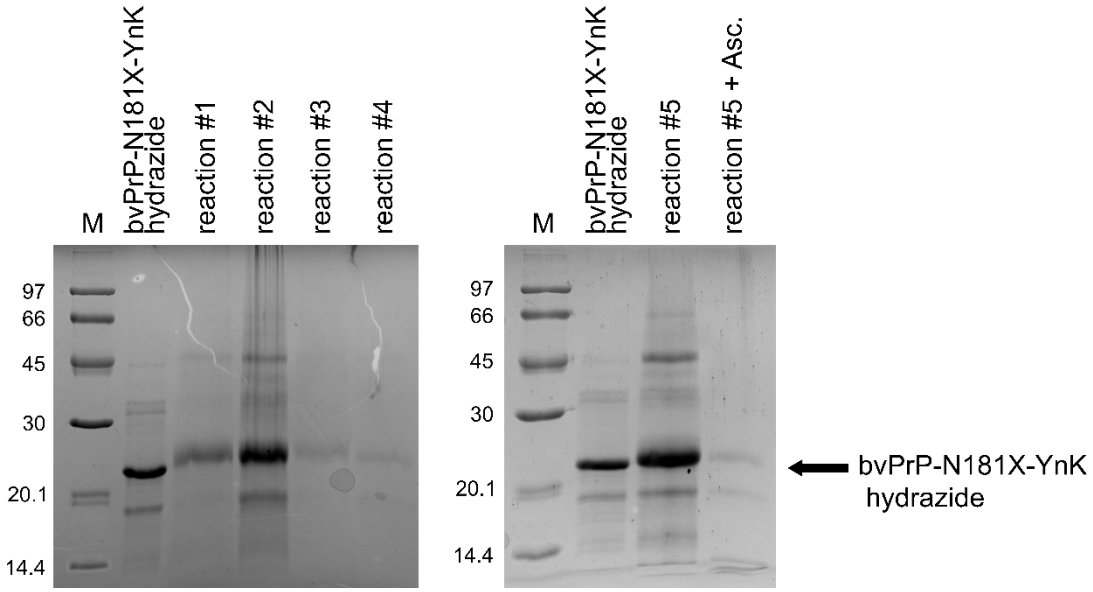

Figure 59: SDS-PAGEs of bvPrP-N181X-YnK CuAAC glycan conjugation reaction samples. The gels show samples from Reaction #1 to #5, with a second reaction #5 sample after sodium ascorbate addition (reaction #5 + Asc.) as well as unreacted bvPrP-N181X-YnK hydrazide samples. Masses of the low molecular weight protein marker (M) are displayed in kDa.

Here, all reaction samples are accompanied by an increase in size compared to the hydrazide educt (23,111 Da). However, as the contaminant bands also visibly increased in mass, it cannot be concluded that any reaction was performed successfully. Furthermore, the expected product mass of 23,474 Da, corresponding to a 373 Da mass increase, may not be visible using an SDS-PAGE with 15 % of acrylamide and may require a significantly increased percentage to successfully separate the respective bands, if feasible at all. Additionally, samples of reactions #1, #3, #4, and #5 with added ascorbate show hardly visible bands, which may correspond to insufficient sample amount, the catalytic reagent equiv. used, the DMF solvent concentration, increase of precipitation with longer reaction times or solubilization issues during sample preparation.

Overall, it could not be determined whether the monitoring problems mask successful synthesis of the azide-alkyne coupled product or, if in fact the reaction conditions are unsuitable to conduct this reaction and require adaptation. However, when assessing all reactions performed it is suggested that a high degree of precipitation mostly occurs at high catalytic pre-mix concentrations, such as recorded for reactions #1, #2 and #4. Similar findings have also been reported during the previous CuAAC reactions conducted for ncAA integrity verifications (see 4.2, 4.3). These results correspond to the reported aggregation tendencies of recombinant PrP at high copper concentrations, which may undergo reversible aggregation at low, non-physiological temperatures.[51,57] Furthermore, proteins in general may precipitate due to the presence of CuAAC reactants such as $CuSO_4$ or sodium

ascorbate.[58] Nevertheless, this finding was contradicted by reactions #3 and #4, as the former did not exhibit additional precipitation after restarting the reaction with more pre-mix and the latter exhibited precipitate disappearance at RT over time. Moreover, reactions #1 and #3 indicate that a high DMF solvent percentage used during pre-mix assembly or the reaction itself, respectively, are presumably accompanied by sodium ascorbate precipitation. However, this exact result could not be reported during the remaining reactions and may have been masked by general precipitation occurrences. The solubilization experiments performed with reaction #5 indicate that 6 M GdnHCl may alleviate some solubility issues and enable reaction monitoring. Nevertheless, this finding was not evaluated further. Additionally, the continued presence of precipitate during treatment with the various solvents mentioned above indicates the possibility that samples also did precipitate during LC-MS or analytical HPLC sample preparation, preventing meaningful measurements.

It is suggested that the glycan conjugation reaction is repeated with the bvPrP-N181X-YnK hydrazide dissolved in 6 M GdnHCl, with approximately 10 equiv. of azidomannose to prevent viscosity accompanied by a further reduction of the pre-mix reagent equivalents while keeping the DMF percentage low to prevent potential protein or ascorbate precipitation. Moreover, an addition of EDTA to remove the copper ions from the protein prior to measurement, as mentioned in literature, may alleviate PrP aggregation and enable reaction monitoring.[51,59] Alternatively, if these changes do not enable LC-MS or HPLC monitoring, the resulting product may be assessed through a tryptic digest to infer product formation.

4.6 N-*ε*-(prop-2-ynyloxycarbonyl)-L-lysine (YnK) synthesis

Due to the increasing costs posed by continuous YnK demand for recombinant bvPrP-N181X-YnK expression, a more affordable alternative in the form of organic synthesis was explored further. The procedure published by the Lemke group utilizes a cheap starting material in the form of Boc-L-Lys-OH and allows the direct application of the synthesized YnK hydrochloride salt in protein expression without any prior purification steps.[48] This reaction was performed in cooperation with a PhD student from the Becker group (A. Mägde).

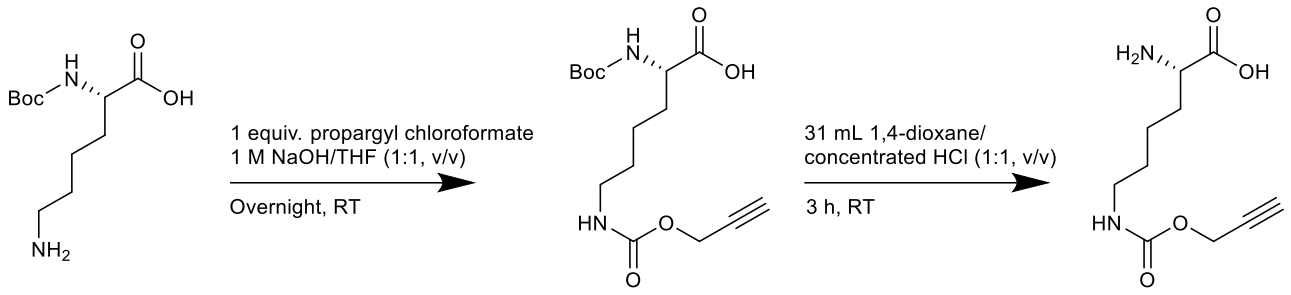

Figure 60: Reaction scheme of the synthesis of YnK.

YnK synthesis was conducted in two steps at a 9.85 mmol scale by first functionalizing the *ε*-amine group of 1.2 equiv. Boc-L-Lys-OH with propargyl chloroformate *via* nucleophilic substitution in basic conditions at RT overnight.[60] Following acidification, extraction with EtOAc, $MgSO_4$ assisted drying of the organic phase and solvent removal, a yellow oil was received. For the second step, the yellow oil was redissolved in a 1:1 1,4-dioxane/concentrated HCl solution without further purification and left to react for 3 h at RT, causing Boc removal. A waxy, brown product with a yield of 2.665 g (10.05 mmol, 102 %) was received after subsequent solvent removal, re-solubilization of the distillation residue in 1 M HCl and lyophilization. The product identity was then verified *via* LC-MS, ^{1}H-NMR as well as ^{13}C-NMR. In addition to the high yield, which is also reported in the original literature[48], the surplus yield of the received YnK product (MW=228) suggests the formation of side products, which presumably are the lysine educt without its Boc protecting group (MW=146) as well as the Boc-containing intermediate (MW=328), possibly also accompanied by incomplete solvent removal. As visible in the LC-MS spectrum (**Figure 61**), the two detected compounds exhibit mass deviations of +10 and +29 from the suspected masses respectively, and these deviations could not be assigned further.

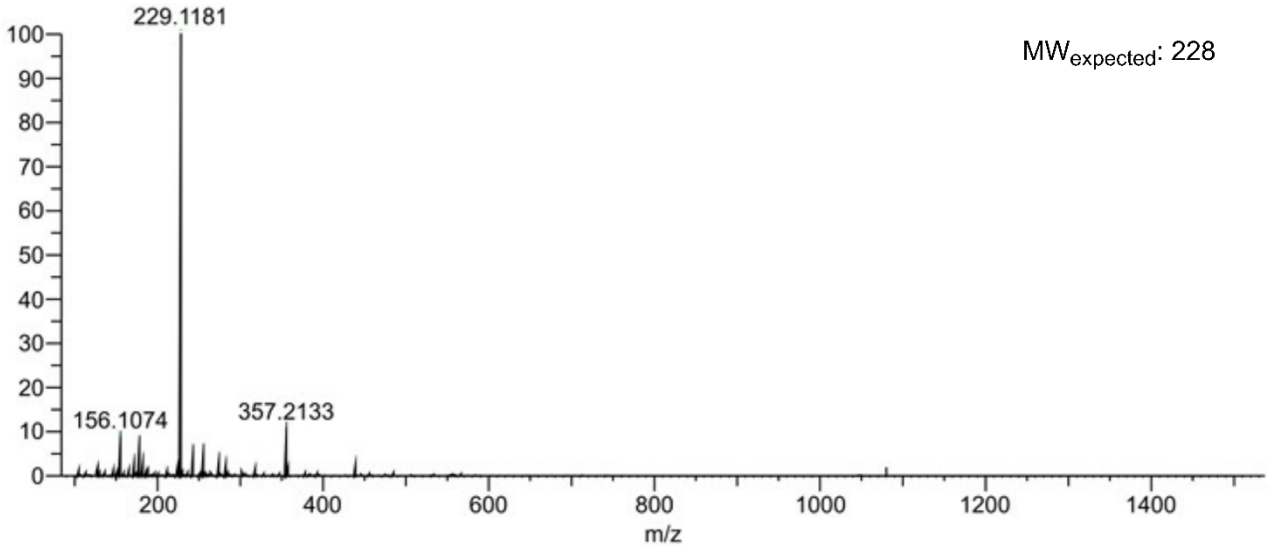

Figure 61: Deconvoluted LC-MS spectrum of the synthesized YnK sample.

The presence of side-products is also detectable in the ^{1}H-NMR spectrum and is mainly exhibited by the presence of an additional integrated proton. Moreover, the carboxylic proton is also missing from the spectrum, therefore resulting in two additional protons.

5. Conclusion

The aim of this thesis was to semi-synthetically produce two full-length bvPrP variants with appended C-terminal GPI-anchor mimics as well as glycan mimicking modifications at the native N-glycosylation positions 181 and 197 *via* a combination of GCE, EPSL and CuAAC techniques.

Protein expressions in the presence of the ncAA AzK, bearing an azide moiety, were conducted to generate the recombinantly produced N-terminal segments as intein fusion proteins. However, it was discovered that the bvPrP-N181X-AzK azide functionality is reduced to an amine during the intein cleavage reaction, presumably by the DTT present in the cleavage solution.[52] This renders the AzK containing protein hydrazides unusable for subsequent CuAAC conjugations, as evidenced by an unsuccessful reaction with Fluor 488 alkyne. bvPrP-N197X-AzK could not be assessed due to product loss during RP-HPLC purification. Its generation was not repeated due to the azide reduction issues also making this variant useless for further experiments. Following these discoveries, protein expression of the bvPrP-N181X variant was conducted with the DTT-stable ncAA YnK, which contains an alkyne functionality instead. Experiments showed that, unlike bvPrP-N181X-AzK, the YnK intein fusion protein does not undergo any unwanted side-reactions during the cleavage reaction but was obtained in lower, but still good amounts. Therefore, the generated protein hydrazide was suitable for subsequent CuAAC reactions, as demonstrated by a successful conjugation to Fluor 488 azide. However, the subsequent CuAAC reaction performed with an azidomannose glycan could not be monitored due to precipitation of the analytes. Thus, it is suggested that this reaction is repeated using adapted conditions and is evaluated *via* tryptic digest if the monitoring problems persist.

A selenoester conversion and subsequent EPSL reaction was conducted with bvPrP-WT hydrazide and GPI-diselenide to infer the general feasibility of the reactions. While the selenoester conversion conditions generated the bvPrP-WT selenoester reliably at high yields, subsequent EPSL and deselenization required repeated attempts as the reactions are very sensitive to any mistakes made during preparation or the reactions themselves. The desired bvPrP-WT-GPI was finally obtained, however, to generate the yields described by Kulkarni *et al*.[40] it is required that the standard reaction conditions during EPSL are adapted suitably to achieve higher ligation efficiencies.

The synthesis of the YnK ncAA was also conducted successfully and should lower the economic burden for the production of the modified protein variants in greater amounts. Successful incorporation of YnK synthesized in-house was also demonstrated.

If the issues regarding glycan conjugation and EPSL mentioned above can be solved, sufficient amounts of bvPrP-GPI variants can be produced reliably to evaluate the influence of N-glycosylation on the conformation and stability of bvPrP in biophysical experiments. Moreover, the combination of the techniques applied during this thesis, namely GCE, EPSL and CuAAC, show promising results to reliably generate complex modified semi-synthetic proteins.

6. Literature

(1) Sigurdson, C. J.; Bartz, J. C.; Glatzel, M. Cellular and Molecular Mechanisms of Prion Disease. *Annual Review of Pathology: Mechanisms of Disease* **2019**, *14*, 497–516.

(2) Myers, R.; Cembran, A.; Fernandez-Funez, P. Insight From Animals Resistant to Prion Diseases: Deciphering the Genotype – Morphotype – Phenotype Code for the Prion Protein. *Front. Cell. Neurosci.* **2020**, *14* (254).

(3) Sikorska, B.; Liberski, P. P. Human Prion Diseases: From Kuru to Variant Creutzfeldt-Jakob Disease. In *Protein Aggregation and Fibrillogenesis in Cerebral and Systemic Amyloid Disease*; J. Harris, Ed.; Subcellular Biochemistry, Vol. 65; Springer Dordrecht, 2012; Vol. 65, pp 457–496.

(4) Arshad, H.; Bourkas, M. E. C.; Watts, J. C. The Utility of Bank Voles for Studying Prion Disease. In *Progress in Molecular Biology and Translational Science*; Elsevier B.V., 2020; Vol. 175, pp 179–211.

(5) Barria, M. A.; Gonzalez-Romero, D.; Soto, C. Cyclic Amplification of Prion Protein Misfolding. In *Amyloid Proteins. Methods in Molecular Biology*; Sigurdsson, E. M., Calero, M., Gasset, M., Eds.; Humana Press, 2012; Vol. 849, pp 199–212.

(6) Fernández-Borges, N.; Chianini, F.; Eraña, H.; Vidal, E.; Eaton, S. L.; Pintado, B.; Finlayson, J.; Dagleish, M. P.; Castilla, J. Naturally Prion Resistant Mammals: A Utopia? *Prion* **2012**, *6* (5), 425–429.

(7) Kovač, V.; Šerbec, V. Č. Prion Protein: The Molecule of Many Forms and Faces. *Int. J. Mol. Sci.* **2022**, *23* (3).

(8) Callender, J. A.; Sevillano, A. M.; Soldau, K.; Kurt, T. D.; Schumann, T.; Pizzo, D. P.; Altmeppen, H.; Glatzel, M.; Esko, J. D.; Sigurdson, C. J. Prion Protein Post-Translational Modifications Modulate Heparan Sulfate Binding and Limit Aggregate Size in Prion Disease. *Neurobiol. Dis.* **2020**, *142*.

(9) Baskakov, I. V.; Katorcha, E.; Makarava, N. Prion Strain-Specific Structure and Pathology: A View from the Perspective of Glycobiology. *Viruses* **2018**, *10* (12).

(10) Hackl, S.; Becker, C. F. W. Prion Protein—Semisynthetic Prion Protein (PrP) Variants with Posttranslational Modifications. *Journal of Peptide Science* **2019**, *25* (10).

(11) Scheckel, C.; Aguzzi, A. Prions, Prionoids and Protein Misfolding Disorders. *Nat. Rev. Genet.* **2018**, *19* (7), 405–418.

(12) Capellari, S.; Strammiello, R.; Saverioni, D.; Kretzschmar, H.; Parchi, P. Genetic Creutzfeldt-Jakob Disease and Fatal Familial Insomnia: Insights into Phenotypic Variability and Disease Pathogenesis. *Acta Neuropathol.* **2011**, *121* (1), 21–37.

(13) Palmer, M. S.; Dryden, A. J.; Hughes, J. T.; Collinget, J. Homozygous Prion Protein Genotype Predisposes to Sporadic Creutzfeldt-Jakob Disease. *Nature* **1991**, *352* (6333), 340–342.

(14) Pocchiari, M.; Puopolo, M.; Croes, E. A.; Budka, H.; Gelpi, E.; Collins, S.; Lewis, V.; Sutcliffe, T.; Guilivi, A.; Delasnerie-Laupretre, N.; Brandel, J. P.; Alperovitch, A.; Zerr, I.; Poser, S.; Kretzschmar, H. A.; Ladogana, A.; Rietvald, I.; Mitrova, E.; Martinez-Martin, P.; De Pedro-Cuesta, J.; Glatzel, M.; Aguzzi, A.; Cooper, S.; Mackenzie, J.; Van Duijn, C. M.; Will, R. G. Predictors of Survival in Sporadic Creutzfeldt-Jakob Disease and Other Human Transmissible Spongiform Encephalopathies. *Brain* **2004**, *127* (10), 2348–2359.

(15) Shibuya, S.; Higuchi, J.; Shin, R.-W.; Tateishi, J.; Kitamoto, T. Protective Prion Protein Polymorphisms against Sporadic Creutzfeldt-Jakob Disease. *The Lancet* **1998**, *351* (9100), 419.

(16) Asante, E. A.; Smidak, M.; Grimshaw, A.; Houghton, R.; Tomlinson, A.; Jeelani, A.; Jakubcova, T.; Hamdan, S.; Richard-Londt, A.; Linehan, J. M.; Brandner, S.; Alpers, M.; Whitfield, J.; Mead, S.; Wadsworth, J. D. F.; Collinge, J. A Naturally Occurring Variant of the Human Prion Protein Completely Prevents Prion Disease. *Nature* **2015**, *522* (7557), 478–481.

(17) Makarava, N.; Chang, J. C. Y.; Molesworth, K.; Baskakov, I. V. Posttranslational Modifications Define Course of Prion Strain Adaptation and Disease Phenotype. *Journal of Clinical Investigation* **2020**, *130* (8), 4382–4395.

(18) Wille, H.; Requena, J. R. The Structure of PrP^{Sc} Prions. *Pathogens* **2018**, *7* (1).

(19) Sajnani, G.; Silva, C. J.; Ramos, A.; Pastrana, M. A.; Onisko, B. C.; Erickson, M. L.; Antaki, E. M.; Dynin, I.; Vázquez-Fernández, E.; Sigurdson, C. J.; Carter, J. M.; Requena, J. R. PK-Sensitive PrP^{Sc} Is Infectious and Shares Basic Structural Features with PK-Resistant PrP^{Sc}. *PLoS Pathog.* **2012**, *8* (3).

(20) de la Torre, D.; Chin, J. W. Reprogramming the Genetic Code. *Nat. Rev. Genet.* **2021**, *22* (3), 169–184.

(21) Wals, K.; Ovaa, H. Unnatural Amino Acid Incorporation in E. Coli: Current and Future Applications in the Design of Therapeutic Proteins. *Front. Chem.* **2014**, *2* (15).

(22) Hoesl, M. G.; Budisa, N. Recent Advances in Genetic Code Engineering in Escherichia Coli. *Curr. Opin. Biotechnol.* **2012**, *23* (5), 751–757.

(23) Huang, Y.; Zhang, P.; Wang, H.; Chen, Y.; Liu, T.; Luo, X. Genetic Code Expansion: Recent Developments and Emerging Applications. *Chem. Rev.* **2025**, *125* (2), 523–598.

(24) Shandell, M. A.; Tan, Z.; Cornish, V. W. Genetic Code Expansion: A Brief History and Perspective. *Biochemistry* **2021**, *60* (46), 3455–3469.

(25) Arranz-Gibert, P.; Patel, J. R.; Isaacs, F. J. The Role of Orthogonality in Genetic Code Expansion. *Life* **2019**, *9* (3), 58.

(26) Isaacs, F. J.; Carr, P. A.; Wang, H. H.; Lajoie, M. J.; Sterling, B.; Kraal, L.; Tolonen, A. C.; Gianoulis, T. A.; Goodman, D. B.; Reppas, N. B.; Emig, C. J.; Bang, D.; Hwang, S. J.; Jewett, M. C.; Jacobson, J. M.; Church, G. M. Precise Manipulation of Chromosomes in Vivo Enables Genome-Wide Codon Replacement. *Science* **2011**, *333* (6040), 348–353.

(27) Nakamura, Y.; Gojobori, T.; Ikemura, T. Codon Usage Tabulated from International DNA Sequence Databases: Status for the Year 2000. *Nucleic Acids Res.* **2000**, *28* (1), 292.

(28) Yi, H. Bin; Lee, S.; Seo, K.; Kim, H.; Kim, M.; Lee, H. S. Cellular and Biophysical Applications of Genetic Code Expansion. *Chem. Rev.* **2024**, *124* (11), 7465–7530.

(29) Li, J.; Chen, P. R. Development and Application of Bond Cleavage Reactions in Bioorthogonal Chemistry. *Nat. Chem. Biol.* **2016**, *12* (3), 129–137.

(30) Baker, A. S.; Deiters, A. Optical Control of Protein Function through Unnatural Amino Acid Mutagenesis and Other Optogenetic Approaches. *ACS Chem. Biol.* **2014**, *9* (7), 1398–1407.

(31) Baumann, A. L.; Hackenberger, C. P. R. Modern Ligation Methods to Access Natural and Modified Proteins. *Chimia* **2018**, *72* (11), 802–808.

(32) Wang, Z. A.; Cole, P. A. Methods and Applications of Expressed Protein Ligation. In *Expressed Protein Ligation: Methods and Protocols.*; Vila-Perelló, M., Ed.; Methods in Molecular Biology, Vol. 2133; Humana: New York, NY, 2020; pp 1–13.

(33) Thompson, R. E.; Muir, T. W. Chemoenzymatic Semisynthesis of Proteins. *Chem. Rev.* **2020**, *120* (6), 3051–3126.

(34) Thapa, P.; Zhang, R.-Y.; Menon, V.; Bingham, J.-P. Native Chemical Ligation: A Boon to Peptide Chemistry. *Molecules* **2014**, *19* (9), 14461–14483.

(35) Conibear, A. C.; Watson, E. E.; Payne, R. J.; Becker, C. F. W. Native Chemical Ligation in Protein Synthesis and Semi-Synthesis. *Chem. Soc. Rev.* **2018**, *47* (24), 9046–9068.

(36) Chu, N.; Cole, P. A. Protein Semisynthesis. In *Total Chemical Synthesis of Proteins*; Brik, A., Dawson, P., Liu, L., Eds.; Wiley-VCH: Weinheim, 2021; pp 307–326.

(37) Kulkarni, S. S.; Sayers, J.; Premdjee, B.; Payne, R. J. Rapid and Efficient Protein Synthesis through Expansion of the Native Chemical Ligation Concept. *Nat. Rev. Chem.* **2018**, *2* (4), 1–17.

(38) Jin, K.; Li, X. Advances in Native Chemical Ligation–Desulfurization: A Powerful Strategy for Peptide and Protein Synthesis. *Chemistry - A European Journal* **2018**, *24* (66), 17397–17404.

(39) Agouridas, V.; El Mahdi, O.; Diemer, V.; Cargoët, M.; Monbaliu, J. C. M.; Melnyk, O. Native Chemical Ligation and Extended Methods: Mechanisms, Catalysis, Scope, and Limitations. *Chem. Rev.* **2019**, *119* (12), 7328–7443.

(40) Kulkarni, S. S.; Watson, E. E.; Maxwell, J. W. C.; Niederacher, G.; Johansen-Leete, J.; Huhmann, S.; Mukherjee, S.; Norman, A. R.; Kriegesmann, J.; Becker, C. F. W.; Payne, R. J. Expressed Protein Selenoester Ligation. *Angewandte Chemie - International Edition* **2022**, *61* (20).

(41) Spriestersbach, A.; Kubicek, J.; Schäfer, F.; Block, H.; Maertens, B. Purification of His-Tagged Proteins. In *Methods in Enzymology*; Lorsch, J. R., Ed.; Academic Press Inc., 2015; Vol. 559, pp 1–15.

(42) Pasupuleti, R.; Riedl, S.; Saltor Núñez, L.; Karava, M.; Kumar, V.; Kourist, R.; Turnbull, W. B.; Zweytick, D.; Wiltschi, B. Lectin-Anticancer Peptide Fusion Demonstrates a Significant Cancer-Cell-Selective Cytotoxic Effect and Inspires the Production of “Clickable” Anticancer Peptide in Escherichia Coli. *Protein Science* **2023**, *32* (12).

(43) Briand, L.; Marcion, G.; Kriznik, A.; Heydel, J. M.; Artur, Y.; Garrido, C.; Seigneuric, R.; Neiers, F. A Self-Inducible Heterologous Protein Expression System in Escherichia Coli. *Sci. Rep.* **2016**, *6*.

(44) Palmer, I.; Wingfield, P. T. Preparation and Extraction of Insoluble (Inclusion-Body) Proteins from Escherichia Coli. *Curr. Protoc. Protein Sci.* **2012**, *70*, 6.3.1.–6.3.20.

(45) Da Silva Correia, S. M.; Schmitz, M.; Fischer, A.; Hermann, P.; Zerr, I. Role of Different Recombinant PrP Substrates in the Diagnostic Accuracy of the CSF RT-QuIC Assay in Creutzfeldt-Jakob Disease. *Cell Tissue Res.* **2023**, *392* (1), 301–306.

(46) Agrahari, A. K.; Bose, P.; Jaiswal, M. K.; Rajkhowa, S.; Singh, A. S.; Hotha, S.; Mishra, N.; Tiwari, V. K. Cu(I)-Catalyzed Click Chemistry in Glycoscience and Their Diverse Applications. *Chem. Rev.* **2021**, *121* (13), 7638–7956.

(47) Neumann, S.; Biewend, M.; Rana, S.; Binder, W. H. The CuAAC: Principles, Homogeneous and Heterogeneous Catalysts, and Novel Developments and Applications. *Macromol. Rapid Commun.* **2020**, *41* (1).

(48) Milles, S.; Tyagi, S.; Banterle, N.; Koehler, C.; VanDelinder, V.; Plass, T.; Neal, A. P.; Lemke, E. A. Click Strategies for Single-Molecule Protein Fluorescence. *J. Am. Chem. Soc.* **2012**, *134* (11), 5187–5195.

(49) Fornelli, L.; Toby, T. K. Characterization of Large Intact Protein Ions by Mass Spectrometry: What Directions Should We Follow? *Biochim. Biophys. Acta Proteins Proteom.* **2022**, *1870* (4).

(50) Klaene, J. J.; Ni, W.; Alfaro, J. F.; Zhou, Z. S. Detection and Quantitation of Succinimide in Intact Protein via Hydrazine Trapping and Chemical Derivatization. *J. Pharm. Sci.* **2014**, *103* (10), 3033–3042.

(51) Juliani do Amaral, M.; Mohapatra, S.; Ribeiro Passos, A.; Sousa Lopes da Silva, T.; Sampaio Carvalho, R.; da Silva Almeida, M.; Sá Pinheiro, A.; Wegmann, S.; Cordeiro, Y. Copper Drives Prion Protein Phase Separation and Modulates Aggregation. *Sci. Adv.* **2023**, *9* (44).

(52) Gao, C.; Fisher, Z. B.; Edgar, K. J. Azide Reduction by DTT or Thioacetic Acid Provides Access to Amino and Amido Polysaccharides. *Cellulose* **2019**, *26* (1), 445–462.

(53) Wiltschi, B.; Casas, M. G.; Stargardt, P.; Mairhofer, J. Decoupling Protein Production from Cell Growth Enhances the Site-Specific Incorporation of Noncanonical Amino Acids in E. Coli. *ACS Synth. Biol.* **2020**, *9* (11), 3052–3066.

(54) Hackl, S.; Ng, X. W.; Lu, D.; Wohland, T.; Becker, C. F. W. Cytoskeleton-Dependent Clustering of Membrane-Bound Prion Protein on the Cell Surface. *Journal of Biological Chemistry* **2021**, *296* (100359).

(55) Araman, C.; Thompson, R. E.; Wang, S.; Hackl, S.; Payne, R. J.; Becker, C. F. W. Semisynthetic Prion Protein (PrP) Variants Carrying Glycan Mimics at Position 181 and 197 Do Not Form Fibrils. *Chem. Sci.* **2017**, *8* (9), 6626–6632.

(56) Olschewski, D.; Seidel, R.; Miesbauer, M.; Rambold, A. S.; Oesterhelt, D.; Winklhofer, K. F.; Tatzelt, J.; Engelhard, M.; Becker, C. F. W. Semisynthetic Murine Prion Protein Equipped with a GPI Anchor Mimic Incorporates into Cellular Membranes. *Chem. Biol.* **2007**, *14* (9), 994–1006.

(57) Thakur, A. K.; Srivastava, A. K.; Srinivas, V.; Chary, K. V. R.; Rao, C. M. Copper Alters Aggregation Behavior of Prion Protein and Induces Novel Interactions between Its N- and C-Terminal Regions. *Journal of Biological Chemistry* **2011**, *286* (44), 38533–38545.

(58) Hong, V.; Presolski, S. I.; Ma, C.; Finn, M. G. Analysis and Optimization of Copper-Catalyzed Azide-Alkyne Cycloaddition for Bioconjugation. *Angewandte Chemie - International Edition* **2009**, *48* (52), 9879–9883.

(59) Lallana, E.; Riguera, R.; Fernandez-Megia, E. Reliable and Efficient Procedures for the Conjugation of Biomolecules through Huisgen Azide-Alkyne Cycloadditions. *Angewandte Chemie - International Edition* **2011**, *50* (38), 8794–8804.

(60) Tyagi, S.; Lemke, E. A. Genetically Encoded Click Chemistry for Single-Molecule FRET of Proteins. In *Methods in Cell Biology*; Conn, P. M., Ed.; Academic Press Inc., 2013; Vol. 113, pp 169–187.

7. Appendix

7.1 Softwares

Writing program: Word (Microsoft)

Bibliography software: Mendeley (Elsevier)

MS data analysis program: MassLynx (Waters)

NMR data analysis program: MestreNova (Mestrelab Research)

Graphics: Origin2025 (OriginLab), ChemDraw (Revvity Signals)

Image editing program: Inkscape (open source), Paint (Microsoft)

Search engines: Google Search (Google), Google Scholar (Google), PubMed (NCBI), Scopus (Elsevier)

7.2 bvPrP amino acid sequences

7.2.1 bvPrP-WT (residues 23-231):

MKKRPKPGGWNTGGSRYPGQGSPGGNRYPPQGGGTWGQPHGGGWGQPHGGGWG
QPHGGGWGQPHGGGWGQGGGTHNQWNKPSKPKTNMKHVAGAAAAGAVVGGLGGY
MLGSAMSRPMIHFGNDWEDRYYRENMNRYPNQVYYRPVDQYNNQNNFVHDCVNITIKQ
HTVTTTTKGENFTETDVKMMERVVEQMCVTQYQKESQAYYEGRSS

7.2.2 bvPrP-N181X (residues 23-231):

MKKRPKPGGWNTGGSRYPGQGSPGGNRYPPQGGGTWGQPHGGGWGQPHGGGWG
QPHGGGWGQPHGGGWGQGGGTHNQWNKPSKPKTNMKHVAGAAAAGAVVGGLGGY
MLGSAMSRPMIHFGNDWEDRYYRENMNRYPNQVYYRPVDQYNNQNNFVHDCVXITIKQ
HTVTTTTKGENFTETDVKMMERVVEQMCVTQYQKESQAYYEGRSS

The red X (X) denotes the mutation site at residue 181, where the native asparagine was replaced with an amber stop codon, allowing the incorporation of the ncAA of choice through amber codon suppression.

7.2.3 bvPrP-N197X (residues 23-231):

MKKRPKPGGWNTGGSRYPGQGSPGGNRYPPQGGGTWGQPHGGGWGQPHGGGWG
QPHGGGWGQPHGGGWGQGGGTHNQWNKPSKPKTNMKHVAGAAAAGAVVGGLGGY
MLGSAMSRPMIHFGNDWEDRYYRENMNRYPNQVYYRPVDQYNNQNNFVHDCVNITIKQ
HTVTTTTKGEXFTETDVKMMERVVEQMCVTQYQKESQAYYEGRSS

The red X (X) denotes the mutation site at residue 197, where the native asparagine was replaced with an amber stop codon, allowing the incorporation of the ncAA of choice through amber codon suppression.

7.2.4 *Mxe* GyrA intein-7x His-tag-CBD:

CITGDALVALPEGESVRIADIVPGARPNSDNAIDLKVLDRHGNPVLADRLFHSGEHPVYTV
RTVEGLRVTGTANHPLLCLVDVAGVPTLLWKLIDEIKPGDYAVIQRSAFSVDCAGFARGKP
EFAPTTYTVGVPGLVRFLEAHHRDPDAQAIADELTDGRFYYAKVASVTDAGVQPVYSLRV
DTADHAFITNGFVSHATGLTGIHHHHHHHHSGLNSGLTTNPGVSAWQVNTAYTAGQLVTYN
GKTYKCLQPHTSLAGWEPSNVPALWQLQ

The sequence in magenta denotes the intein, the 7x His-tag is orange and the CBD sequence is blue.

7.3 T7x33 vector annotation

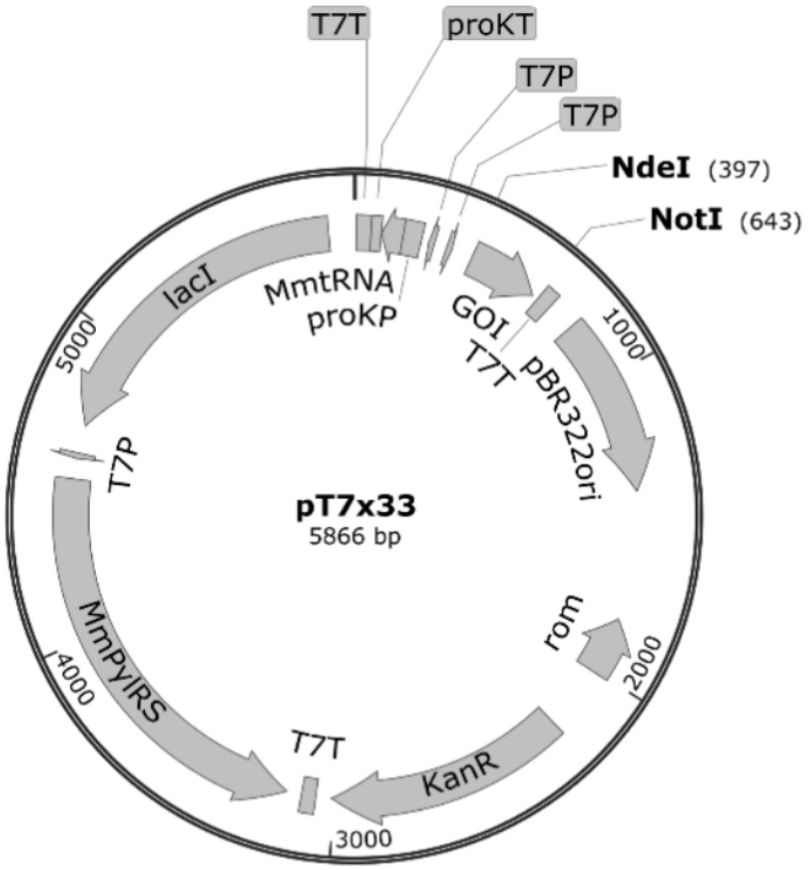

Appendix figure 1: Schematic depiction of the T7x33 vector without a bvPrP fusion construct insert. GOI denotes the insertion site for a gene of interest (GOI), lacI the Lac repressor gene, KanR the kanamycin resistance gene, MmPylRS the pyrrolysine aaRS gene originating from *Methanosarcina mazei*, MmtRNA the pyrrolysine specific tRNA gene originating from *Methanosarcina mazei*, NdeI and NotI the respective cutting sites for each restriction enzyme, pBR322ori the origin of replication, proKP and proKT the proK promoter and terminator sequences, rom the repressor of primer, T7P and T7T the respective T7 promoter and terminator sequences. The annotated scheme originates from the first supplement by Wiltschi *et al*.[42]

7.4 YnK synthesis NMR spectra

7.4.1 YnK ^{1}H-NMR spectrum

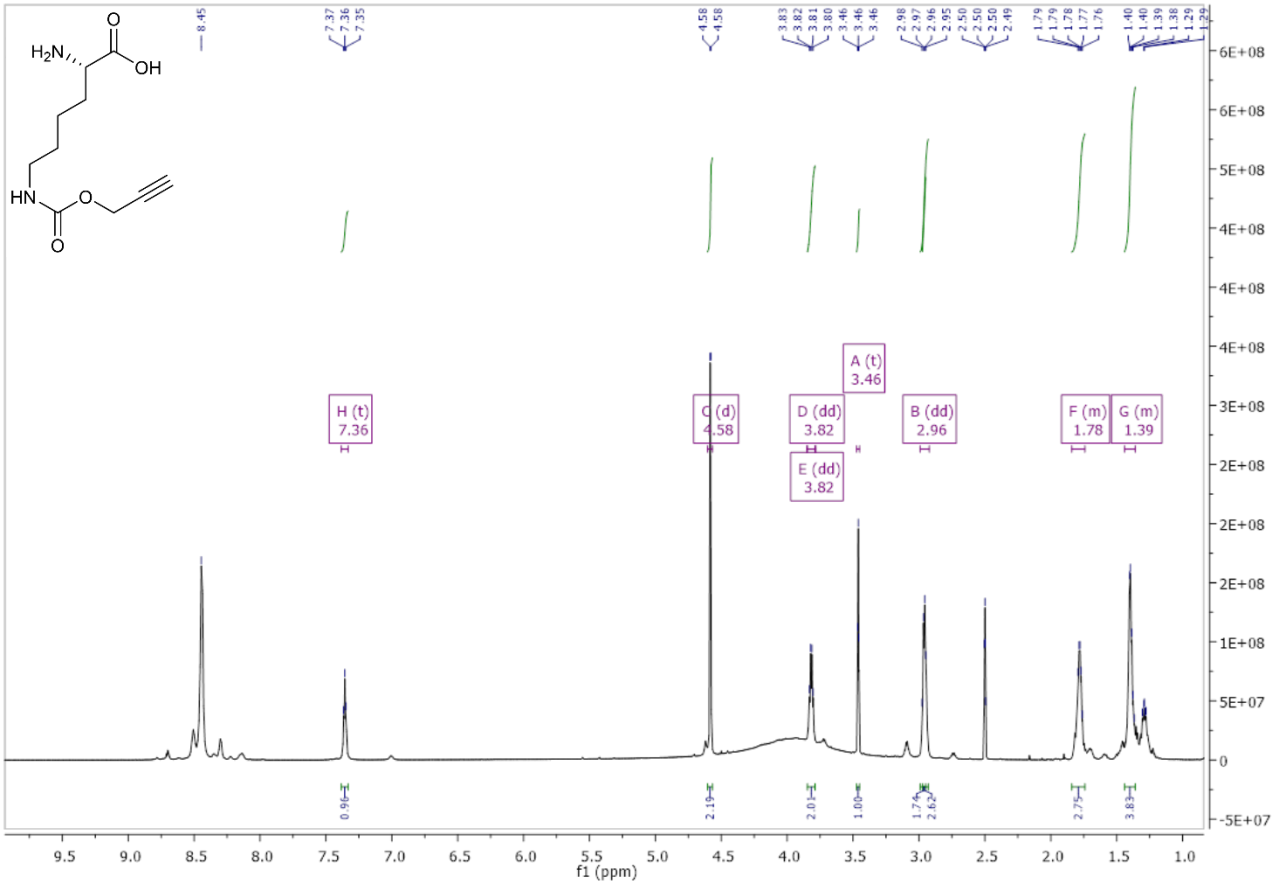

^{1}H NMR (DMSO-d6) [ppm] δ = 13.77 (s, 1H), 8.19 (s, 2H), 7.34 (t, 1H), 4.58 (d, 2H), 3.86 (s, 1H), 3.47 (t, 2H), 2.96 (q, 2H), 1.67-1.79 (m, 2H), 1.21-1.43 (m, 4H).

7.4.2 YnK ^{13}C-NMR spectrum

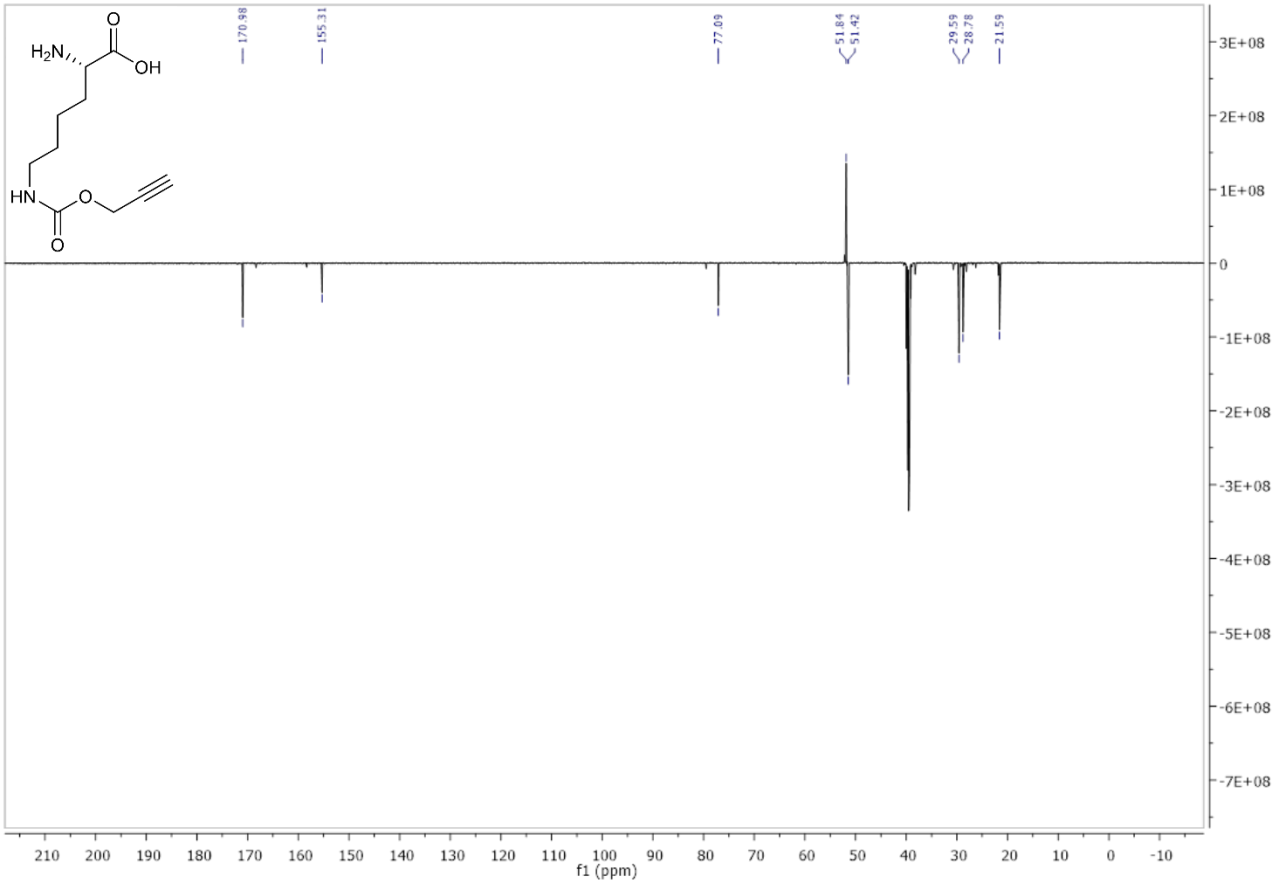

^{13}C NMR (DMSO-d6) [ppm] δ = 170.3, 162.3, 74.5, 74.4, 52.4, 51.7, 39.9, 29.8, 29.0, 21.8.